

# **CELLULOSE FIBRILS IN WOOD CELL WALLS AND THEIR POTENTIAL FOR TECHNICAL APPLICATIONS**

**PhD Thesis**

Faculty of Mathematics, Informatics and Natural Science,  
Department of Biology, University of Hamburg

by

**TANJA ZIMMERMANN**

Zürich 2007

Genehmigt vom Department Biologie  
der Fakultät für Mathematik, Informatik und Naturwissenschaften  
an der Universität Hamburg  
auf Antrag von Professor Dr. D. ECKSTEIN  
Weiterer Gutachter der Dissertation:  
Herr Professor Dr. J. H. SELL  
Tag der Disputation: 09. Februar 2007

Hamburg, den 08. Januar 2007



Professor Dr. Reinhard Lieberei  
Leiter des Departments Biologie

## Acknowledgement

This work was carried out at the Wood Laboratory of the Swiss Federal Laboratories for Materials Testing and Research (Empa), Dübendorf (CH) in collaboration with the University of Hamburg (D).

I am very grateful to my supervisors Prof. Dr. Jürgen Sell and Prof. Dr. Dieter Eckstein. J. Sell inspired me with his enthusiasm for cell wall research and was my scientific mentor at Empa till his retirement in 2002. D. Eckstein accepted to supervise my thesis as a professor at the Chair of Wood Biology, University of Hamburg. He accompanied my thesis in an open-minded and benevolent manner.

A special thank is due to Dr. Klaus Richter, head of the Wood Laboratory at Empa who always supported me and who gave valuable comments on my manuscripts.

Dr. Nico Bordeanu, Anja Fischer, Dr. Raoul Klingner, Evelyn Pöhler and Esther Strub, co-workers or former co-workers of my Wood Science/Biomimetics Research Group are gratefully acknowledged for their support and fruitful discussions.

I am grateful to Prof. Dr. Francis Schwarze and Prof. Dr. Hrvoje Turkulin for critically proof-reading and to Margrit Conradin for assistance in the formatting of the thesis.

Thanks are also due to Dr. Thomas Geiger and Jürg Schleuniger, Laboratory for Functional Polymers at Empa for their support and discussions concerning the cellulose fibril part of my thesis.

I thank Dr. Patrick Schwaller, Laboratory for Materials Technology at Empa Thun who taught me the nanoindentation method and who helped me with the interpretation of the results obtained.

I am grateful to Dr. Peter Lienemann and Urs Gfeller, Laboratory of Solid State Chemistry and Catalysis for their support concerning the X-ray diffraction measurements.

The contributions of Verena Thommen and Peter Reimann, Physics Department of Condensed Matter at the University of Bale are gratefully acknowledged. I was allowed to use the Atomic Force Microscope (AFM) at their laboratory and they advised me how to operate it efficiently. I also thank Prof. Dr. H. J. Hug, Laboratory of Nanoscale Materials Science at Empa who helped me with the interpretation of my AFM images.

I thank Dr. Ingo Burgert, Department of Biomaterials, Max-Planck-Institute of Colloids and Interfaces, Golm (D) for stimulating discussions and help with the mechanical tests on small specimens.

Last but not least, I thank my parents and my husband for all their love and support. Special thanks are due to my step-daughter Amadea and my children Ronja and Kaya who taught me so much. Their infective vitality and laugh always remind me that there is more to life than science and work.

The thesis is dedicated to my son Julian.





## Summary

The wood cell wall, a master piece of evolutionary design has evolved to provide mechanical strength for the living tree. We can learn from the cell wall and use its structures for technical purposes but, further information and insight concerning nanoscale order and assembly of its structural elements is required. In addition, a better understanding of cell wall polymer interactions is important. This knowledge will advance opportunities for new applications of wood and its individual constituents.

In the first part of the thesis the fine structure of the secondary 2 (S2) wall layer on transverse fracture surfaces of different tension-loaded softwoods, hardwoods and reaction wood was studied by field emission scanning electron microscopy (FE-SEM). Softwood tracheids (also in compression wood) and hardwood fibres showed a predominantly radial fragmentation (perpendicular to the other cell wall layers) of the S2 layer. Radial structures were also identified on cross-sections of various hardwood fibres degraded by white rot fungi. By contrast, a disordered fracture pattern was observed in the S2 or G layers of pronounced tension wood cells.

In addition, transverse fracture surfaces and ultra thin sections of Norway spruce tracheids were observed by FE-SEM and transmission electron microscopy (TEM) after pre-treatment of the cell walls with various alkali solutions, acetic and nitric acid and ASAM delignification. In untreated (reference) samples, radial fracture patterns – perpendicular to the compound middle lamella (CML) – were regularly observed. Swelling of the cell wall and a slight reduction in glucomannan led to the disappearance of radial structures and resulted in a disordered fragmentation. As the severity of the alkali treatment increased and acid and ASAM delignification was applied, concentric alignments in the cell wall became more and more discernable. The increasing loss of hemicelluloses and lignin led therefore to distinct changes in the fragmentation patterns of the cell walls. In addition, losses in strength and stiffness could be determined for all chemically treated cell walls.

Atomic Force Microscopy was used to investigate the ultrastructural appearance of transverse wood cell wall surfaces in embedded and polished wood blocks or semi-thin sections of Norway spruce. The images of the polished samples showed randomly arranged wood cell wall components in the secondary 2 (S2) layers of all investigated early- and latewood tracheids. Alignments of the structural components were found in the S2 layer of semi-thin sectioned tracheid cell walls. They were often preferentially aligned in the cutting direction, especially in very thin sections. As the direction of the compound middle lamella (CML) clearly differs from the cutting direction and the direction of the aligned structures, these textures were considered to represent scratch marks.

The ultrastructural appearance changes considerably depending on the applied sample processing and microscopy method. Even slight changes in cell wall constitution markedly influence the interactions of the cell wall components and thus fracture mechanics and ultrastructural appearance of wood cell walls. It is concluded that the random distribution pattern of the cellulose fibril/matrix structure as observed by AFM reflects the underlying original cell wall structure. The wood cell wall components arrange into various structural patterns under different stress conditions and preparation methods modifying the originally random arrangement of the wood cell wall constituents.

The information about the arrangement and interactions of the main chemical wood cell wall constituents is important when considering their exploitation for technical purposes. Especially cellulose as most abundant, renewable and biodegradable natural polymer on earth with its extraordinary mechanical properties is of interest for the development of new composite materials.

The content of cellulose in wood is approximately 45 % and even higher in e.g. annual plants. Within the different cell wall layers of softwood tracheids or hardwood fibres the high tensile strength cellulose exists as a system of fibrils embedded in the matrix substance lignin. The capability of these nano-scaled cellulose fibrils for the reinforcement of polymers was studied in the second, more applied part of the thesis.

For this purpose, fibrils with diameters below 100 nanometer and lengths of several tens of micrometers were either mechanically or chemically/mechanically isolated from a commercial softwood sulphite pulp. Homogeneous, translucent fibril films and polymer composites with polyvinyl alcohol and hydroxypropyl cellulose were prepared. For mechanical characterisation, tensile tests and nanoindentation experiments were carried out. The addition of fibrils led to an up to threefold higher Modulus of Elasticity (MOE) and an up to fivefold higher tensile strength of the polymers. The results from the mechanical tests can be related to the results obtained from the TEM and AFM characterisations. A significant increase in the mechanical properties was measured for the films with fibril contents of 10 wt% compared to the films with lower fibril ratio. A network formation could only be observed for composites with a fibril ratio of at least 10 wt%. The existence of fibril networks has therefore been found to be of great importance for the mechanical properties of nanocomposites.

According to the results, extensive applications of cellulose fibrils in coatings, adhesives, medicine, packaging or transportation may have great potential. A prime challenge is the compounding of cellulose fibrils with natural polymers for the development of a new class of cellulose bio-nanocomposites. Therefore, a chemical modification of cellulose fibrils will be necessary to match the hydrophilic or hydrophobic nature of the polymer matrix. In future, characteristics of different matrices could be directly influenced by functionalising the hydroxyl groups of cellulose fibrils.

## List of abbreviations and definitions

AFM	Atomic Force Microscopy
CML	Compound Middle Lamella (primary wall and middle lamella)
DP	Degree of Polymerisation
$E_{\text{indent}}$	Indentation modulus
FE-SEM	Field Emission Scanning Electron Microscopy
G-Layer	Gelatinous layer
HPC	Hydroxypropyl cellulose
LM	Light Microscopy
MCC	Microcrystalline Cellulose
MFC	Microfibrillated Cellulose
MOE	Modulus of Elasticity
PEO	Polyethylene oxide
PVA	Polyvinyl alcohol
PVP	Polyvinyl pyrrolidone
RH	Relative humidity
S1	Secondary one layer (outer layer of the secondary cell wall)
S2	Secondary two layer (the thick middle layer of the secondary wall)
S3	Secondary three layer (inner layer of the secondary cell wall)
TEM	Transmission Electron Microscopy
wt%	Weight percent
Cellulose fibrils	Cellulose, the principal component of the wood cell wall exists as a system of fibrils, a single fibril has a diameter of about 3.5 nanometer.
Cellulose fibril aggregates	Single cellulose fibrils are normally aggregated or agglomerated to larger structural units with cross section sizes of about 10 to 30 nm.
Cellulose fibril agglomerations	See cellulose fibril aggregates
Cellulose whisker	Crystalline cellulose chains, normally isolated from cellulose fibres by acid hydrolysis
Fracture/Fragmentation pattern	The aligned features in the S2 of fractured samples are described as fracture or fragmentation patterns.

Microstructure	Defined as structures that have micrometer dimensions and are visible by light microscopy
Ultrastructure/Nanostructure	Defined as structures that have nanometer dimensions and are visible by high resolution microscopy methods like FE-SEM, TEM or AFM

## Contents

1	Introduction .....	11
1.1	Background.....	11
1.1.1	Wood cell wall structure.....	11
1.1.2	Cellulose fibrils.....	13
1.1.3	Cellulose nanocomposites.....	14
1.2	Objectives of the study .....	14
2	Materials and Methods .....	16
2.1	Wood cell wall structure.....	16
2.1.1	Sample pre-treatment.....	16
2.1.2	Sample preparation .....	16
2.1.3	Microscopic characterisation .....	18
2.1.4	X-ray diffraction.....	19
2.2	Cellulose fibrils.....	19
2.2.1	Separation and characterisation of cellulose fibrils .....	19
2.2.2	Production of cellulose nanocomposites .....	22
2.2.3	Mechanical characterisation of cellulose nanocomposites.....	22
2.2.4	Morphological characterisation of cellulose nanocomposites .....	23
3	Results and Discussion .....	24
3.1	Wood cell wall structure.....	24
3.1.1	Fractured softwood tracheids and hardwood fibres .....	24
3.1.2	Fungi treated hardwood fibres.....	25
3.1.3	Chemically treated spruce tracheids .....	26
3.1.4	Embedded and polished spruce tracheids .....	26
3.2	Cellulose fibrils.....	28
3.2.1	Morphology of separated cellulose fibrils .....	28
3.2.2	Mechanical properties of cellulose nanocomposites.....	29
3.2.3	Morphological properties of cellulose nanocomposites.....	30
4	Conclusions .....	31
4.1	Wood cell wall structure.....	31
4.2	Cellulose fibrils.....	32
5	References .....	34
5.1	Appendix.....	39

## Appendix

The present thesis is based on five peer reviewed publications: one book article and four journal papers:

- A Zimmermann, T., and J. Sell. 2004. Field Emission SEM studies on softwood tracheids and hardwood fibres - A review of activities at the EMPA Wood Laboratory. In: Wood fibre cell walls. Methods to study their formation, structure and properties. Eds. Schmitt, U., P. Ander, J. R. Barnett, A. M. C. Emons, and S. Tschegg, COST Action E20. pp. 175-186  
Own contribution: conception of the studies, literature research, sample preparation, bending tests and FE-SEM investigations, discussion of the results, outline and writing of the article
- B Zimmermann, T., V. Thommen, P. Reimann, and H. J. Hug. 2006. Ultrastructural appearance of embedded and polished wood cell walls as revealed by Atomic Force Microscopy. *Journal of Structural Biology* 156: 363-369  
Own contribution: conception of the study, literature research, AFM investigations, and discussion of the results, outline and writing of the article
- C Zimmermann, T., K. Richter, N. Bordeanu, and J. Sell. 2007. Arrangement of cell wall constituents in chemically treated Norway spruce tracheids. *Wood and Fiber Science*, in press  
Own contribution: conception of the study, literature research, sample preparation, FE-SEM and TEM investigations, and discussion of the results, outline and writing of the article
- D Zimmermann, T., E. Pöhler, and T. Geiger. 2004. Cellulose fibrils for polymer reinforcement. *Advanced Engineering Materials* 6(9): 754-761  
Own contribution: conception of the study, contribution to literature research, contribution to sample preparation, fibril extraction, their characterisation and compounding, tensile testing of the respective composites, contribution to data evaluation, and discussion of the results, outline and writing of the article
- E Zimmermann, T., E. Pöhler, and P. Schwaller. 2005. Mechanical and morphological properties of cellulose fibril reinforced nanocomposites. *Advanced Engineering Materials* 7(12): 1156-1161  
Own contribution: conception of the study, literature research, sample preparation, nanoindentation experiments and AFM investigations, discussion of the results, outline and writing of the article

---

# 1 Introduction

## 1.1 Background

Recent developments in nanotechnology, material science and engineering provide new technical expertise to the production of advanced materials from natural products. Identification and exploitation of this knowledge should enable the sustainable conversion of forest-based raw materials such as wood into innovative high-value materials.

With the focus on near-future applications of nanotechnology in the forest product sector, exploratory research and development in the following areas will be relevant (Iversen et al. 2005):

- Basic research and development in the area of wood and pulp fibre cell wall nanostructure:
  - e.g. hierarchical structure of cell walls
  - organisation and distribution of fibre wall components
  - enzymatic modification of fibre components
  - chemical and physical modifications of fibre components
- Exploratory research and development aiming at the industrial utilisation of nano-scaled cellulose fibrils:
  - isolation of cellulose fibrils from different raw materials
  - chemical modification of cellulose fibrils
  - aggregation and deaggregation processes
  - physical and mechanical characterisation of fibril strength and networking properties in applications
  - performance of cellulose fibrils in nanocomposites

Several of these aspects are addressed in this thesis. The properties of wood based materials, e.g. fibre or cellulose fibril based products depend on the properties of the chemical constituents and their arrangement and interaction within the cell wall. Respective information at the macroscopic level is well documented, but at the micro- or nano level more work is needed to understand cell wall constitution and interactions of wood polymers. Thus, the first chapter/part of the thesis deals with the arrangement and the interactions of the main chemical constituents in wood cell walls. Based on the obtained knowledge, the second part then exploits the capability of the high strength cellulose fibrils for technical applications.

### 1.1.1 Wood cell wall structure

Wood has been widely used as an engineering material for thousands of years because of its extraordinary properties, e.g. a high mechanical strength and a high strength to weight ratio. The excellent mechanical properties of wood are a direct result of its hierarchical internal structure at all length scales (Booker and Sell 1998). Wood cell wall research seeks to understand and exploit the relationships between the complex architecture of wood cell walls at the micro- and nanometer scale and the material properties of wood and its fibres.

At the microscopic level, the wood cell wall which can be described as a natural composite is organised in layers with different thicknesses and different ratios of cellulose, the matrix material lignin and hemicellulose (Brändström 2001; Harada and Côté 1985; Wardrop 1964). Within the different cell wall layers, cellulose exists as a system of fibrils with diameters of 3-4 nm aggregated in larger structural units (Fengel 1970; Frey-Wyssling 1968; Heyn 1977). The cellulose fibril aggregates are surrounded by the polymers lignin and hemicelluloses. The arrangement as well as the interactions of these chemical constituents at the nanometer level has to date not been completely resolved.

The nanoscale structure of softwood tracheid cell walls was determined by a combination of various preparation and different high resolution techniques. The original structure of cross sections is still strongly debated. The images presented by e.g. Fahlén and Salmén (2002) or Ruel et al. (1978) showed that the thickest cell wall layer (S2) solely consists of concentric lamellae, whereas the measurements of Sell and Zimmermann (1993) or Schwarze and Engels (1998) revealed a radial arrangement of the fibril/matrix structure (perpendicular to the compound middle lamella). *Figure 1* shows these structural arrangements in a schematic secondary wall model. In contrast to both models, a random texture of cell wall components within the S2 layer of softwood tracheids was recently described by Donaldson and Frankland (2004).

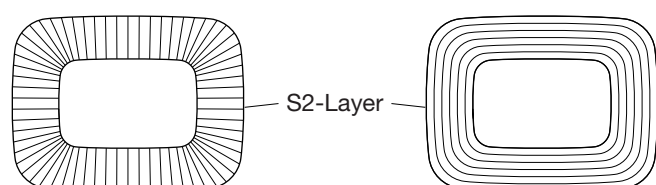


*Fig. 1: Schematic model of the thick S2 layer of a softwood tracheid secondary wall showing preferential structural orientations in either radial, i.e. perpendicular to the other layers (left) or lamellar directions (right)*

It has been suggested that different organisation patterns do coexist (Sell and Zimmermann 1998; Singh and Daniel 2001). Another hypothesis is that the wood cell wall components arrange into various structural patterns under different stress conditions and preparation methods (Zimmermann et al. 2006) (**Paper C**). Indeed, a morphological re-arrangement process following plastic deformation of wood has been described by Keckes et al. (2003). They found evidence for a molecular stick-slip mechanism similar to the motion of dislocations in crystalline materials. In detail, a re-formation of the amorphous matrix between the cellulose fibrils within the cell wall was proposed. A similar mechanism may explain the formation of different ultrastructural patterns observed in the past.

Further studies are necessary to demonstrate the influence of different mechanical, enzymatic or chemical impacts on the ultrastructural appearance of wood cell wall transverse sections. Interactions of the cell wall constituents should be the main focus.

Basic knowledge about the arrangement and the sizes of cellulose fibrils or fibril aggregates within the cell wall is a pre-condition when considering their potential for technical applications. Thus, the findings regarding cell wall ultrastructure obtained in the first part of the thesis provided the basis for the second more applied part on the isolation and characterisation of cellulose fibrils from wood pulp as well as their compounding in polymer matrices.



### 1.1.2 Cellulose fibrils

Nanotechnology is the study and engineering of matter at the dimensions of 1 to 100 nanometers, where the physical, chemical or biological properties are fundamentally different from those of the bulk material. By expanding our knowledge and control of matter at such levels, new ways in product development can be opened (Moon et al. 2006). Thus, the interest of the research community in developing environmentally friendly nanocomposites, that use renewable polymers, has grown intensively in recent years (Iversen et al. 2005).

With a total quantity on earth of  $10^{11}$  tons (Coughlan 1985), cellulose is the most abundant, renewable and biodegradable natural polymer on earth (Mathew et al. 2006). In wood tracheids or fibres that have diameters in the micrometer and length in the millimetre range cellulose acts as a structural element with a content of approximately 45 %. Within the different cell wall layers of fibres the high tensile strength cellulose exists as a system of fibrils embedded in the matrix substance lignin (*Figure 2*). One single cellulose fibril is approx. 3-4 nm thick and several tens of micrometers long and consists of a crystalline part linked to amorphous domains. The cellulose chains are stabilised laterally by hydrogen bonds between hydroxyl groups (Fengel and Wegener 1989).

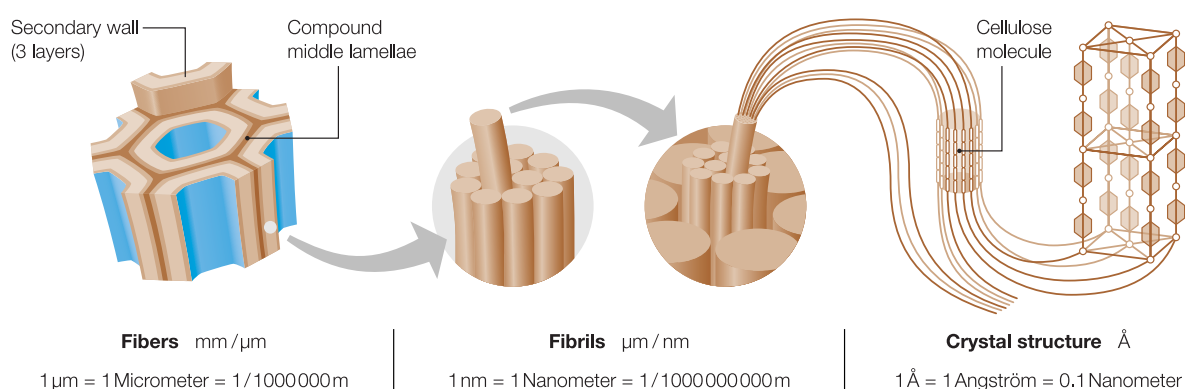


*Fig. 2: Scheme of a wood cell wall showing the compound middle lamella, and three layers of the secondary wall. Cellulose, the principal component of the cell wall, exists as a system of fibrils. Parts of the fibrils are arranged in an orderly fashion and provide crystalline properties to the wall (Zimmermann et al. 2004).*

The extraordinary mechanical properties of the crystal structure are of great interest. Thus, the modulus of elasticity of the perfect crystal of native cellulose has been calculated by different authors (Michell 1989; Northolt and de Vries 1985; Tashiro and Kobayashi 1991; Wainwright et al. 1982) and estimated between 130 GPa up to 250 GPa. The tensile strength of the crystal structure was assessed to be approximately 0.8 GPa up to 10 GPa. Table 1 in **Paper D** illustrates the interrelation between the length scale and the strength and stiffness of cellulose structures.

To use the potential of fibrils, the fragmentation of cellulose fibres into smaller units has been continuously attempted. The Microfibrillated Cellulose (MFC) with diameters in the nanometer range and aspect ratios (fibre length divided by diameter) between 50 and 100 (Boldizar et al. 1987) is a form of expanded high-volume cellulose, obtained through a mechanical homogenisation process of e.g. wood pulp. The Microcrystalline Cellulose (MCC) with particle sizes between 10 and 15  $\mu\text{m}$  and aspect ratios of about 3 (Boldizar et al. 1987) is generated by acid hydrolysis of various plant fibres (Herrick 1984; Turbak et al. 1983).

---

MFC and MCC are normally not applied for reinforcement purposes; although these cellulose structures have high strength properties. As they form a stable gel, they are often used as paint or ink thickener, pharmaceutical tablet binder or rheology-control agent in food.

### 1.1.3 Cellulose nanocomposites

It has recently become apparent that biological nanofibres (diameter 20-40 nm) are of great interest in new nanocomposite materials (Berglund 2004). A first book about the processing, characterisation and properties of cellulose nanocomposites has been published with a book chapter based on the **Papers D and E** of this thesis (Oksman and Sain 2006).

Some studies have reported on cellulose whiskers or fibrils obtained from organic materials like sugar beet pulp (Dinand et al. 1999; Heux et al. 1999), potato tuber cells (Dufresne et al. 2000), wheat straw (Dufresne et al. 1997; Helbert et al. 1996), tunicin (Angles and Dufresne 2000; Chanzy et al. 2000; Favier et al. 1995) or crab shell chitin (Nair and Dufresne 2003). These whiskers or fibrils were used as reinforcement components in synthetic polymers and biopolymers for the production of films and lacquers. Depending on the portion of cellulose, the composites showed improved mechanical properties.

The production of cellulose nanocomposites with fibrils of a high aspect ratio for load-bearing applications is fairly new. In particular, the possible fields of application of cellulose fibrils separated from wood pulp were hardly investigated. In addition to the expected high strength advantages, wood as basis material for the extraction of cellulose fibrils is inexpensive and constantly available.

Although there are several studies on the separation of cellulose fibrils from plant fibres or special marine animals, certain problems have not been sufficiently solved. The isolation/disintegration of cellulose without severe degradation and at reasonable costs is still difficult. Another problem is the dispersion of cellulose fibrils in polymer matrices, especially when they are hydrophobic. To date, it is not possible to obtain dry re-dispersible cellulose fibrils.

## 1.2 Objectives of the study

### Wood cell wall structure

The first part of the thesis aimed to accomplish basis knowledge of the wood cell wall structure. The main objective was to investigate the arrangement of cellulose fibrils respectively cellulose fibril agglomerates on transverse surfaces of the S2 layer of softwood tracheid cell walls, especially Norway spruce, and of hardwood fibres. The different sample processing methods used are described hereafter. The prepared samples were characterised by various high resolution microscopy techniques.

#### Sub-Goals

1. Morphological characterisation (FE-SEM) of soft- and hardwood, reaction wood and transverse sections of wood treated with decay fungi (**Book Article A**).

- 
2. Morphological (FE-SEM, TEM) and mechanical characterisation (strength, elasticity) of chemically pre-treated Norway spruce transverse sections (**Paper C**).
  3. AFM characterisation of embedded and polished, respectively microtomed Norway spruce transverse sections (**Paper B**).

### **Cellulose fibrils**

The overall objective of this part of the thesis was to evaluate the potential of cellulose fibrils, respectively cellulose fibril agglomerates for the use in technical applications.

#### **Sub-Goals**

1. Separation of cellulose fibril agglomerates at the greatest possible lengths and diameters below 100 nm from sulphite pulp with methods also capable for a later industrial up-scaling (combination of mechanical and / or chemical methods) (**Paper D**).
2. Morphological characterisation of the obtained cellulose fibrils by FE-SEM and TEM (determination of sizes, networking) (**Paper D**).
3. Determination of the Degree of Polymerisation (DP) of the basis material and the obtained fibrils (**Paper D**).
4. Compounding of the separated cellulose fibrils with suitable model polymers to evaluate their reinforcing effect (**Paper D**).
5. Analysis of the fibril alignment and the assumption of network formation in fibril reinforced polymer films by TEM and AFM (**Paper E**).
6. Investigation of the mechanical properties of cellulose fibril reinforced polymer films (e.g. determination of the tensile strength, MOE and hardness by conventional tensile testing as well as nanoindentation) (**Paper D+E**).
7. Evaluation of potential technical applications of cellulose nanocomposites.

---

## 2 Materials and Methods

### 2.1 Wood cell wall structure

An important hypothesis is that the imaged structure of transverse sections strongly depends on the pre-treatment and preparation method of wood samples. Different sample processing pathways were selected to evaluate the resulting ultrastructural appearances by FE-SEM, TEM or AFM (**Paper B and C**).

#### 2.1.1 Sample pre-treatment

##### Chemical pre-treatment

The treatments were designed to dissolve the binding components hemicellulose and lignin with increasing severity. Alkaline treatment with NaOH and KOH was used for selective hemicellulose degradation. Acetic treatment and ASAM pulping was designed for intensive degradation of both, hemicelluloses and lignin, leaving the cellulose generally unaltered (**Paper C**).

##### Chemical analysis

To demonstrate the effects of the various chemical treatments applied, the samples were submitted to total hydrolysis with sulphuric acid, the hydrolysed carbohydrates were separated by borate complex ion exchange chromatography, and detected photometrically with copper-2,2-bicinchonate reagent according to Uremovic et al. (1994) (**Paper C**).

##### Exposure to white rot fungi

Larsen et al. (1995), Schwarze and Engels (1998) and Schwarze and Fink (1999) investigated softwood tracheids or hardwood fibres exposed to white rot fungi by LM, SEM or TEM. From the results obtained, they derived information about the arrangement of cell wall constituents. The latter biological pre-treatment method was applied and two different white rot fungi using the following host-fungus combinations were selected: sycamore (*Acer pseudoplatanus*) with *Flammulina velutipes*, beech (*Fagus sylvatica*) and small-leaved lime (*Tilia cordata*) with *Ganoderma applanatum*. Wood blocks were obtained from the sapwood of living trees and inoculated according to Schwarze and Fink (1999) (**Book Article A**).

#### 2.1.2 Sample preparation

##### Fracturing

In earlier investigations (Sell and Zimmermann 1993, 1998) fracturing was used as a sample preparation method. According to these studies, 3-point bending tests were applied to loosen the cell wall structure on transverse sections of wood specimens for evaluation of the resulting fracture patterns. In addition, the

---

bending strength and the Modulus of Elasticity (MOE) of the samples were calculated (**Book Article A** and **Paper C**).

### **Drying**

Conventional Scanning Electron microscopy requires absolutely dry ( $u = 0\%$ ) wood. Thus, samples from the outermost tension zone of the fractured samples were dried in a vacuum oven at 40 °C and 10 mbar for 12 hours (**Book Article A + Paper C**).

Samples treated with wood decay fungi for examination with FE-SEM were dehydrated in an ethanol series (**Book Article A**); the chemically treated samples intended for TEM were dehydrated in an acetone series prior to embedding (**Paper C**).

The wood used for sample preparation for the AFM measurements (main method/pathway 1) was conditioned in a climate chamber at 35 % RH and 23 °C to reach a moisture content of approx. 7 % (**Paper B**). In pathway 3, the influence of high shrinkage stresses on the tracheid cell wall structure should be evaluated. Therefore, the respective samples were oven dried for 12 hours at 102 °C to a moisture content of 0 % prior to embedding.

### **Embedding**

For the preparation of (ultra) thin as well as polished sections for LM, TEM or AFM investigations the samples have to be embedded into a rigid supporting resin.

Samples treated with wood decay fungi were embedded into methacrylate (LR White) (**Book Article A**).

The chemically treated samples for TEM investigations were embedded following the methodology proposed by Spurr (1969) (**Paper C**).

The wood blocks prepared for AFM were embedded into Specifix-20 resin and curing agent from Struers, an epoxy resin also used for ceramic or metallic samples which have to be polished in further processing steps (**Paper B**).

### **Microtoming**

The surface of hardwood fibre cell walls degraded at an early stage by white rot fungi was smoothened perpendicular to the fibres by cutting with a rotary microtome (diamond knife) prior to their observation by FE-SEM (**Book Article A**).

(Ultra) thin sections were prepared for the following purposes:

Approximately 100 nm thin sections of the chemically treated samples were produced and stained with  $\text{KMnO}_4$  to compare TEM images of tracheid cross sections with FE-SEM images of fractured transverse surfaces (**Paper C**).

---

Semi-thin sections of 0.5  $\mu\text{m}$ , 1  $\mu\text{m}$  and 5  $\mu\text{m}$  thickness were prepared by microtoming from the not polished underside of one embedded spruce wood block taken from pathway 1 (**Paper B**). Subsequent AFM analysis intended to clarify if this preparation method may induce artefacts.

## **Polishing**

Here, we studied the influence of a sample preparation method which is normally applied for metallic or ceramic specimens. In pathway 1 the samples were non-directionally polished, thus the polishing direction was changed by discrete 90-degree-steps after each grain size to avoid any artificially induced orientation of the wood cell wall components. In pathway 2 a possible influence of directional polishing was evaluated. Instead of changing the polishing direction, a fixed polishing angle of about 45 ° to the direction of the xylem rays was chosen (**Paper B**).

### **2.1.3 Microscopic characterisation**

#### **FE-SEM characterisation of fractured samples**

The dried samples (see above) were glued on a specimen holder using carbon-adhesive and sputtered with a platinum layer of approx. 10 nm. The samples were investigated in a Field Emission SEM (Jeol 6300F) at an acceleration voltage of 5 kV and working distance of 24 mm (**Book Article A + Paper C**).

#### **TEM characterisation of microtomed samples**

The prepared sections (see above) were examined with a Philips STEM CM30 transmission electron microscope (**Paper C**).

#### **AFM characterisation of polished and microtomed samples**

Different positions of polished and microtomed cell walls of randomly selected early- and latewood tracheids were imaged with a Nanoscope IVa Dimension TM 3100 AFM (**Paper B**). All images were acquired in Tapping Mode. The principle is shown in *Figure 3*. During Tapping Mode the cantilever is driven with constant amplitude, at a fixed frequency above its resonance. During scanning, the z-position of the sample is regulated to keep the oscillation amplitude at the chosen amplitude setpoint (here about 90 % of the free oscillation amplitude). Under ideal circumstances the output of the z-feedback then shows the sample topography.

Simultaneously with the topography, the cantilever amplitude (error of feedback) and the cantilever phase were recorded. The phase image typically reflects local mechanical properties such as the sample stiffness.

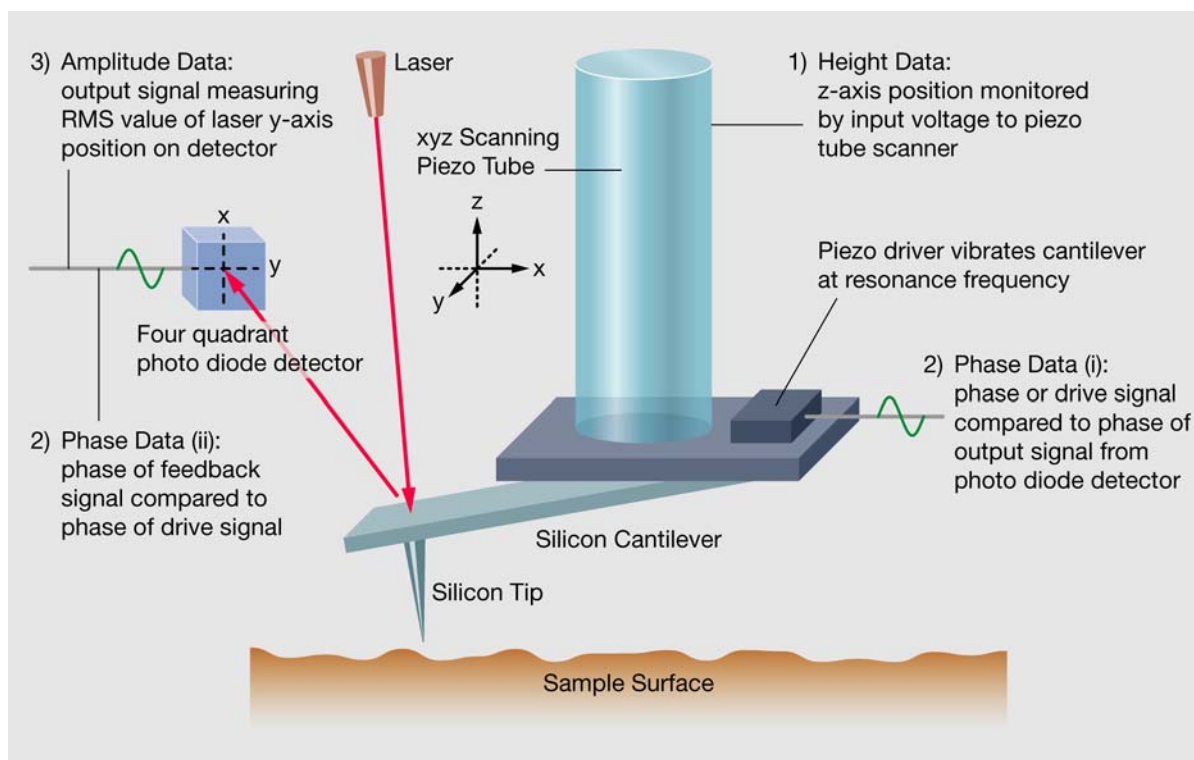


Fig. 3: 1) The height data is obtained by monitoring changes in the length of the z-axis on the xyz scanning piezo tube. Input voltage to the scanning piezo tube is proportional to the length of the tube and any change in the z axis is plotted as a topographical map of the sample surface. 2) The phase data monitors the change of phase signal of the input drive signal with respect to the phase change in oscillating cantilever. 3) The amplitude of the cantilever oscillation is monitored by the photodiode detector. The RMS (Root Mean Square) value of the laser signal in the y- axis of the detector is recorded for each segment on a given raster of the probe tip.

## 2.1.4 X-ray diffraction

To assess the possible influence of the alkali treatments on the supermolecular structure of cellulose, XRD measurements were carried out (**Paper C**). The tangential surfaces of the sample sticks treated with 10% (cold and hot water extraction) and 18% NaOH as well as 24% KOH were prepared by microtoming the surface and a thoroughly washing with deionized water. The samples were then investigated with a diffractometer (X'Pert Pro, Panalytical, Netherlands) using Ni-filtered Cu K $\alpha$  radiation ( $\lambda = 0.15418$  nm).

## 2.2 Cellulose fibrils

### 2.2.1 Separation and characterisation of cellulose fibrils

#### Separation of cellulose fibrils from sulphite pulp

One important precondition of this part of the study was to develop a simple disintegration method with the possibility for future industrial up-scaling.

As basis material a commercially available sulphite pulp (rich in hemicelluloses and mainly composed of softwood tracheids) from the company Borregaard was used. Two separation methods/pathways were undertaken:

*Pathway 1, mechanical separation (Paper D+E):*

1. First, wet sulphite pulp with a dry content of 30 % was reduced to small pieces with a laboratory mixer (FA IKA; 20000 rpm, 25 s).
2. The pulp was then dispersed in deionised water. For suspensions up to 2 litres, the pulp fibres were treated with an ultra-turrax (FA IKA; 24000 rpm, 8 h) at 5-10° C to separate the fibril bundles from the wooden cell wall. For larger quantities a closed dispersing system (FA Kinematica AG, Megatron MT 300; 22000 rpm, 320 min, *Figure 4*) was used.
3. A further dispersing and homogenisation of the cellulose fibrils was achieved by application of a microfluidizer M-110 y (FA Microfluidics; 1000 bar, 60 min, *Figure 5*). The method consists of a solely mechanical treatment that separates the fibrils under high pressure and therefore applies shearing-stress to the fibre axis.

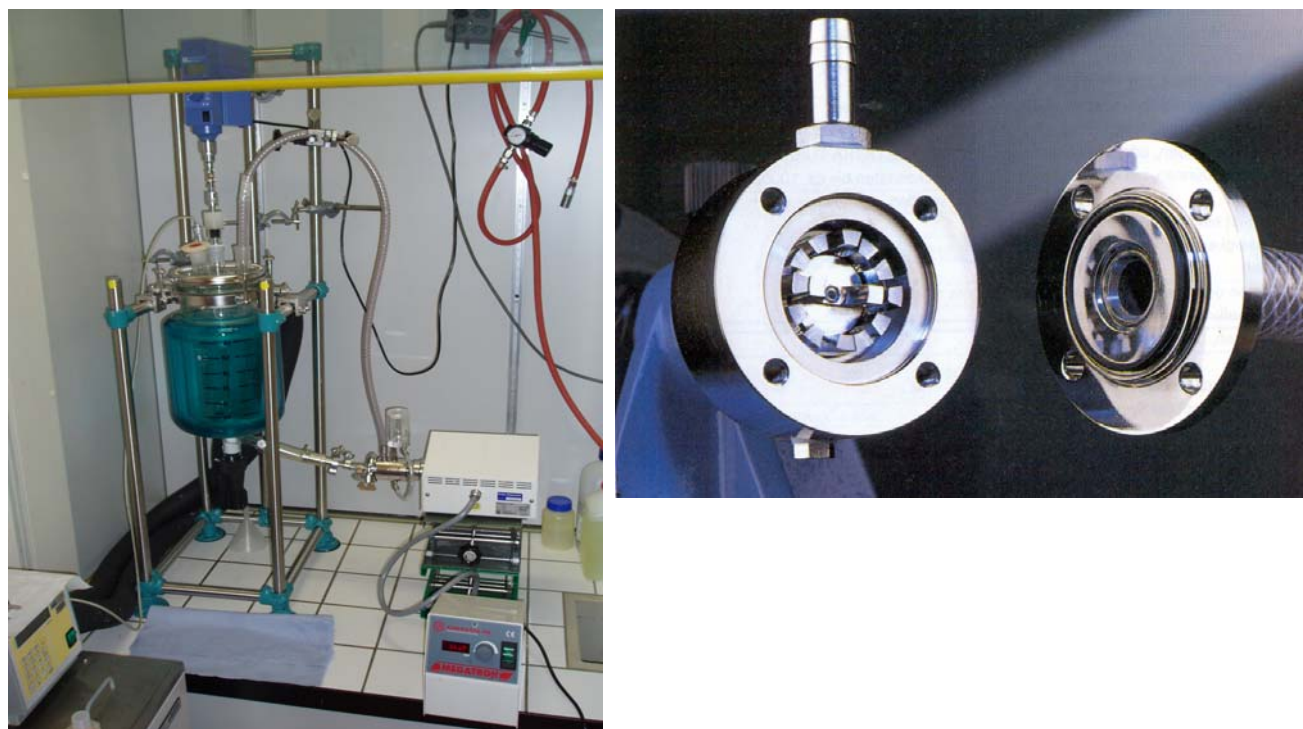


*Fig 4.: Inline dispersing system with an integrated ultra-turrax (FA Kinematica AG, Megatron MT 300)*



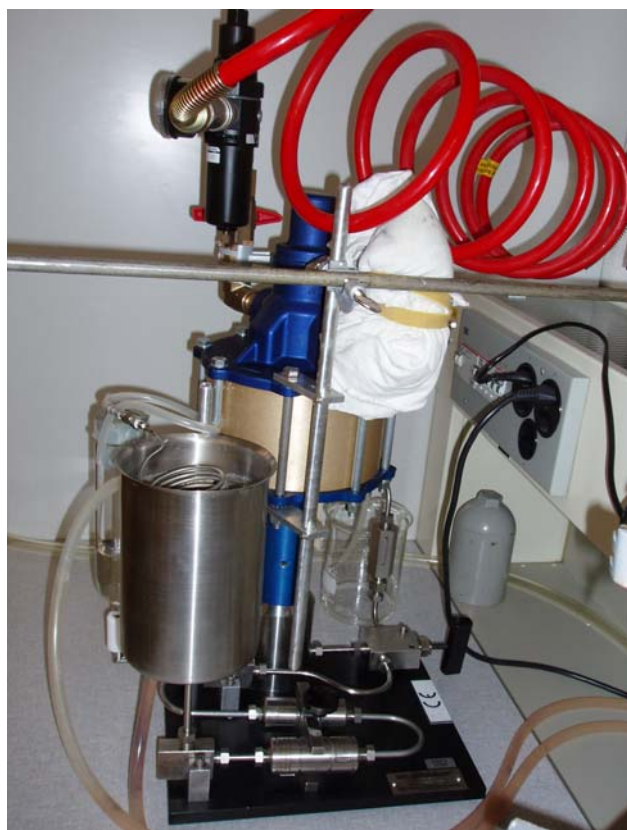


Fig. 5: High Pressure homogeniser (FA Microfluidics)

*Pathway 2, chemical/mechanical separation (**Paper D**):*

1. Oven dried pulp was weighed in a solution of sulphuric acid (10 wt%) and stirred at 60°C for 16 hours. The obtained suspension was centrifugated (5000 rpm) and washed several times in deionised water. Afterwards the solution was neutralised with sodium hydroxide (0.1 N).
2. Further disintegration of the cellulose fibril bundles was obtained by using the same homogenisation step as described in pathway 1 (3).

**FE–SEM characterisation of fibrils**

For the preparation of samples for Field Emission Scanning Electron Microscopy (DB235S-FEG and JEOL 6300F), glimmer plates were fixed with a conducting carbon on specimen holder. A drop of a diluted fibril/water suspension (1:20) was put on the glimmer plates. The samples were air-dried and the remaining fibrils were sputtered with a platinum layer of about 5 nm (BALTEC MED 020 coating system). The images were taken with accelerating voltages between 5 and 18 kV (**Paper D**).

---

### TEM characterisation of fibrils

For investigations of isolated fibrils uncoated 300 mesh copper grids were drawn through the fibril suspension. The stuck fibrils were stained with 1 wt% uranyl acetate and examined with a Philips CM200 transmission electron microscope at an accelerating voltage of 120 kV (**Paper D**).

### Determination of the Degree of Polymerisation (DP)

The DP was determined to get information about the degradation of the amorphous domains after mechanical or chemical/mechanical disintegration of the cellulose.

The wood pulp as reference material and the obtained fibrils (see above, pathway 1 and 2) were dried for 16 hours at a temperature of 105 °C. A defined ratio of cellulose was solved in acetone. From the pure solvents and also from the testing solutions, the running time through a marked distance of a viscosimeter was determined. The viscosity number as well as the degree of polymerisation (DP) of the cellulose was then calculated by the obtained running times and the defined cellulose portion (Anonymous 1981) (**Paper D**).

### 2.2.2 Production of cellulose nanocomposites

The intention was to evaluate the reinforcing potential of the cellulose fibrils. For this purpose two compatible water soluble model polymers, polyvinyl alcohol (PVA, FA Aldrich, Mw= 85000-146000 g/mol) and low viscosity hydroxypropyl cellulose (HPC, FA Aqualon, Mw= 80000 g/mol) were chosen.

The polymers were solved in the aqueous fibril suspensions with different solid contents (1, 5, 10 and 20 wt%) at a temperature of 60 °C. The obtained suspensions were casted in silicone forms (*Figure 6*) and dried at standardised conditions (23 °C/50 % RH) for seven days (solution casting method). Additionally, films out of pure cellulose fibril suspensions and pure HPC and PVA were also prepared (**Paper D**).

### 2.2.3 Mechanical characterisation of cellulose nanocomposites

#### Tensile Tests

Tensile specimens were stamped out of the casted films according to EN ISO 527-4, Anonymous (1997) (*Figure 7*). Tensile tests were then conducted using a Zwick Z010 universal testing machine with a 200 N load cell. The tests were carried out at 20 °C/65 % RH with a loading speed of 50 mm/min. The tensile strength as well as the MOE of the samples was calculated.



Fig. 6: Silicone form for the casting of fibril suspensions

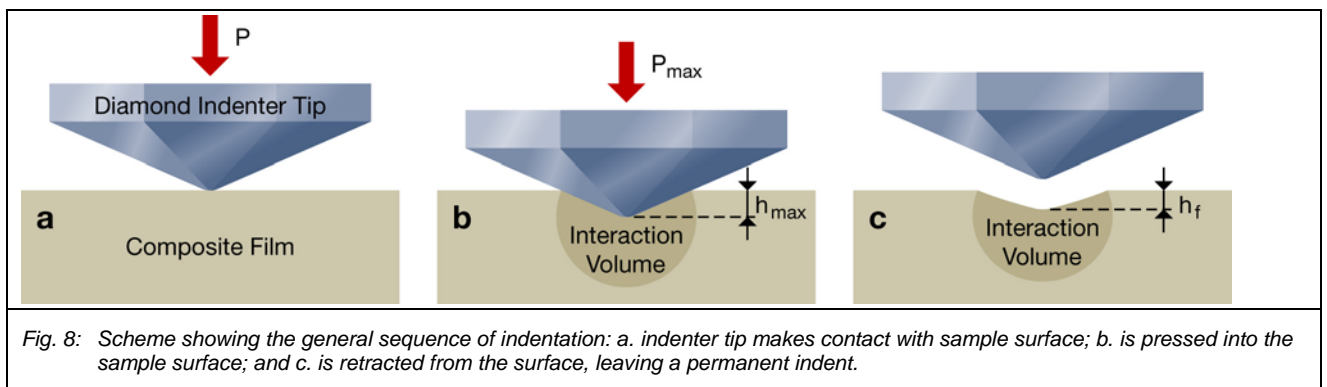


Fig. 7: Tensile specimens stamped out of the casted films

## Nanoindentation

One reason for the performance of nanoindentation experiments was the fact that the elongation of the composite films was only determined from the longitudinal motion of the testing machine. Therefore, it was assumed that the numeric MOE values calculated from the tensile tests may be underestimated.

In the nanoindentation experiments a diamond indentation body was inserted into the specimen. The applied normal load  $P$  and the displacement into the surface  $h$  were continuously measured during loading and unloading (Fischer-Cripps 2002). The indentation modulus ( $E_{\text{indent}}$ ) was calculated from the unloading part of the curve as the unloading is a purely elastic recovery process. The full procedure is described by Oliver and Pharr (2004) as well as in more detail in **Paper E**. Figure 8 is showing the general sequence of indentation.



### 2.2.4 Morphological characterisation of cellulose nanocomposites

The reason for the morphological characterisation of the cellulose composites was the analysis of the fibril alignment and the assumption of network formation in reinforced HPC films.

---

### TEM characterisation of composite films

A small extract (2x2 mm<sup>2</sup>) of the HPC-composite containing 20 wt% fibrils was embedded in polymethylmethacrylate (PMMA) resin. Ultra thin sections (approx. 60 nm thick) of the transverse film surfaces were sectioned using an ultramicrotome fitted with a diamond knife. The sections were mounted on Formvar coated grids and examined with a Philips CM200 transmission electron microscope at an accelerating voltage of 120 kV (**Paper E**).

### Evaluation of TEM images

The Image Processing Tool Kit 5.0, Adobe Photoshop was used for the evaluation of the interspace mesh areas of the cellulose fibril networks imaged by TEM.

### AFM characterisation of composite films

Small pieces (5x5 mm<sup>2</sup>) of the HPC composite films of all fibril portions were glued (superglue, Turbo Klebstofftechnik GmbH, Bazenheid, CH) onto aluminium sample holders and examined with a NanoScope IVa Dimension™ 3100 AFM using Tapping Mode™. Images were taken in height mode, where the deflection of the cantilever is directly used to measure the z position, and in phase mode, where the phase shift of the cantilever is used to determine differences in material constitution.

## 3 Results and Discussion

### 3.1 Wood cell wall structure

#### 3.1.1 Fractured softwood tracheids and hardwood fibres

On transverse-fracture surfaces, the thick secondary 2 (S2) wall layer of softwood tracheids (also in compression wood) and hardwood fibres exhibited predominantly an orientation of cellulose fibril agglomerations perpendicular to the compound middle lamella (CML) (i.e. radial orientation relative to the longitudinal cell axis). The fibril agglomerations had diameters between approximately 20 and 100 nm. In contrast, the S2 and G-layers of tension wood fibres revealed randomly arranged cell wall components without any kind of preferential orientation on transverse cross sections (**Book Article A**).

The origin of the imaged radial structures in the cell wall is explained by a higher packing density and stronger adhesion of fibrils in the radial direction compared to the circumferential one. However, many researchers provide evidence that the S2 consists of concentric lamellae. Thus, it is also supposed that radial and concentric structures may coexist in cell walls.

Another possibility is that the tensile fracture conditions themselves encourage a distinct radial crack propagation in the S2 layer (Fahlén and Salmén 2002; Zimmermann and Sell 1997). Radial lamellation may

be caused by the fracture process itself by a lateral contraction due to tension-strain perpendicular to the cell axis.

However, radial structures within the S2 perpendicular to the other cell wall layers have also been found in independent investigations using different methods. For instance, TEM investigations (Pöhler 1995; Singh et al. 1998) and studies on bio deterioration of cell walls of soft- and hardwoods with fungi (Larsen et al. 1995; Schwarze and Engels 1998; Schwarze and Fink 1999) indicate a radial arrangement of cell wall constituents.

As radial arrangements have never been observed in unaffected or normal wood it is conceivable that external impacts lead to re-formations of the cell wall constituents as recently postulated by Keckes et al. (2003). Independent of the genuine cell wall structure as well as the origin of radial structures on fracture surfaces of softwood tracheids or hardwood fibres, the functional advantages of such structures are obvious (Booker and Sell 1998). The bending stiffness and thus the buckling resistance under longitudinal compressive load may be markedly higher in cell walls where a radial arrangement of structural components is induced resulting in transverse reinforcements.

### 3.1.2 Fungi treated hardwood fibres

Transverse sections of the S2 of partially delignified hardwood fibre and vessel cell walls (sycamore, small-leaved lime, beech) exhibited radial degradation patterns of the fibril/matrix structure within the S2 layer. These structures resemble fragmentation patterns found in the S2 of sound softwood tracheid or hardwood fibre cell walls (**Book Article A**). Similar to sound wood, the partially delignified samples also showed concentric (tangential) structural features within the S2 layer, which were however, less distinct than the radial structures (*Figure 9*).

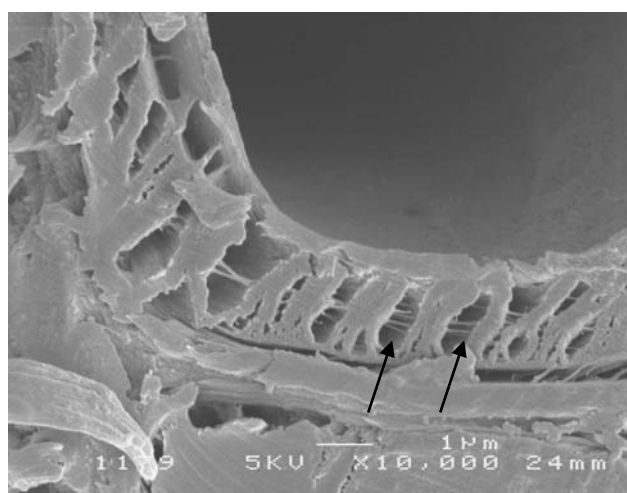


Fig. 9: FE-SEM micrograph: Transverse section of a fibre cell wall of sycamore artificially inoculated with *Flammulina velutipes*. In addition to radial structures, the S2 layer shows also concentrically oriented elements (arrows).

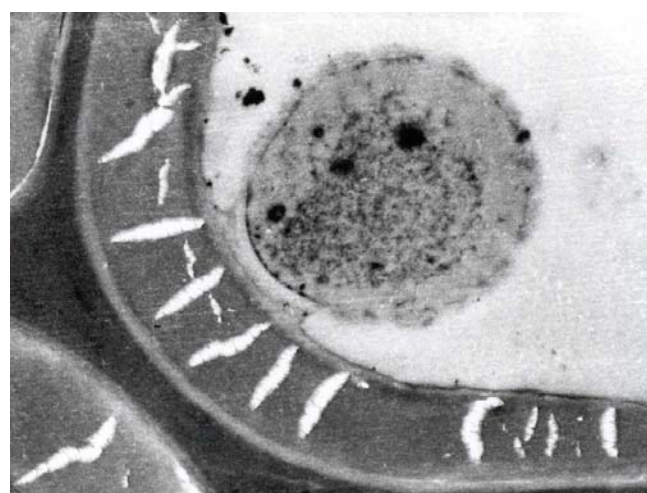


Fig. 10: TEM image out of a study published by Schwarze and Fink 1999: At an early stage of fungal degradation radial and concentric clefts are visible.

---

This result corresponds with findings of Schwarze and Fink (1999). The authors published a light microscopic and TEM study, revealing characteristic radial and concentric clefts in transverse sections of Norway spruce secondary walls during early stages of decay by the white rot fungus *Stereum sanguinolentum* (Figure 10).

However, it is unclear and should be investigated in further research studies, whether decay fungi elucidate an underlying (radial or lamellar) structure or if the radial structures are induced by the penetration directions of low molecular weight substances or enzymes secreted by hyphae.

### 3.1.3 Chemically treated spruce tracheids

Chemical treatment of spruce tracheids was associated with changes in the fragmentation of the S2 wall layer (**Paper C**). Swelling of the cell wall and a slight reduction in hemicelluloses (in this case especially glucomannan) after treatment with NaOH or KOH led to the disappearance of radial structures and resulted in a disordered fragmentation. For all alkaline treatments in different concentrations no lattice conversion of cellulose (transformation of parallel cellulose I to antiparallel cellulose II) was observed. The X-ray diffraction patterns for all alkali treated samples were typical for cellulose I (Borysiak and Garbarczyk 2003; Mansikkamäki et al. 2005). Thus, mercerisation and therefore changes in the lattice structure of cellulose are not the reason for the observed re-arrangement of cell wall constituents.

Substantial degradation of hemicelluloses and lignin after treatment with acetic acid and nitric acid or sodium sulphite and sodium hydroxide, respectively, was linked to increasing formation of distinct lamellar arrangements (concentric rings parallel to each other) within the S2. The increasing loss of hemicelluloses and lignin resulted therefore in distinct changes in the fragmentation patterns of the cell walls.

Simultaneously with the loss of binding components and the changes in fragmentation, the strength and stiffness of the samples decreased. Thus, even a slight change in carbohydrate composition (e.g. 2 % reduction of mannose) resulted in strength and stiffness losses. A distinct degradation of all hemicelluloses and lignin (e.g. reduction of unhydrolyzed residue of about 18 %) caused sample deformations as well as a sharp decline in MOE and bending strength.

The possible interactions between cellulose fibril aggregates and matrix material are discussed in **Paper C**. Especially the hemicellulose glucomannan, known to be closely associated with the cellulose fibril agglomerates (Salmén and Olsson 1998), is supposed to play a decisive role for fracture mechanics and the assembly of the cell wall constituents. It is concluded that even slight changes in cell wall constitution influence the interactions of the chemical cell wall components and thus fracture mechanics as well as ultrastructural appearance of wood cell walls. However, within this study it was not possible to derive the initial arrangement of the cell wall components.

### 3.1.4 Embedded and polished spruce tracheids

The sample topography of the embedded and polished spruce samples showed height differences below one micrometer, suitable for high resolution AFM phase contrast imaging. All AFM phase images of the thick



S2 cell wall layer of latewood (shown in **Paper B**) and earlywood tracheid cross sections (compare *Figs. 11 and 12*) obtained from embedded and polished samples showed randomly distributed cell wall components without any kind of preferential orientation. This is also true for the samples which were oven dried at 102 °C prior to embedding as well as for the samples polished only in one direction. AFM images obtained from microtomed sections showed alignments of the structural components in the S2 layer of the tracheid cell walls, they were often preferentially orientated in the cutting direction.

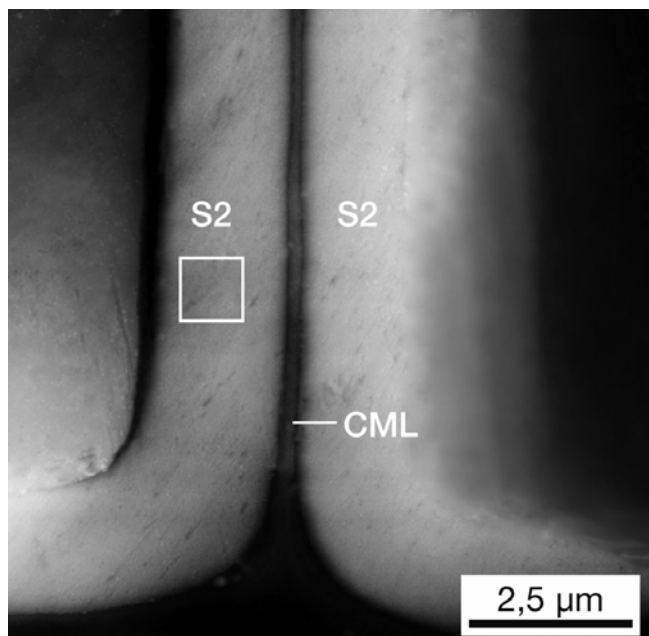


*Fig. 11: AFM height image of a transverse section of a non-dried earlywood spruce tracheid. The compound middle lamella (CML) and the thick secondary 2 wall layers (S2) are clearly discernable.*

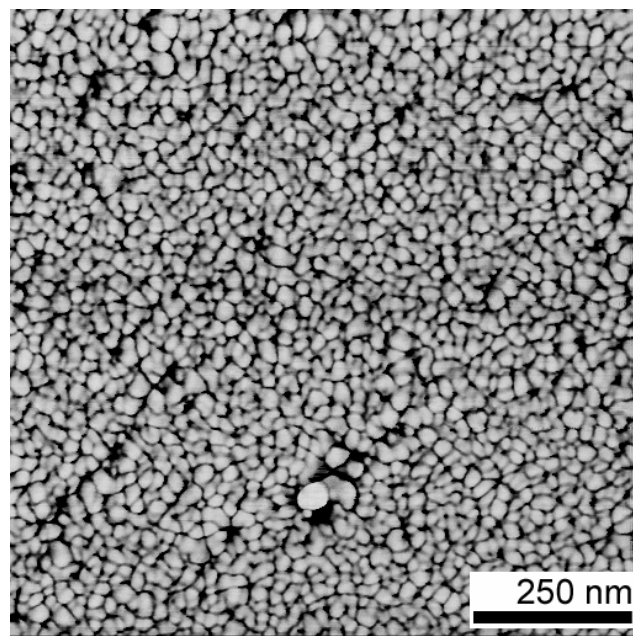


*Fig. 12: AFM phase image of a part of the thick S2 wall layer highlighted in Figure 11. Lighter areas consist of cellulose fibril aggregates, darker areas are considered to be matrix material. The image shows a random distribution of cellulose fibril aggregates and matrix material with no preferential orientation.*

The studies (3.1.1-3.1.4) show that high quality images can be obtained with different sample preparation and high resolution microscopic techniques resulting in a lamellar, radial or random distribution of cell wall components. This is also obvious from the literature: Many TEM micrographs of ultra thin sections of embedded spruce or pine tracheid cell walls showed that the S2 consists of concentric helical lamellae with small, but slightly varying inclinations (5 ° to 30 °) of the cellulose fibrils to the cell axis, e.g., Daniel and Nilsson (1984), Kerr and Goring (1975) and Ruel et al. (1978). Similar results were obtained by tapping mode AFM by Fahlén and Salmén (2002) and (2003). They embedded freeze-dried spruce samples in epoxy resin and cut 0.5 micrometer thick cross sections using a rotary microtome. The micrographs showed concentric lamellae inside the S2 layer consisting of individual cellulose fibril aggregates.

In contrast, radial arrangements of the cellulose fibril/matrix structure (perpendicular to the compound middle lamella) were found by SEM and light microscopy in decayed wood (Larsen et al. 1995; Schwarze and Engels 1998), respectively and by SEM on fractured (Sell and Zimmermann 1993) transverse surfaces of Norway spruce.

Similar to the presented AFM results, disordered arrangements have been reported by Donaldson (2001) who compared high resolution TEM micrographs with model calculations. For the latter, he assumed that the

---

cellulose fibrils are randomly arranged in weakly defined clusters. More recently Donaldson and Frankland (2004) reported a random crystal cavity formation within the S2 of iodine stained wood. They assumed that this appears to be an indication for the underlying random nature of the cell wall nanostructure.

It has been intensively discussed whether these different ultrastructural appearances observed in the past and the random arrangement of cell wall constituents detected by the AFM investigations might be influenced by the applied sample processing steps as drying, embedding, preparation of thin sections, polishing or fracturing (compare paragraph 4 in **Paper B**).

In our studies we demonstrated that the observed random texture of embedded and polished cell wall transverse sections does not depend on high shrinkage stresses caused by severe drying and not on directional polishing. We therefore propose that the described embedding and polishing process should be used as an alternative sample preparation strategy. On the other hand, we showed that microtoming does cause preferential orientations of the structural components along the cutting direction, especially in very thin sections. This leads to the conclusion that the observed texture without any kind of preferential orientation merely reflects the underlying random nature of the cell wall nanostructure.

## 3.2 Cellulose fibrils

### 3.2.1 Morphology of separated cellulose fibrils

Mechanical disintegration of pulp fibres resulted in fibril structures with diameters between 20 and 100 nm and estimated lengths of several tens of micrometers. Due to the high density of hydroxyl groups at their surfaces (Fengel and Wegener 1989), the fibrils strongly interacted and formed networks. Thus, it was not possible to determine the exact lengths of the fibrils. Chemical breakdown with sulphuric acid combined with mechanical homogenisation resulted in even finer fibril structures with diameters below 50 nanometers. The fibrils became shorter but their lengths were still in the range of micrometers (**Paper D**). The decomposition of cellulose by the two disintegration methods could also be demonstrated by the degree of polymerisation (DP). After mechanical isolation of cellulose fibrils the DP decreased by about 50 %. Due to a stronger degradation of amorphous domains in cellulose, the chemical disintegration with sulphuric acid led to a stronger drop of the DP of about 80 %.

The discussion part in **Paper D** compares different methods used for the separation of cellulose fibrils from organic fibres. Shearing stresses to the longitudinal fibre axis (in our case caused by a homogenisation process under high pressure, up to 1000 bar), the use of acid and its concentration, the disintegration temperature and time are the influencing parameters for the resulting fibril dimensions. Network formation as well as the stability of such networks has been proposed to be of great importance for high reinforcement efficiency (Dufresne et al. 1997; Hajji et al. 1996; Helbert et al. 1996) (compare also 3.2.3).



---

### 3.2.2 Mechanical properties of cellulose nanocomposites

#### Tensile Tests

The highest reinforcing effect was found for the HPC-composites with solely mechanically isolated fibrils. Even though the fibrils were orientated at random in the matrix material, the Modulus of Elasticity (MOE) increased threefold (fibril content 20 wt%) compared to the unfilled polymer. The tensile strength even showed a fivefold increase (**Paper D**).

Results of different studies where cellulose microcrystals, whiskers or cellulose fibrils were successfully used for the reinforcement of hydrophilic or hydrophobic matrices have been compared (**Paper D**). Frequently, the addition of fillers is accompanied by an increase in strength and stiffness at the expense of reduced elongation to rupture. Wu et al. (2002) synthesized a polyurethane/cellulose nanocomposite and found next to an improvement of the mechanical properties an increase in the elongation to rupture. This is in accordance with our results: For HPC composites with a fibril loading of 5 wt% the elongation to rupture increased fivefold. The good mechanical performance of cellulose nanocomposites and particularly the high elongation to rupture could benefit from network formations (found in **Paper E**) as well as an interfacial coupling or crosslinking between cellulose and polymer matrix. The highly extended surface area of networked fibrils generates an increased bond density resulting in a crack delay mechanism. As a consequence of the nano-scaled dimensions of the fibrils, fracture sites will be smaller and more widely distributed in the material volume. The failure of the nanostructured material is therefore delayed and the strength is increased (Nakagaito and Yano 2006).

#### Nanoindentation

Nanoindentation experiments have been carried out for HPC with mechanically isolated cellulose fibrils in different concentrations as these composites showed the best performance in the tensile tests (**Paper E**). Generally, the MOE as well as the hardness increased with increasing filling threshold. However, the samples showed two-threefold higher MOE values when compared with those obtained in tensile tests.

The apparent differences in the deformation behaviour between tensile (tensile tests) and compressive (nanoindentation) loading may be explained by the fact that tensile and indentation tests do not probe the same material volumes and regions. In fact, tensile tests analyse a large volume of material, which includes defects, whereas in nanoindentation the deformation zone is localised to a volume of a few hundred micrometer. Another important factor could be the lower strain rate during the tensile tests, in our case  $0.008 \text{ sec}^{-1}$ , compared with much higher strain rates in the nanoindentation experiments. Here, the strain rate decreased from  $2.25 \text{ sec}^{-1}$  at the beginning of the loading cycle to  $0.03 \text{ sec}^{-1}$  when reaching its maximum load. Wood e.g. shows an increased stiffness with high strain rates. Finally, the numeric values calculated from conventional tensile testing might be underestimated as the elongation of the samples was only determined from the longitudinal motion of the testing machine. It is reasonable to assume that due to the shift of the tensile testing machine, the measured strain was too high for all composite films and therefore the calculated MOE values were too low.

As most important result, both mechanical characterisation methods indicate that the optimal filling rate of HPC is between 10 wt% and 20 wt%.

---

### 3.2.3 Morphological properties of cellulose nanocomposites

A homogeneous fibril distribution as well as the formation of a rigid network resulting from hydrogen bonds between adjacent and overlapping fibrils was proposed to explain the improved mechanical behaviour of reinforced composites (Favier et al. 1995; Zimmermann et al. 2004). Actually, the TEM investigations on HPC composite films (**Paper E**) showed that the cellulose fibrils are homogeneously dispersed within the polymer matrix. During the drying step no fibril agglomerations occurred. To the knowledge of the author, it was possible for the first time to show network formation of cellulose fibrils within the polymer matrix. The determination of mesh size areas of these structures showed a high statistical spread with predominantly small mesh sizes. The TEM results were confirmed by AFM for the composites with a fibril loading of 10 wt% and 20 wt%. However, also structural irregularities and inhomogeneities on the surface of the HPC composite films with denser and more translucent areas were detected. Thus, the distribution of the cellulose fibrils was not equal all over the films. For the films with a low fibril content (e.g. 1 wt% or 5 wt%) no network formation at all could be detected. The fibril concentrations seemed to be too small for intensive interactions between single fibrils.

The results were compared with those obtained in other morphological studies dealing with the distribution of cellulose whiskers or fibrils in various polymer matrices, e.g. Dufresne and Vignon (1998) or Dufresne et al. (2000). Especially SEM and TEM were often used for the investigation of the surface morphology of fractured nanocomposite films.

In summary, the findings of the TEM and AFM characterisations can be related to the results obtained from tensile testing and nanoindentation. A significant increase in the mechanical properties was measured for the films with fibril contents of 10 wt% compared to the films with lower fibril portions. As a network formation could only be observed for composites with a fibril portion of at least 10 wt%, the existence of fibril networks appears to be of great importance for the mechanical properties of nanocomposites.

---

## 4 Conclusions

### 4.1 Wood cell wall structure

- Depending on the applied chemical or fungi pre-treatment and sample preparation method, transverse fracture surfaces, microtomed or polished sections of the S2 layer showed radially, concentrically or randomly arranged cell wall constituents.
- It is suggested that the dissimilar ultrastructural appearances in the presented studies but also in the discussed literature are induced during sample processing. The wood cell wall components arrange into various structural patterns under different stress conditions and preparation methods.
- Hemicelluloses and lignin are important components that are associated with fracture mechanics and the resulting fragmentation pattern. The fracture process and the resulting fragmentation pattern of the cell wall are very sensitive to alterations of the chemical composition of the wood cell wall (**Paper C**).
- The hemicellulose glucomannan seems to play a special role for the interactions between the cell wall constituents. Even small losses of glucomannan influence their interactions and therefore the ultrastructural appearance of transverse sections.
- The helical organisation of tracheid or fibre cell walls may also have an influence when re-orientations occur in the cell wall. As the cellulose fibrils are spirally arranged in the S2 layer, its deformation due to chemical treatment, microtoming or fracturing processes may have caused the different structural arrangements.
- This might especially be the case when preparing ultra thin sections. It was found that microtoming of thin sections (e.g. 0.5  $\mu\text{m}$ ) does cause preferential orientations depending on the cutting direction even in well embedded samples.
- In **Paper B** evidence was obtained that the disordered structure does not depend on drying and directional polishing. It can therefore be concluded that the observed texture reflects the underlying random nature of the cell wall nanostructure.
- Hence, the described polishing process is proposed as an alternative sample preparation strategy.

For future studies it is of foremost importance to investigate underlying interactions of cell wall components and to understand the mechanisms of re-orientations of cell wall constituents. It is also inalienable to think about single processing steps during sample preparation and to investigate the possible impacts for the ultrastructural appearance of the samples.

---

## 4.2 Cellulose fibrils

- Cellulose fibrils with diameters below 100 nm and lengths of several tens of micrometers were isolated out of sulphite pulp by mechanical dispersion and high pressure (1000 bar) homogenisation processes. The treatment resulted in nano-scaled fibril networks.
- Chemical breakdown with sulphuric acid combined with mechanical homogenisation resulted in even finer fibril structures with diameters below 50 nm. The fibrils were explicitly shorter but even in the micrometer range.
- The high Modulus of Elasticity (MOE) as well as the good aspect ratio of cellulose fibrils is an ideal requirement for a reinforcing application in polymers. Thus, fibril reinforced PVA and HPC showed – compared with the pure polymer – an up to threefold higher MOE and a fivefold higher tensile strength. Also the elongation to rupture increased distinctly. It is proposed that the good mechanical performance and particularly the high elongation to rupture benefits from the interfacial coupling or a cross linking between cellulose and polymer matrix. Due to the small dimensions of the fibrils, potential fracture sites in the composites will be smaller and more widely distributed in the material volume.
- An advantage of the nano-scale dimensions of the cellulose fibril networks is the possibility for the reinforcement of transparent polymers. The fibrils have much smaller dimensions than the wavelength of visible light. Thus, only a minimal light scattering occurs. Cellulose microfibrils can reinforce transparent polymers providing strength and stiffness without hindering the optical transparency.
- Nanoindentation is a suitable and easy to handle method for the mechanical characterisation of cellulose nanocomposites.
- TEM and AFM are very useful for the morphological characterisation of cellulose nanocomposites. To the knowledge of the author network formation within the polymer for fibril contents of at least 10 % was demonstrated here for the first time.
- The combination of tensile testing and/or nanoindentation, TEM and AFM allow to explain the mechanical behaviour of the HPC nanocomposites and to determine the optimal filling rate for cellulose fibrils.

### Challenge for the future and possible application areas

Cellulose fibrils could be very useful for an application in waterborne coatings or adhesives to improve properties like hardness, cohesive and adhesive strength, stiffness, application, exploitation or thermal creep. Application developments in electronics (LCD panels) where the transparency of cellulose nanocomposites could be used or in “nanopapers” for filter and membrane applications are also conceivable.

A challenge for future research activities is the combination of cellulose fibrils or whiskers with natural polymers. This will lead to the development of a new class of biodegradable and environmental friendly bio-nanocomposites with a potentially remarkable improvement of material properties when compared with the matrix polymers. Extensive applications in medicine, packaging or transportation are conceivable. Possible

---

raw materials for this new class of bio-nanocomposites are natural biopolymers like Poly lactic acid (PLA), Poly hydroxy butyrate (PHB), Poly hydroxy alcanoate (PHA) or cellulose esters.

The combination of cellulose fibrils with hydrophobic (bio)polymers will lead to some challenging problems that have to be solved. The crystalline cellulose chains of cellulose fibrils are connected to one another by hydrogen bonds which result in an agglomeration or entanglement of the fibrils. High energy is required to overcome this strong bonding. In order to reduce the interaction between hydroxyl groups, after mechanical or chemical/mechanical treatment, the cellulose fibril agglomerates obtained in our study were kept in water suspensions. Removal of this solvent would lead to a re-agglomeration of the fibrils. As water is the normally used carrier for the dispersion of cellulose fibrils, their application has been mostly restricted to water soluble polymers.

To expand the use of bio-based nanocomposites for high-value applications, it is necessary to reduce the re-agglomeration and entanglement of cellulose fibrils and to improve their dispersion in hydrophobic polymers. A future challenge is therefore the chemical modification of cellulose fibrils, e.g. by chemical surface modification (esterification and etherification reactions) or by a coating of cellulose fibrils. A promising approach would also be the use of water soluble carrier polymers like polyethylene oxide (PEO) or polyvinyl pyrrolidone (PVP).

In future, it is conceivable, that characteristics (e.g. fire resistance) of different matrices could be directly influenced by functionalising the hydroxyl groups of cellulose fibrils.

---

## 5 References

- Angles, M. N., and A. Dufresne. 2000. Plasticized starch/tunicin whiskers nanocomposites. 1. Structural analysis. *Macromolecules* 33 (22): 8344-8353.
- Anonymous. 1981. Cellulose in dilute solutions - Determination of limiting number - Part 2: Method in iron(III) sodium tartrate complex (EWNN<sub>mod NaCL</sub>) solution. ISO 5351/2.
- \_\_\_\_\_. 1997. Plastics - Determination of tensile properties - Part 4: Test conditions for isotropic and orthotropic fibre-reinforced plastic composites. EN 527-4.
- Berglund, L. 2004. Cellulose based nanocomposites. In Mohanty, A. K., M. Misra and L. T. Drzal. *Natural fibers, biopolymers, and biocomposites*. CRC Press LLC. pp. 807-832.
- Boldizar, A., C. Klason, J. Kubat, P. Naslund, and P. Saha. 1987. Prehydrolyzed cellulose as reinforcing filler for thermoplastics. *International Journal of Polymer Materials* 11 (4): 229-262.
- Booker, R. E., and J. Sell. 1998. The nanostructure of the cell wall of softwoods and its functions in a living tree. *Holz als Roh- und Werkstoff* 56: 1-8.
- Borysiak, S., and J. Garbarczyk. 2003. Applying the WAXS method to estimate the supermolecular structure of cellulose fibres after mercerisation. *Fibres & Textiles in Eastern Europe* 11 (5): 104-106.
- Brändström, J. 2001. Micro- and ultrastructural aspects of Norway spruce tracheids: a review. *IAWA Journal* 22 (4): 333-353.
- Chanzy, H., B. Ernst, J.-Y. Cavaille, and V. Favier. 2000. Cellulose microfibril-reinforced polymers and their applications. United States Patent, Elf Atochem. S.A., France. 6103790.
- Coughlan, M. P. 1985. Cellulose hydrolysis - The potential, the problems and relevant research at galway. *Biochemical Society Transactions* 13 (2): 405-406.
- Daniel, G., and T. Nilsson 1984. Studies on the S2 layer of *Pinus sylvestris*. Department of Forest Products 154.
- Dinand, E., H. Chanzy, and M. R. Vignon. 1999. Suspensions of cellulose microfibrils from sugar beet pulp. *Food Hydrocolloids* 13 (3): 275-283.
- Donaldson, L., and A. Frankland. 2004. Ultrastructure of iodine treated wood. *Holzforschung* 58 (3): 219-225.
- Donaldson, L. A. 2001. A three-dimensional computer model of the tracheid cell wall as a tool for interpretation of wood cell wall ultrastructure. *IAWA Journal* 22 (3): 213-233.
- Dufresne, A., J. Y. Cavaille, and W. Helbert. 1997. Thermoplastic nanocomposites filled with wheat straw cellulose whiskers. 2. Effect of processing and modeling. *Polymer Composites* 18 (2): 198-210.
- Dufresne, A., D. Dupeyre, and M. R. Vignon. 2000. Cellulose microfibrils from potato tuber cells: Processing and characterization of starch-cellulose microfibril composites. *Journal of Applied Polymer Science* 76 (14): 2080-2092.
- Dufresne, A., and M. R. Vignon. 1998. Improvement of starch film performances using cellulose microfibrils. *Macromolecules* 31 (8): 2693-2696.

- 
- Fahlén, J., and L. Salmén. 2002. On the lamellar structure of the tracheid cell wall. *Plant Biology* 4 (3): 339-345.
- \_\_\_\_\_. 2003. Cross-sectional structure of the secondary wall of fibers as affected by processing. *Journal of Materials Science* 38: 119-126.
- Favier, V., H. Chanzy, and J. Y. Cavaille. 1995. Polymer nanocomposites reinforced by cellulose whiskers. *Macromolecules* 28 (18): 6365-6367.
- Fengel, D. 1970. Ultrastructural behavior of cell wall polysaccharides. In Page, D. H. *The physics and chemistry of wood pulp fibres*. Tappi 53 (3).
- Fengel, D., and G. Wegener 1989. *Wood - Chemistry, Ultrastructure, Reactions*. Walter de Gruyter, Berlin, New York. 613 pp.
- Fischer-Cripps, A. 2002. *Nanoindentation*. Springer, New York. pp. 224
- Frey-Wyssling, A. 1968. The ultrastructure of wood. *Wood Science and Technology* 2: 73-83.
- Hajji, P., J. Y. Cavaille, V. Favier, C. Gauthier, and G. Vigier. 1996. Tensile behavior of nanocomposites from latex and cellulose whiskers. *Polymer Composites* 17 (4): 612-619.
- Harada, H., and W. A. Coté 1985. *Structure of wood*. Academic Press, Orlando. pp. 1-42.
- Helbert, W., J. Y. Cavaille, and A. Dufresne. 1996. Thermoplastic nanocomposites filled with wheat straw cellulose whiskers .1. Processing and mechanical behavior. *Polymer Composites* 17 (4): 604-611.
- Herrick, F. W. 1984. Process for preparing microfibrillated cellulose. United States Patent. 4481077.
- Heux, L., E. Dinand, and M. R. Vignon. 1999. Structural aspects in ultrathin cellulose microfibrils followed by C-13 CP-MAS NMR. *Carbohydrate Polymers* 40 (2): 115-124.
- Heyn, A. N. J. 1977. The ultrastructure of wood pulp with special reference to the elementary fibril of cellulose. *Tappi* 60 (11): 159-161.
- Iversen, T., T. Larsson, M. Lindström, L. Wagberg, J. Ekstedt, L. Berglund, J. Laine, and M. Oesterberg 2005. Nanoforest - a nanotechnology roadmap for the forest products industry. *STFI-Packforsk* 48.
- Keckes, J., I. Burgert, K. Frühmann, M. Müller, K. Kölln, M. Hamilton, M. Burghammer, S. von Roth, S. Stanzl-Tschegg, and P. Fratzl. 2003. Cell-wall recovery after irreversible deformation of wood. *Nature Materials* 2: 810-812.
- Kerr, A. J., and D. A. I. Goring. 1975. Ultrastructural arrangement of the wood cell wall. *Cellulose Chemistry and Technology* 9: 563-573.
- Larsen, M. J., J. E. Winandy, and F. Green. 1995. A proposed model of the tracheid cell wall of Southern Yellow pine having an inherent radial structure in the S2 layer. *Material und Organismen* 29 (3): 197-210.
- Mansikkamäki, P., M. Lahtinen, and K. Rissanen. 2005. Structural changes of cellulose crystallites induced by mercerisation in different solvent systems, determined by powder X-ray diffraction method. *Cellulose* 12: 233-242.
- Mathew, A. P., A. Chakraborty, K. Oksman, and M. Sain. 2006. The structure and mechanical properties of cellulose nanocomposites prepared by twin screw extrusion. In Oksman, K. and M. Sain. *Cellulose*

- 
- Nanocomposites - Processing, Characterization and Properties. American Chemical Society, Washington, DC. pp.114-131.
- Michell, A. J. 1989. Wood cellulose-organic polymer composites. Composites Asia Pacific, Adelaide, Australia, Composites Institute of Australia. pp. 66-81.
- Moon, R. J., R. Frihart, and T. Wegner. 2006. Nanotechnology Applications in the Forest Products Industry. Forest Products Journal 56 (5): 4-10.
- Nair, K. G., and A. Dufresne. 2003. Crab shell chitin whisker reinforced natural rubber nanocomposites. 2. Mechanical behavior. Biomacromolecules 4 (3): 666-674.
- Nakagaito, A. N., and H. Yano. 2006. Nanocomposites based on cellulose microfibril. In Oksman, K. and M. Sain. Cellulose Nanocomposites - Processing, Characterisation and Properties. American Chemical Society, Washington, DC. pp. 151-168.
- Northolt, M. G., and H. de Vries. 1985. Angewandte Makromolekulare Chemie 133: 183.
- Oksman, K., and M. Sain 2006. Cellulose nanocomposites - processing, characterization and properties. American Chemical Society, Washington DC. pp. 256.
- Oliver, W. C., and G. M. Pharr. 2004. Measurement of hardness and elastic modulus by instrumented indentation: Advances in understanding and refinements to methodology. Journal of Materials Research 19 (1): 3-20.
- Pöhler, E. 1995. Chemische und mikroskopische Untersuchungen zum Delignifizierungsverlauf beim ASAM- und Kraftaufschluss. Diploma thesis. Wood Chemistry, Federal Research Centre for Forestry and Forest Products.
- Ruel, K. F., F. Barnoud, and D. A. I. Goring. 1978. Lamellation in the S2 layer of softwood tracheids as demonstrated by scanning transmission electron microscopy. Wood Science and Technology 12: 287-291.
- Salmén, L., and A. M. Olsson. 1998. Interaction between hemicelluloses, lignin and cellulose: Structure-property relationships. Journal of pulp and paper science 24 (3): 99-103.
- Schwarze, F. W. M. R., and J. Engels. 1998. Cavity formation and the exposure of peculiar structures in the secondary wall (S2) of tracheids and fibres by wood degrading basidiomycetes. Holzforschung 52 (2): 117-123.
- Schwarze, F. W. M. R., and S. Fink. 1999. Radial and concentric clefts in the secondary wall (S2) of Norway spruce tracheids during incipient stages of decay by *Stereum sanguinolentum* (Alb. & Schw.: Fr.). Material und Organismen 33 (1): 51-64.
- Sell, J., and T. Zimmermann. 1993. Radial fibril agglomerations of the S2 on transverse-fracture surfaces of tracheids of tension-loaded spruce and white fir. Holz als Roh- und Werkstoff 51: 384.
- \_\_\_\_\_. 1998. The fine structure of the cell wall of hardwoods on transverse- fracture surfaces. Holz als Roh- und Werkstoff 56 (5): 365-366.
- Singh, A. P., and G. Daniel. 2001. The S2 layer in the tracheid walls of *Picea abies* wood: Inhomogeneity in lignin distribution and cell wall microstructure. Holzforschung 55 (4): 373-378.



- 
- Singh, A. P., J. Sell, U. Schmitt, T. Zimmermann, and B. Dawson. 1998. Radial striation of the S2 layer in mild compression wood tracheids of *Pinus radiata*. *Holzforschung* 52: 563-566.
- Spurr, A. R. 1969. A low-viscosity epoxy resin embedding medium for Electron Microscopy. *Journal of Ultrastructure Research* 26 (1-2): 31 ff.
- Tashiro, K., and M. Kobayashi. 1991. Theoretical evaluation of 3-dimensional elastic-constants of native and regenerated celluloses - role of hydrogen-bonds. *Polymer* 32 (8): 1516-1530.
- Turbak, A. F., F. W. Snyder, and K. R. Sandberg. 1983. Microfibrillated cellulose, a new cellulose product: properties, uses and commercial potential. *Journal of Applied Polymer Science* 37: 815-827.
- Uremovic, A., T. Dokk Glawischnig, J. Schuseil, B. Saake, A. Borchmann, A. Herrmann, and J. Puls. 1994. Chromatographische Untersuchungen zur quantitativen Bestimmung der Holzzucker. *Holz als Roh- und Werkstoff* 52: 347-354.
- Wainwright, S. A., W. D. Biggs, J. D. Currey, and J. M. Gosline 1982. *Mechanical design in organisms*. Princeton University Press.
- Wardrop, A. B. 1964. The structure and formation of the cell wall in xylem. Academic Press, New York. pp. 87-134.
- Wu, Q., X. Liu, and L. A. Berglund 2002. Polymer nanocomposites based on cellulose. *Proceedings of the 23rd Riso International Symposium on Material Science: Sustainable Natural and Polymeric Composites - Science and Technology*, Riso National Laboratory, Roskilde, Denmark. pp. 107-113
- Zimmermann, T., E. Pöhler, and T. Geiger. 2004. Cellulose fibrils for polymer reinforcement. *Advanced Engineering Materials* 6 (9): 754-761.
- Zimmermann, T., and J. Sell. 1997. Das Feingefüge der Zellwand auf Querbruchflächen von längszugbeanspruchten Laubhölzern. *Forschungs- und Arbeitsberichte Holz* 115 (35): 1-32.
- Zimmermann, T., V. Thommen, P. Reimann, and H. J. Hug. 2006. Ultrastructural appearance of embedded and polished wood cell walls as revealed by Atomic Force Microscopy. *Journal of Structural Biology* 156: 363-369



## **5.1 Appendix**

### **Book Article A**



# **Field Emission SEM studies on softwood tracheids and hardwood fibres - A Review of Activities at the EMPA Wood Laboratory**

by

**Tanja Zimmermann and Jürgen Sell**  
**EMPA, Swiss Federal Laboratories for Materials Testing and Research,**  
**Wood Laboratory, Dübendorf, Switzerland**  
**Ueberlandstrasse 129, CH-8600 Dübendorf**

## **SUMMARY**

To learn more about the fine structure of the S2 wall layer, transverse fracture surfaces of tension-loaded softwoods, hardwoods and reaction wood were studied by high resolution FE-SEM. As the fracture process loosens the cell wall, its components become clearly visible. Softwood tracheids (also in compression wood) and hardwood fibres exhibited a predominantly radial orientation (i.e. perpendicular to the other layers) of the fibril/matrix structure of the S2 layer. Similar structures were found on cross-sections of various hardwoods degraded by white rot fungi. By contrast, no preferential orientation was discovered in the S2 or G layer of pronounced tension wood cells.

Such structures may be assumed to provide functional benefits to the strengthening tissue: the sandwich-like structure may enhance the buckling resistance of the tracheids and fibre cell walls, and thus the bending stiffness of the whole tree.

It is conceivable that the tension wood fibres of hardwood trees, subjected only to longitudinal tension, do not need compression stiffening which would explain the absence of transverse fibril agglomerations in this case.

In other studies, a poly laminated concentric arrangement of the cellulose/lignin- polyose matrix is postulated and clearly documented.

Given these findings, we concluded that concentric and radial arrangements do, in fact, co-exist in the S2 of softwood tracheids and hardwood fibres.

**Key words:** FE-SEM, fine structure, S2 layer, transverse fracture surfaces, softwood, hardwood, reaction wood, white rot fungi

## INTRODUCTION

The cell wall structure on the macro-, micro-, and nanoscale largely determines the properties of wood and the stability of the living tree. As yet, not all structural features are fully understood. In particular, the arrangement of cellulose fibrils and the lignin/polyose matrix in the individual cell wall layers of softwood tracheids and hardwood fibres is still under debate.

Since 1993, the EMPA Wood Laboratory has conducted a number of studies aimed at clarifying the relationship between the fine structure of wood cell walls and their function in a living tree.

Initial studies on transverse fracture surfaces of spruce tracheids used a high-resolution FE-SEM to investigate the influence of temperature, wood moisture content, and load duration on the fine structure of tension-fractured surfaces of bending-loaded samples (Zimmermann et al. 1994).

This clearly demonstrated the impact of loading conditions, especially load duration, on the tension strength and deformation of the microscopic fracture-surface of the cell tissue, and cell wall; brittle fractures in the cell wall were plainly distinguishable from ductile fractures. In some cases, the fractured surfaces resembled smooth cross-sections of cut wood (Figure 1). Heat and moisture increased the ductile character of fractured surfaces (Figure 2).

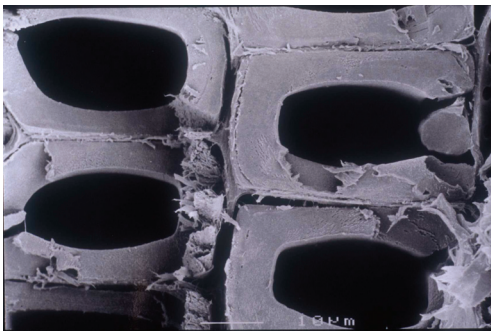


Fig. 1: FE-SEM micrograph: Transverse-fracture surface of latewood tracheids, subjected to impact bending at 20 °C/35 % RH. Extremely brittle fracture with clean surface of S2 layer; the fibril/matrix structure is not visible. Delaminations between S1 and S2.

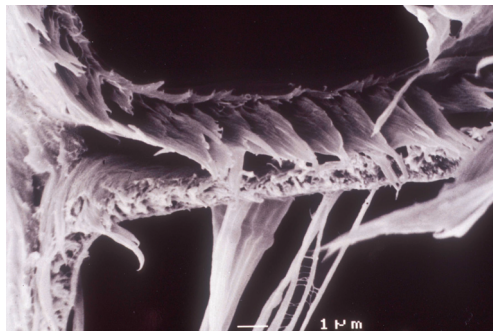


Fig. 2: FE-SEM micrograph: Transverse fracture surface of earlywood tracheids, subjected to long-term bending at 60 °C/95 % RH. Extremely ductile fracture with severe deformation of entire cell wall tissue.

The ductile fracture process clearly loosens the cell wall tissue and partly separates the different wood components (unlike the smooth cross-sections of microtome cut wood). We exploited this effect in studying the fine structure of the cell wall.

The results of various investigations before and after the start of COST E20, “Wood Fibre Cell wall Structure”, are presented below.

## MATERIAL AND METHODS

### **Fracturing**

The morphological fine structure of the cell wall of spruce (*Picea abies*), White fir (*Abies alba*), pine (*Pinus radiata*), beech (*Fagus sylvatica*), oak (*Quercus robur*, *Quercus petraea*), and, to a lesser extent, of other hardwood species was examined by FE-SEM.

3 point bending tests were performed to loosen the cell wall structure of previously climatised wood sticks and thus enable a microscopic differentiation of its elements on transverse-fracture surfaces.

Samples of about 5mm x 5mm were prepared from the outermost tension zones of the fracture surfaces. They were carefully dried for 12 hours in a vacuum oven at 40 °C and 0 torr, glued onto a specimen holder and sputtered with a platinum layer of about 10 nm. The samples were investigated with a Jeol 6300F microscope at an acceleration voltage of 5 kV and a working distance of 24 mm.

### **Exposure to white rot fungi and microtoming**

For comparison, two different white-rot fungi were selected using the following host-fungus combinations: sycamore (*Acer pseudoplatanus*) with *Flammulina velutipes*, beech (*Fagus sylvatica*) and small-leaved lime (*Tilia cordata*) with *Ganoderma applanatum*.

Wood blocks were obtained from the sapwood of living trees and inoculated in accordance with the procedures laid down by Schwarze and Fink (1999). The samples were fixed in Karnovskys fixative for 24 hours, then washed in a 0.05M phosphate buffer and post-fixed in 1% osmium tetroxide. They were then washed in the same buffer before dehydration in an ethanol series. After dehydration, the samples were embedded in LR White (methacrylate). After polymerisation, one surface was smoothed perpendicular to the fibre by cutting with a rotation microtome (diamond knife). The embedding material was then solved out by repeated washing in acetone (96%). A number of these samples were prepared for FE-SEM as described above.

## RESULTS AND DISCUSSION

### **Fine structure of softwood tracheids and hardwood cell walls**

On transverse-fracture surfaces, the by far thickest secondary layer (S2) of cell walls in spruce and White fir exhibits an orientation of fibril agglomerations perpendicular to the compound middle lamella (CML) (i.e. radial orientation relative to the longitudinal axis of the cell, Figure 3). These structures may stem from a higher packing density and stronger adhesion of the fibrils in the radial direction compared to the circumferential direction.

Concentric lamellae of the S2 fibrils (parallel to the CML), as described in many studies, were not found. As far as discernible by FE-SEM, the single fibrils or fibril bundles of the S2 are roughly between 20 and 100 nm in diameter. The tangential width of the fibril agglomerations lies between 0.1 and 1 µm. In the radial direction the fibril agglomerations cover a considerable portion of the S2 width (Figure 4). They frequently extend from the S1 to the S3. These results are described in detail in Sell and Zimmermann (1993 a and b).

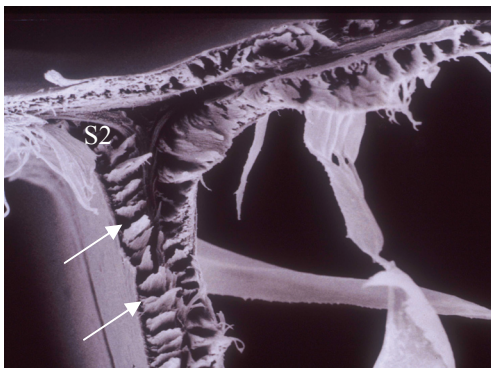


Fig. 3: FE-SEM micrograph: Transverse-fracture surface (tension zone) of earlywood tracheid cell walls of spruce, subjected to long-term bending at 20 °C/35 % RH. The ductile fracture exhibits distinct radial agglomerations of the cellulose fibril/matrix structure within the S2 (arrows). The cell wall seems to have a sandwich-like structure.

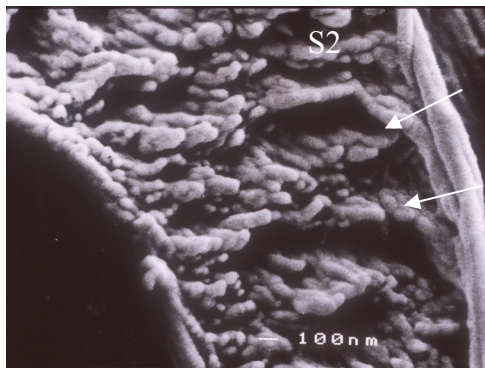


Fig. 4: FE-SEM micrograph: Transverse-fracture surface (tension zone) of earlywood tracheid cell wall of spruce, subjected to long-term bending at 20 °C/95 % RH. Radially agglomerated cellulose fibrils or fibril bundles (arrows) about 20 to 100 nm in diameter become visible at high magnifications.

As with softwood tracheids, distinct fibril/matrix agglomerations were observed in the S2 layer of the fibre cell walls of all hardwoods studied (Figures 5, 6). The agglomerations are mostly oriented in a perpendicular, or partly perpendicular direction to the CML and the S1 and S3-layers. Concentric (tangential) structures “(lamellae)” were also sporadically observed in the S2 layer. A few cell walls even exhibited mixed radial and tangential fibril orientations on transverse-fracture surfaces within a single S2-layer. However, only fibre cells (libriform and tracheid fibres) displayed the radial or partially radial structural arrangements within the S2, which were absent from parenchyma cells and vessels. These exhibited only a polylamellar (concentric) structure of the transverse-fracture surface of the entire cell wall (Figures 7, 8).

These findings on the structure of the S2 layer, which differ from previous studies published over the past decades, have been comprehensively discussed with regard to the possible influence of artefacts by Zimmermann and Sell (1997) and Sell and Zimmermann (1998). The tensile fracture conditions, in particular, could encourage a distinctly radial crack propagation in the S2 layer. Yet, the more or less pronounced radial orientation of fibril agglomerations and thus, implicitly, of the lignin matrix of the cell wall has since been confirmed by several independent investigations using various different methods. For instance, transmission electron microscopic investigations (Pöhler 1995; Singh et al. 1998) and decomposition studies on the cell wall of hardwoods with fungi (Larsen et al. 1995; Schwarze and Engels 1998; Schwarze and Fink 1999) have provided confirmation of a radial arrangement of lignin and/or cellulose in the S2 layer.



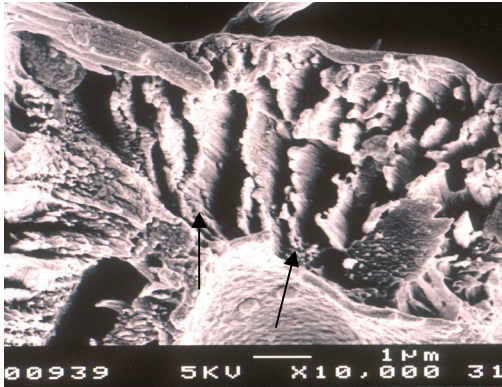


Fig. 5: Transverse-fracture surface (tension zone) of a beech libriform fibre, subjected to short-term static bending at 20 °C/85 % RH. Relatively severely deformed cell wall, with radial agglomerations of fibril/matrix structure (arrows) extending over whole S2 cross section.



Fig. 6: Transverse-fracture surface (tension zone) of oak fibres; subjected to impact bending at 20 °C/35 % RH. Distinct preferentially radial orientations of fibril/matrix structure within S2 (arrows); deposited extractives in cell lumen.

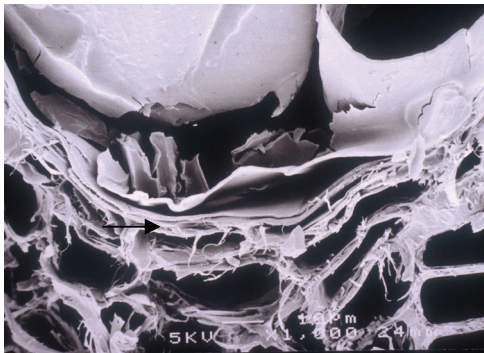


Fig. 7: Transverse-fracture surface of cell wall area of an earlywood vessel in chestnut; unlike fibres, no radial structures are visible. In fact, the cell wall seems to consist of numerous concentric lamellae (arrow).

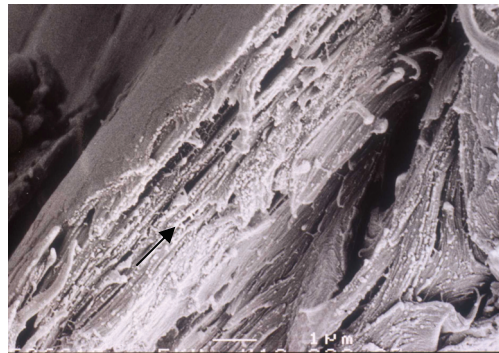


Fig. 8: Transverse-fracture surface of cell wall area of an earlywood vessel in oak. The cell wall seems to consist of numerous concentric lamellae (arrow).

### ***Fine structure of reaction wood***

The compression wood examined exhibits the fibril/matrix orientation of the thick S2 cell wall layer observed in normal wood with a markedly preferential orientation approximately transverse to the CML (Figure 9) (Zimmermann and Sell 2000). TEM observations by Singh et al. (1998) of ultra thin sections of samples taken from *Pinus radiata* revealed radial striations in the S2 layer with the same orientation as the radial structures seen with the FE-SEM (Figure 10).

While the S2 and G layers of beech fibres from mild tension wood exhibit transverse structures, sometimes in opposite directions, no preferential orientation is discernible of the cel-

lulose fibril/matrix structure of the S2 or G layer of pronounced tension wood cell walls (Figures 11, 12) (Zimmermann and Sell 2000).

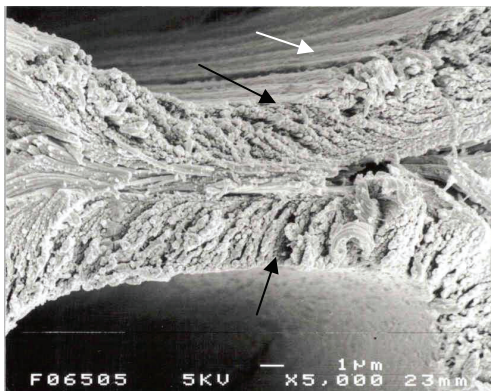


Fig. 9: Transverse-fracture surface (tension zone) of cell wall from tracheid of pine (*Pinus radiata*) mild compression wood. A preferential orientation of the cellulose fibrils rather perpendicular to the CML (arrows) is discernible. Indicatively, slight deep (radial) fissures are discernible transverse to the CML (white arrow).

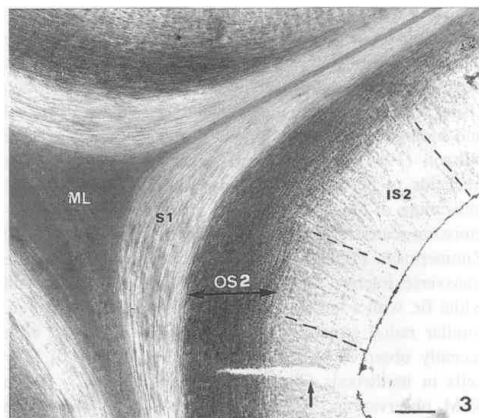


Fig. 10: Transverse section through corner region of mild compression wood tracheids. The secondary wall is differentiated into 3 morphological distinct regions, the S1, OS2 and IS2. The IS2 wall appears to be striated in a direction largely perpendicular to the plane of the middle lamella (ML) (stippled line). TEM micrograph, from Singh et al. (1998).

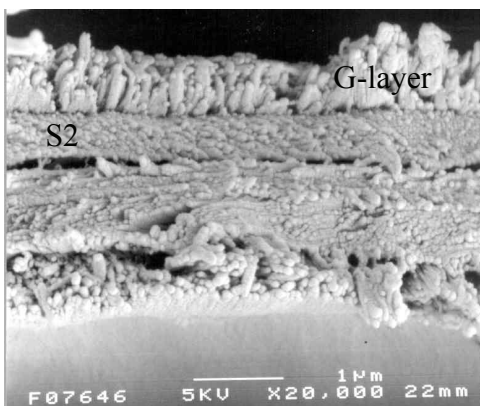


Fig. 11: Transverse-fracture surface (tension zone) of elm fibre cell walls. No preferential orientation of the cellulose fibrils in the S2 or G-layer is discernible.

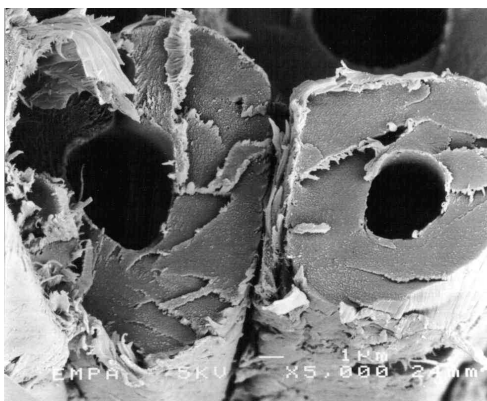


Fig. 12: Transverse-fracture surface (tension zone) of two beech fibre cells. The fracture of the thick G layer is so brittle that no fibril orientation is discernible

#### ***Fine structure of fungi-degraded wood***

Here, in contrast to the other investigations, *transverse sections* of hardwood cell walls (sycamore, small-leaved lime and common beech) degraded at an early stage by white rot fungi were used for investigation by FE-SEM. The structural features observed were com-

pared with the cell wall structure typically found on transverse-fracture surfaces of sound wood.

Transverse sections (TS) of partially delignified hardwood fibre and vessel cell walls exhibited characteristic structural features, also observed on the fracture surfaces of sound wood. This was particularly evident for the radial arrangement (i.e. perpendicular to the middle lamella) of the fibril/matrix structure within the S2 layer (Figure 13).

Like sound wood, the partially delignified samples also showed tangential (concentric) structural features within the S2, though these were less pronounced than the radial structures. The results match the findings of Schwarze and Fink (1999) who published a light microscopic and TEM study, showing characteristic radial and concentric clefts in transverse sections of Norway spruce secondary walls during the early stages of decay caused by the white rot fungus *Stereum sanguinolentum*.

During the incipient stages of lignin degradation, the greatest loss of cell wall substance was initially observed within the S2. While this layer often underwent extensive degradation, the S3 layer, and often the S1 and CML, appeared to remain more or less intact.

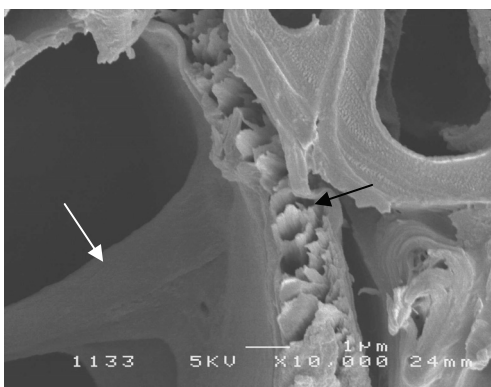


Fig. 13: TS of two adjacent sycamore fibres, artificially inoculated with *Flammulina velutipes*, at an early stage of delignification. A hypha is growing within the lumen on the S3 layer (white arrow). This layer shows no visible structural alterations, whereas the underlying S2 layer has been partially degraded. Preferential delignification of the S2 results in the exposure of fibril agglomerations, arranged perpendicular to the CML (black arrow).

### ***Discussion of controversial theories***

The literature describes the cell wall as an arrangement of lamellae with different thicknesses and different portions of their main chemical components. The helical orientation of the cellulose fibrils, or their inclination to the longitudinal cell axis, also varies between the different layers of the secondary wall: the thin S1 (adjacent to the CML), the thick S2, and the thin S3 (adjacent to the cell lumen). A review of the structure and formation of the cell wall is given by Wardrop (1964); Harada and Coté (1985) and Brändström (2001).

Given its obvious importance for the mechanical properties of wood, the fine structure of the thick S2 investigated in the presented studies is of particular interest. The different descriptions of this structure are not always consistent.

Studies by many researchers show evidence that the S2 consists of concentric helical lamellae with minor, though slightly varying inclinations ( $5^{\circ}$  to  $30^{\circ}$ ) to the cell axis, e.g. Kerr and Goring (1975); Ruel and Goring (1978); Daniel and Nilsson (1984). The ultrastructural model proposed by Kerr and Goring (1975) for the arrangement of lignin, cellulose and hemicellulose in the S2-layer of the wood cell wall is shown in Figure 14.



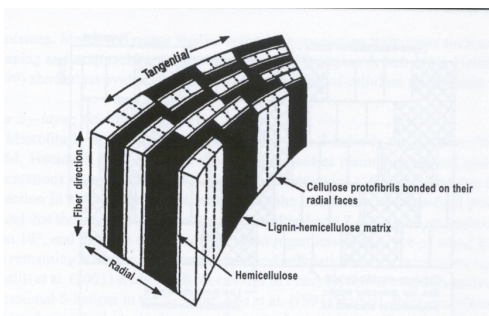


Fig. 14: Cell wall model from Kerr and Goring (1975)

Our studies revealed similar radial arrangements (i.e. perpendicular to the other layers) of the fibril/matrix structure on transverse-fracture surfaces of softwood tracheids and hardwood fibres as well as on cross-sections of fungi degraded hardwood fibre cell walls. The results are described in detail in this paper and are largely incorporated in Sell and Zimmermann (1993); Sell (1994) and Sell and Zimmermann (1998). They led to a modification of a cell wall model proposed by Côté (in Core et al. 1979), Figure 15.

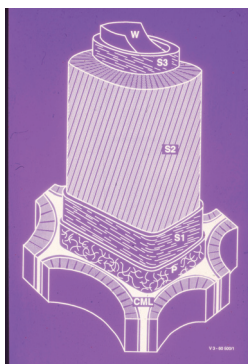


Fig. 15: Cell wall model after Côté (1965) from Core et al. (1979) showing the different cell wall layers. The model is modified by (heavily schematic) radial agglomerations of fibrils on the cross-section of the S2. Dimensions and character of the (white) intermediate zones are not identified.

The origin of these structures has been explained by a higher packing density and stronger adhesion of the fibrils in the transverse direction compared to the circumferential direction (Sell and Zimmermann 1998). Other authors have confirmed some kind of radial lamellation in the S2, e.g. Larsen et al. (1995); Pöhler (1995); Schwarze and Engels (1998); Singh et al. (1998); Schwarze and Fink (1999) and Singh and Daniel (2001). It seems that both structures do coexist.

Until now, however, it could not be excluded that the radial as well as circumferential structures appear to be depended on preparation techniques used to study the cell wall fine structure (Donaldson 2001, Fahlén and Salmén 2003). Consequently, confirmation of the results by other methods remains necessary.

In an FE-SEM and TEM investigation by Zimmermann (2003), spruce cell walls were modified by a gradual dissolution of chemical components, mainly polyoses and lignin. This study revealed both radial and lamellar structural arrangements of the cellulose fibril/matrix structure. Both weathering and a slight reduction in polyoses resulted in a disordered, a distinct degradation of polyoses and/or lignin in lamellar arrangements (i.e. parallel to the other layers) of the fibril/matrix structure. The results of the study provide further evidence for the coexistence of radial and lamellar structural arrangements in wood cell wall layers.

### ***Biomechanical aspects***

Our interest focused not on the fine structure of the wood cell wall itself, but on the functional benefits of such structures in a living tree.

The proposed radial fibril assembly within the S2 or, in other words, fibril agglomerations perpendicular to the “cross-banding faces” S1 and S3, is likely to enhance the mechanical properties of the entire tree. The bending stiffness and thus the buckling resistance under axial compression of such a sandwich-like cell wall could be significantly higher than for a cell wall consisting of concentric lamellae. The bending stiffness of the whole stem to wind pressure or the forces of gravity would thus increase. This is particularly important for wood with moisture contents (MC) close, or above the fibre saturation point where its strength is significantly reduced. Such a situation occurs in the compression zone of a living tree under bending load which lies in the outer sapwood where the MC far exceeds the saturation point. A model test demonstrated the benefits to the stiffness of the wood cell wall of “standing” structural elements in the S2 layer (1994).

This topic is discussed by Booker and Sell (1998) and Sell (1994). They review findings on the nanostructure of the cell wall of softwoods and discuss the probable relationship between microfibril orientation in the secondary cell wall layers and potential threats to the survival of trees such as excessive vibration and crack propagation within the stem.

## **CONCLUSIONS**

The main purpose of this review is to outline research at the EMPA Wood Laboratory into the fine structure of wood cell walls.

The various studies on softwoods and hardwoods, revealed cellulose fibril/matrix arrangements in the S2 layer perpendicular to the other cell wall layers. These structures may stem from a higher packing density and stronger adhesion of the fibrils in the radial direction compared to the circumferential direction. This suggests higher bond strength in the radial than in the tangential direction between fibril agglomerations in the S2. On transverse-fracture surfaces (in particular with ductile fractures), the structure of the entire secondary wall thus exhibits a sandwich-like form. It consists of the S1 and S3 layers acting as faces and the S2 as core, with fibril agglomerations perpendicular to the face layers. This arrangement might enhance the bending stiffness and buckling resistance of the cell wall and the axial compression strength of the wood in the standing tree.

Many other studies postulate and clearly document a poly laminated concentric (i.e. circumferential) arrangement of the cell wall components. As yet, it has not been conclusively explained why various microscopic, chemical and other methods used in numerous former investigations have revealed concentric and/or radial arrangements of the cellulose fibril/matrix structure of the S2 in the cell wall of softwood tracheids and hardwood fibres. It is therefore, quite plausible that these structures coexist for good ontogenetic, physiological, and mechanical reasons.

The findings from investigations into reaction wood suggest that the cell walls of normal wood, and especially of compression wood, are stiffened against longitudinal compression and buckling by the observed compressed arrangement of S2 layer fibrils perpendicular to the CML.

By contrast, this compression stiffening of the cell walls might not be required in the tension wood fibres of hardwood trees subjected only to longitudinal tension which would explain the absence of radial fibril agglomerations in this case.

Further studies are needed to identify which chemical component might be responsible for a stronger adhesion between cellulose fibrils in one direction or the other.

The aim is to develop a convincing cell wall model that reconciles the different investigations showing concentric and/or radial (perpendicular to the other cell wall layers) arrangements of the cellulose fibril/lignin-polyoses matrix structure of the S2 in softwood and hardwood cell walls.

## REFERENCES

- Booker, R. E., J. Sell. 1998. The nanostructure of the cell wall of softwoods and its functions in a living tree. *Holz- als Roh- und Werkstoff* 56: 1-8.
- Brändström, J. 2001. Micro- and ultrastructural aspects of Norway spruce tracheids: a review. *IAWA Journal* 22 (4): 333-353.
- Core, H. A., W. A. Côté, A. C. Day. 1979. Wood structure and identification. Syracuse University Press, New York, Syracuse. Second edition, 169 pp.
- Daniel, G., T. Nilsson. 1984. Studies on the S2 layer of *Pinus sylvestris*. Department of Forest Products, Uppsala: 1-34.
- Donaldson, L. A. 2001. A three-dimensional computer model of the tracheid cell wall as a tool for interpretation of wood cell wall ultrastructure. *IAWA Journal* 22 (3): 213-233.
- Fahlén, J., L. Salmén. 2003. On the lamellar structure of the tracheid cell wall. *Plant Biology* 4 (3): 339-345.
- Harada, H., W. A. Côté. 1985. Structure of wood. Academic Press, Orlando.
- Kerr, A. J., D. A. I. Goring. 1975. Ultrastructural arrangement of the wood cell wall. *Cellulose Chem. and Technol.* 9: 563-573.
- Larsen, M. J., J. E. Winandy, F. Green. 1995. A proposed model of the tracheid cell wall of southern yellow pine having an inherent radial structure in the S2 layer. *Material und Organismen* 29 (3): 197-210.
- Pöhler, E. 1995. Chemische und mikroskopische Untersuchungen zum Delignifizierungsverlauf beim ASAM- und Kraftaufschluss. Diplomarbeit, Universität Hamburg.
- Ruel, K. F., D. A. I. Goring 1978. Lamellation in the S2 layer of softwood tracheids as demonstrated by scanning transmission electron microscopy. *Wood Science and Technology* 12: 287-291.
- Schwarze, F. W. M. R., J. Engels. 1998. Cavity formation and the exposure of peculiar structures in the secondary wall (S2) of tracheids and fibres by wood degrading basidiomycetes. *Holzforschung* 52: 117-123.
- Schwarze, F. W. M. R., S. Fink. 1999. Radial and concentric clefts in the secondary wall (S2) of Norway spruce tracheids during incipient stages of decay by *Stereum sanguinolentum* (Alb. & Schw.: Fr.). *Material und Organismen* 33(1).
- Sell, J., T. Zimmermann. 1993 a. Radial fibril agglomerations of the S2 on transverse-fracture surfaces of tension-loaded spruce and white fir. *Holz- als Roh- und Werkstoff* 51(6): 384.
- Sell, J., T. Zimmermann. 1993 b. Das Gefüge der Zellwandschicht S2 – Untersuchungen mit dem Feldemissions-Rasterelektronenmikroskop an Querbruchflächen von Fichten- und Tannenholz. *Forschungs- und Arbeitsberichte Abt. Holz*, 115 (28), 27 Seiten.
- Sell, J. 1994. Mechanical aspects of new SEM observations on the fibril/ matrix structure of the S2 layer of softwood tracheids. *Proceedings, Plant Biomechanics Conference, Montpellier, France*: 163 – 164.
- Sell, J., T. Zimmermann. 1998. The fine structure of the cell wall of hardwoods on transverse-fracture surfaces. *Holz als Roh- und Werkstoff* 56: 365-366.
- Singh, A. P., J. Sell, U. Schmitt, T. Zimmermann, B. Dawson. 1998. Radial striation of the

- S2 layer in mild compression wood tracheids of *Pinus radiata*. *Holzforschung* 52: 563-566.
- Singh, A. P., G. Daniel. 2001. The S2 layer in the tracheid walls of *Picea abies* wood: Inhomogeneity in lignin distribution and cell wall microstructure. *Holzforschung* 55 (4): 373-378.
- Wardrop, A. B. 1964. The structure and formation of the cell wall in xylem. Academic Press, New York.
- Zimmermann, T., J. Sell, D. Eckstein. 1994. Rasterelektronenmikroskopische Untersuchungen an Zugbruchflächen von Fichtenholz. *Holz als Roh- und Werkstoff* 52: 223 –229.
- Zimmermann, T., J. Sell. 1997. Das Feingefüge der Zellwand auf Querbruchflächen von längszugbeanspruchten Laubhölzern. *Abteilungs- und Arbeitsberichte Holz*, Nr. 35: 1 –37.
- Zimmermann, T., J. Sell. 2000. Comparison of the biomechanical properties of the fine structure of the cell wall of normal and reaction wood. *Proceedings, Plant Biomechanics Conference*, D – Badenweiler, 186 – 192.
- Zimmermann, T. to be submitted to *Holzforschung* in 2003. Structural and fractographic studies on chemically treated wood.





## **Paper B**



# Ultrastructural appearance of embedded and polished wood cell walls as revealed by Atomic Force Microscopy

T. Zimmermann<sup>a,\*</sup>, V. Thommen<sup>b</sup>, P. Reimann<sup>b</sup>, H.J. Hug<sup>c</sup>

<sup>a</sup> Empa, Swiss Federal Laboratories for Materials Testing and Research, Wood Laboratory, Ueberlandstrasse 129, CH-8600 Duebendorf

<sup>b</sup> University of Basel, Physics Department of Condensed Matter, Klingelbergstrasse 82, CH-4056 Basel

<sup>c</sup> Empa, Laboratory of Nanoscale Materials Science, Ueberlandstrasse 129, CH-8600 Duebendorf

Received 21 December 2005; received in revised form 13 June 2006; accepted 21 June 2006

Available online 29 June 2006

## Abstract

Atomic Force Microscopy (AFM) was used to investigate the ultrastructural appearance of transverse wood cell wall surfaces in embedded and polished Norway spruce wood blocks. The prepared surfaces showed only little height differences, suitable for high resolution AFM phase contrast imaging. Our results revealed randomly arranged wood cell wall components in the thick secondary 2 (S2) layers of the tracheid cell walls. It is concluded that the observed distribution pattern of the cellulose fibril/matrix structure is close to the original cell wall structure. In this context, the plasticity of wood cell wall components to re-arrange and adjust to different conditions resulting in diverse structural pattern is discussed.

© 2006 Elsevier Inc. All rights reserved.

**Keywords:** Norway spruce; S2 layer; Wood cell wall structure; AFM; Sample preparation; Polishing

## 1. Introduction

Evolution has continuously adapted the shape and internal structure of wood cell walls to optimize the biomechanical properties of tree stems for highest surviving probability (Mattheck, 1991; Niklas, 1992). At the micro level, the wood cell wall is organized in layers with different thicknesses and different proportions of cellulose and the matrix material lignin and hemicellulose (cf. Brändström, 2001; Harada and Côté, 1985; Wardrop, 1964). Within the different cell wall layers, cellulose exists as a system of fibrils with diameters of 3–4 nm aggregated in larger structural units (Fengel, 1970; Frey-Wyssling, 1968; Heyn, 1977). The cellulose fibril aggregates are surrounded by the polymers lignin and hemicelluloses. In simple terms, the structure of a wood cell wall resembles reinforced concrete, with cellulose and lignin playing the role of steel rods and concrete, respectively. Thus, the cellulose fibril aggregates increase

the tensile strength while the lignin enhances the compressive stability. The arrangement of cellulose fibril aggregates and the matrix material at the nanometer level has to date not been completely resolved.

The nanoscale structure of softwood tracheid cell walls was determined by a combination of various preparation and different high resolution microscopy techniques. The original structure of cross sections is still strongly debated: The images presented by, e.g., Fahlén and Salmén (2002) or Ruel and Goring (1978) showed that the thickest cell wall layer (S2) solely consists of concentric lamellae, whereas the measurements of Sell and Zimmermann (1993a,b) or Schwarze and Engels (1998) revealed a radial arrangement of the fibril/matrix structure (perpendicular to the compound middle lamella). Fig. 1 shows these structural arrangements in a schematic model. In contrast to both models, a random texture of cell wall components within the S2 layer of softwood tracheids was recently found by Donaldson and Frankland (2004). We suppose that the imaged structure must strongly depend on the pre-treatment and preparation of wood samples.

\* Corresponding author. Fax: +41 44 823 40 07.

E-mail address: [tanja.zimmermann@empa.ch](mailto:tanja.zimmermann@empa.ch) (T. Zimmermann).

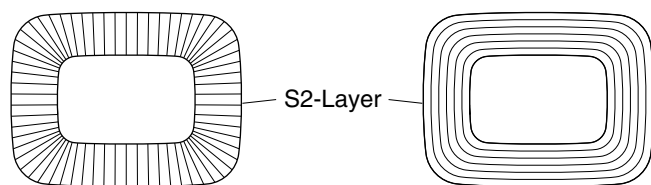


Fig. 1. Schematic model of the thick S2-layer of a softwood tracheid cell wall showing preferential structural orientations in either radial, i.e. perpendicular to the other layers (left) or lamellar directions (right).

In our work, we studied the influence of a sample preparation method which is normally applied for metallic or ceramic specimens. For comparison we also prepared microtomed sections. All samples were investigated by atomic force microscopy.

## 2. Materials and methods

All measurements discussed here were performed on samples prepared from transverse sections (area: 4 mm × 4 mm, length: 15 mm) of sound Norway spruce sapwood (*Picea abies* Karst). Prior to preparation the wood was stored outside for months under cover and afterwards for several weeks in a climate chamber at 35% RH and 23 °C to reach a moisture content of ≈7%. In order to evaluate the effect of pre-treatment (intensive shrinkage and polishing direction) on the ultrastructure, three preparation pathways were followed.

### 2.1. Pathway 1

A total of four samples were prepared: The transverse sections were embedded at ambient temperature into a rigid supporting epoxy resin (SpeciFix-20 resin and curing agent from Struers, mixing ratio 7:1). For this purpose, the samples were placed into cylindrical forms and treated for 10 min. in a vacuum apparatus at ≈200 mbar (Epovac from Struers). Afterwards the cylinder was flooded with the resin and kept under vacuum for 15 min. It is not expected that the low vacuum of 200 mbar caused changes in the cell wall ultrastructure. The embedding process resulted in a full impregnation (lumina and cell walls) of the peripheral zones of the specimens, in the inner zones partly only the lumina were filled with resin (visible by light microscopy). After a curing time of 9 h (curing temperature 50–60 °C), all four cross sections were prepared by two polishing steps, respectively. In step one, polishing was done on a circulating disc (Plano-pol) with several SiC papers of successively smaller grain size (from 30 to 5 μm) and water as a lubricant. The polishing direction was changed by discrete 90°-steps after each grain size to avoid any artificially induced orientation of the wood cell wall components. In step two, the samples were further polished with diamond discs (Phenix, Technotron discs) using a diamond liquid spray with a smallest grain size of 400 nm. During this polishing step, the samples were rotated continuously.

### 2.2. Pathway 2

A total of two samples were prepared following pathway 2. In order to evaluate a possible influence of directional polishing on the ultrastructure, the embedding procedure as described in pathway 1 was repeated. Instead of changing the polishing direction, here a fixed polishing angle of about 45° to the direction of the xylem rays was chosen. This may induce a certain kind of preferential orientation of the structural components in not fully impregnated tracheid cell walls.

### 2.3. Pathway 3

A total of two samples were prepared following pathway 3. This pathway was followed to study the influence of shrinkage stresses on the tracheid cell wall structure that may lead to a mutual change of the ultrastructural arrangements. Before embedding, the samples were oven dried for 12 h at 102 °C to a moisture content of 0%. Then, a polishing procedure equal to that of pathway 1 was performed.

### 2.4. Pathway 4

For comparison sections of 0.5, 1 and 5 μm thickness have been prepared from the not polished underside of one embedded spruce wood block taken from pathway 1. The chosen sample showed well impregnated cell walls (in the peripheral zone and centre zone) as far as visible under the light microscope. The sample was microtomed with a diamond knife. Several sections with the three thicknesses were placed on standard microscopic glass slides.

After the above described preparation pathways, all samples were investigated at standard temperature and humidity (23 °C/60% RH). Different positions of cell walls of randomly chosen early- and latewood tracheids were imaged with a Nanoscope IVa Dimension TM 3100 AFM. A silicon cantilever with a nominal length of 124 μm, a spring constant of 37 N/m, and a resonance frequency of ≈300 kHz was used. In order to minimize the tip-sample interaction forces that may lead to sample deformation, all images were acquired in Tapping Mode. This mode also reduces frictional effects that may cause image distortions. In Tapping Mode, the cantilever is driven with a constant amplitude, at a fixed frequency above its resonance. During the scan the z-position of the sample is regulated to keep the oscillation amplitude at the chosen amplitude setpoint (here about 90% of the free oscillation amplitude). Under ideal circumstances the output of the z-feedback then shows the sample topography.

Simultaneously with the topography, the cantilever amplitude (error of feedback) and the cantilever phase are recorded. The phase image typically reflects local mechanical properties such as the sample stiffness. For dimensional evaluation, image processing software (Image Processing Tool Kit 5.0, Adobe Photoshop) was used.

### 3. Results

The polishing process resulted in a very smooth sample surface that enabled excellent AFM height and phase measurements. The sample topography showed height differences below 1  $\mu\text{m}$ .

Fig. 2a shows the topography (height image) of the transverse surface of a latewood tracheid cell wall from a sample prepared following pathway 1. The compound middle lamella (CML) and the secondary wall layers (S1 and S2) are clearly visible. Figs. 2b–d show higher magnification phase images of the area S2 at the position highlighted by the square in Fig. 2a. The images show the cell wall components as light and dark structures. The cross section size of the light structures is in the range of  $\approx 15$ –30 nm.

All AFM phase images of the thick S2 cell wall layer obtained from the polished samples show randomly distributed cell wall components without any kind of preferential orientation (Figs. 2b–d). This is also true for the samples oven dried at 102°C prior to embedding (pathway 3, Fig. 3a) as well as for the samples polished only in one direction (pathway 2, Fig. 3b). Indeed, the latter samples

show a few preparation marks, but even in a cell wall not fully infiltrated by the embedding resin (Fig. 3b) the directional polishing did not introduce a directional re-ordering of the cell wall components. The width of the light areas is a little bit more heterogeneous but within the same range of dimensions compared to the non directional polished samples.

Only Figs. 3a and b were obtained from inner parts of the respective samples where only the lumina were filled with resin. It is obvious that the dark structures are less distinct in these images.

AFM images obtained from microtomed sections (pathway 4, Figs. 4a and b) show more preparation marks and the cell walls were more deformed than those of the polished samples. Alignments of the structural components were found in the S2 layer of tracheid cell walls, they are often preferentially orientated into the cutting direction, especially in very thin sections, e.g., 0.5  $\mu\text{m}$  sections (Fig. 4a). In addition, the cellulose fibril aggregates seem to be compressed in the direction of microtome cutting. In thicker sections, e.g., 5  $\mu\text{m}$  (Fig. 4b), the basic distribution of wood cell wall components shows only little distortion and

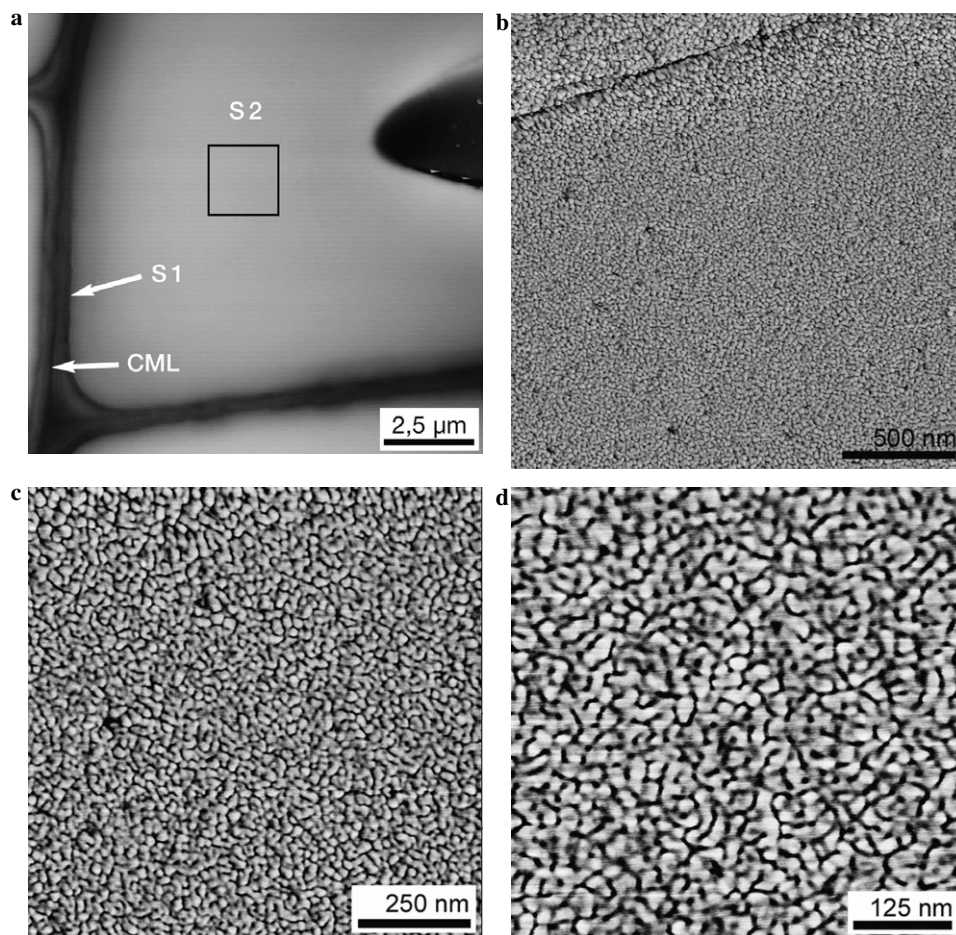


Fig. 2. (a) AFM height image of a transverse section of a non-dried latewood spruce tracheid. Different cell wall layers like the compound middle lamella (CML) and the secondary wall layers 1 and 2 (S1, S2) are discernible. (b) AFM phase image of a part of the thick S2 wall layer highlighted in panel (a). Lighter areas consist of cellulose fibril aggregates, darker areas are considered to be matrix material. (c) Higher magnification of panel (b). The image shows a random distribution of cellulose fibril aggregates and matrix material with no preferential orientation. (d) Higher magnification of Fig. 2c. Single cellulose fibrils (3–4 nm) are not detectable; they appear as aggregates in the range of  $\approx 15$ –30 nm.



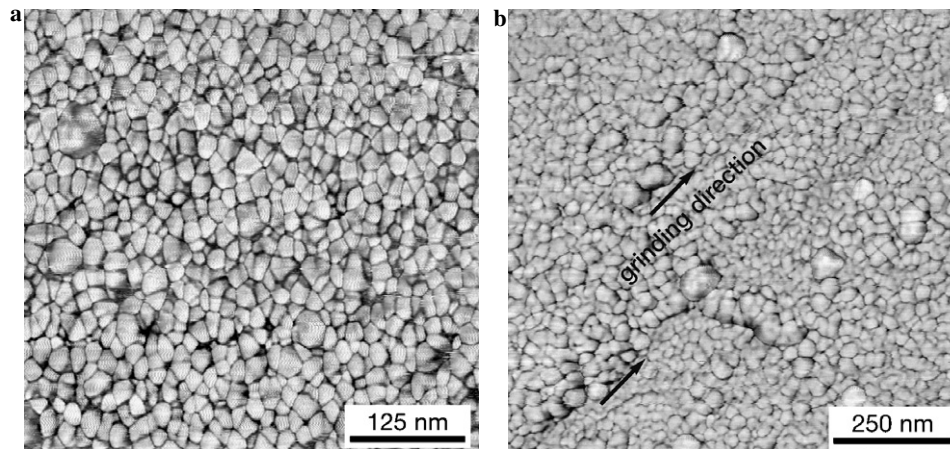


Fig. 3. (a) AFM phase image of a part of the S2 layer from the transverse surface of an oven-dried (at 102 °C) latewood spruce tracheid. The lighter areas, corresponding to cellulose fibril aggregates as well as the darker areas corresponding to matrix material are randomly distributed. (b) AFM phase image of a part of the S2 layer from the transverse surface of a latewood spruce tracheid polished only in one direction (at an angle of 45° to the xylem rays). Even in the presence of distinct abrading marks (arrows), no specific orientation patterns of the cell wall components are detectable.

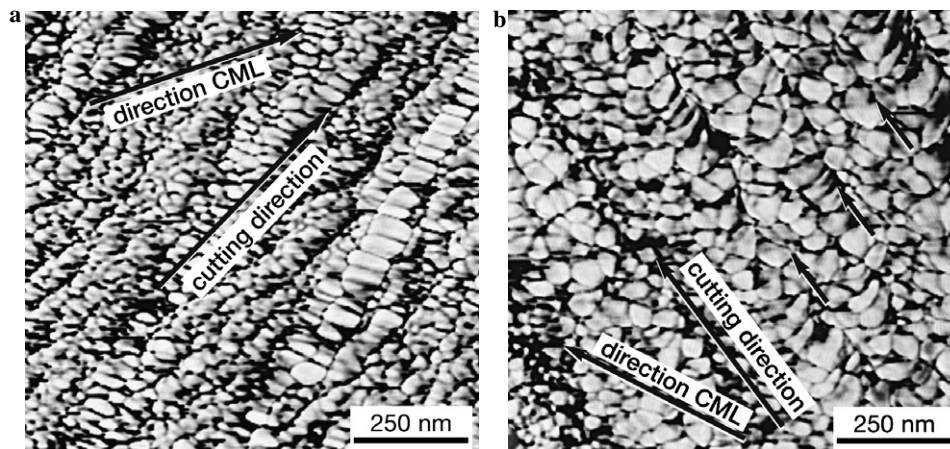


Fig. 4. (a) AFM phase image of a part of the S2 layer from a 0.5 μm thick latewood tracheid cross section; microtomed from the not polished underside of the sample shown in Fig. 2. An aligned orientation of the cell wall components into the cutting direction is visible. Note that the direction of the compound middle lamella (CML) clearly differs from the cutting direction. (b) AFM phase image of a part of the S2 layer from a 5 μm thick latewood tracheid cross section; microtomed from the not polished underside of the sample shown in Fig. 2. Even in the presence of distinct cutting marks (arrows), the degree of orientation is clearly reduced.

a negligible preferential orientation. However, the cutting marks are clearly visible. In Figs. 4a and b, the direction of the compound middle lamella (CML) clearly differs from the cutting direction and the direction of the aligned structures.

Note that the preferential orientation and deformation of the cell wall components visible in Fig. 4a occurred although the microtoming was performed on a well resin embedded sample.

## 4. Discussion

### 4.1. Interpretation of AFM images

Height AFM images simply reflect the topography of a sample that will show preparation induced polishing

scratches under higher magnification conditions. Therefore, only the overview shown in Fig. 2a is a height image. All other images show the phase variation that depends on the mechanical properties of different components in composite materials like wood (Babcock and Prater, 2004). Lighter areas correspond to regions with higher stiffness (Meyer et al., 2004) and are therefore associated with cellulose (Fahlén and Salmén, 2003; Mark, 1967). Consequently, the darker structures are considered to be predominantly matrix material (lignin and hemicelluloses). The cross section size of the lighter areas is in the range of 15–30 nm. Structures of similar size were found by many scientists (e.g., Bailey, 1938; Fahlén and Salmén, 2002, 2003, 2005; Fengel, 1970; Jayme and Koburg, 1959; Kataoka et al., 1992; Kerr and Goring, 1975; Sell and Zimmermann, 1993a,b; Timell, 1989). However, the

naming of these structures unfortunately is rather misleading (e.g., micro- or macrofibril, stripe lamella, cellulose fibril agglomeration). Here, we take the terminology of Fahlén and Salmén who also used AFM as an imaging tool. Hence, the well visible light structures are named cellulose aggregates in our work. Single elementary fibrils which are reported to have diameters of 3–4 nm (Frey-Wyssling, 1968) could not be detected in our study.

#### 4.2. Comparison of ultrastructural appearance of wood cell walls imaged by AFM and other high resolution microscopy methods

For all preparation pathways our AFM images show a random distribution of the wood cell wall components on the thick S2 layers of the examined samples. This clearly disagrees with most other results obtained for softwoods: many TEM micrographs of ultra thin sections of embedded spruce or pine tracheid cell walls show that the S2 consists of concentric helical lamellae with small, but slightly varying inclinations (5–30°) of the cellulose fibrils to the cell axis, e.g., Daniel and Nilsson (1984), Kerr and Goring (1975) and Ruel and Goring (1978). Similar results were obtained by tapping mode AFM by Fahlén and Salmén (2002, 2003). They embedded freeze-dried spruce samples in epoxy resin and cut 0.5 µm thick cross sections using a rotary microtome. The micrographs show concentric lamellae inside the S2 layer built up from individual cellulose fibril aggregates.

In contrast, radial arrangements of the cellulose fibril/matrix structure (perpendicular to the compound middle lamella) were found by SEM and light microscopy on fungi treated (Larsen et al., 1995; Schwarze and Engels, 1998), respectively and by SEM on fractured (Sell and Zimmermann, 1993a,b) transverse surfaces of Norway spruce.

Similar to our results, disordered arrangements have been reported by Donaldson (2001) who compared high resolution TEM micrographs with model calculations. For the latter, he assumed that the cellulose fibrils are randomly arranged in weakly defined clusters. More recently, Donaldson and Frankland (2004) reported a random crystal cavity formation within the S2 of iodine stained wood. They assumed that this appears to be an indication for the underlying random nature of the cell wall nanostructure. This also supports our results.

#### 4.3. Possible reasons for different ultrastructural appearances

The main question is why different observations on the structural arrangement of wood cell wall components on transverse surfaces of the S2 of the same wood species (spruce and pine) have been made. One explanation may be that the ultrastructural appearance is strongly influenced by the applied sample preparation and high resolution microscopy method.

#### 4.4. Drying

Conventional SEM and TEM investigations require oven dried ( $u=0\%$ ) wood. The drying process transfers wood into an unnatural condition. Within the living tree and also during usage wood always possesses a well defined moisture content. It is conceivable that a rigorous drying and the herewith induced high shrinkage stresses prior to embedding (like in pathway 3) may have an impact on the ultrastructural appearance of wood cell walls. In our study, we compare AFM images of rigorously oven dried (at 102 °C to a moisture content of 0%) and climate chamber conditioned wood (at 35% RH, 23 °C to a moisture content of  $\approx 7\%$ ). Apart from slight variations of the size of the cellulose fibril aggregates as well as the matrix material, the ultrastructural appearance was found to be disordered in both cases. Thus, the high shrinkage stresses are found to be inessential for the appearance of the structural arrangement of the cell wall constituents.

#### 4.5. Embedding

An influence of the embedding process on the ultrastructural appearance of tracheid cross sections could be given by stresses arising from the polymerization process of the resin or by a chemical reaction between resin and cell wall constituents. Stress in a complex material like wood may cause a detectable change of the relative sizes of the cell wall components, particularly if they differ in stiffness. Obvious from our investigations is that for fully impregnated cell walls (Figs. 2a and 4a) the dark matrix material (perhaps also permeated resin) is more distinct. However, no differences in the structural arrangement of the components between the sample locations from the peripheral zone (fully embedded) and locations from the inner zone (partially embedded) were found. From this we conclude that the embedding process does not change the ultrastructural appearance of our samples.

Regarding the reactive groups of the resin/curing agent and the wood constituents we found no reasoning for a chemical reaction: the reactive groups of the Specifix-20 resin used are diglycidyl rests that could mainly react with the primary hydroxyl groups of the lignin, cellulose and hemicelluloses. Such ring-opening etherification reactions require relative strong basic conditions (base: sodium hydroxide) (Atalla and Isogai, 2005; Wenz et al., 2005) not given in the embedding process. Additionally, the basicity of the curing agent (present in the embedding process) is too low to induce such a reaction between the resin and the wood components. Moreover, a very important role in ring-opening etherification reactions plays the reaction time. In the applied embedding process the curing time is relatively short (pot life 1 h, curing time 8–10 h), thus reactions between the resin and the wood components can be excluded: e.g., for the reaction between native cellulose and glycidyl ether derivatives the average reaction time is 3 days (Wenz et al., 2005). Furthermore, in our case, cellulose

fibrils, hemicelluloses and lignin are in a fixed compound, so that the reactivity is strongly reduced in comparison with the native components.

#### 4.6. Preparation of thin sections

Donaldson (2001) argues that the preparation of (ultra) thin slices normally used for TEM but also in recent AFM investigations (Fahlén and Salmén, 2002, 2003, 2005) may change the appearance of ultrastructural images: In wood cell walls, the 3–4 nm thick cellulose fibrils (Frey-Wyssling, 1968) enclose an angle of about 5–30° to the longitudinal cell axis. In TEM, the projection of all features within the 60–80 nm ultra thin section is imaged. Donaldson, therefore, calculated that single fibrils running through the TEM section do not appear as circular objects but as about 35 nm long strands. A further mechanism for the observed elongated structures may be a cutting-induced overlap of fibrils passing through the sliced volume. Thus, according to Donaldson, the observation of tangential lamellation within the cell wall may arise from the preparation irrespective of the true arrangement of fibrils in tangential, radial or random patterns. We believe that this explains the lamellar textures observed by several TEM investigations (see above). However, the AFM micrographs of Fahlén and Salmén (2002) also reveal a lamellar structural arrangement. This can not be explained using the above arguments, because the AFM only records surface structures and not a projection as TEM. Our comparative AFM studies on microtomed thin sections also showed aligned structures, especially in very thin sections, e.g., 0.5 µm (Fig. 4a). These structures that are predominantly orientated along the cutting direction clearly represent scratch marks induced by the knife during sectioning. Lamellar structures straight parallel to the compound middle lamella (CML) have not been found. Thus, mechanical strain during the microtoming of thin slices does cause a certain degree of structural re-ordering even in well embedded samples.

#### 4.7. Polishing

Polishing of embedded samples used in our study may be viewed as a form of irregular microscopic cutting process. In contrast to the microtoming that applies forces to thin slices and leads to a macroscopic deformation of the slices, the polishing process only acts on the surface of an otherwise well supported centimetre-sized piece of embedded wood. Thus, the original wood cell wall structure is expected to be preserved by our preparation method. This is further supported by our images obtained on directionally polished samples that did not lead to the formation of oriented structures (Fig. 3b). The imaged cell wall is from the center part of the sample where only the lumina were infiltrated by the resin. Therefore, a structural re-ordering should have been possible.

#### 4.8. Fracturing

SEM images of transverse sections showing structural details could only be obtained on fractured samples. In untreated softwood tracheids typically radial arrangements (perpendicular to the other cell wall layers) of cell wall components were found (Sell and Zimmermann, 1993a,b). This result may be caused by the fracture process itself as discussed by Fahlén and Salmén (2002): they explained the radial agglomerations of cellulose aggregates by a lateral contraction and tension-strain perpendicular to the cell wall axis.

The above discussion shows that high quality images can be obtained with different sample preparation techniques resulting in a lamellar, radial or random distribution of cell wall components.

It has been suggested that different organisation pattern do coexist (Sell and Zimmermann, 1998). Our hypothesis is that the wood cell wall components are extremely plastic and re-arrange into various structural patterns under different stress conditions and preparation methods. Indeed, a morphological healing process following plastic deformation of wood has been discovered by Keckes et al. (2003). They found evidence for a molecular stick-slip mechanism similar to the motion of dislocations in crystalline materials. In detail, a re-formation of the amorphous matrix between the cellulose fibrils within the cell wall was discussed. A similar mechanism could explain the formation of different ultrastructural patterns observed in the past changing the originally random arrangement of the wood cell wall components.

### 5. Conclusion

Random textures of the thick S2 layer on transverse surfaces of Norway spruce tracheids were observed by tapping mode AFM on polished samples. No evidence was obtained for lamellar or radial (perpendicular to the compound middle lamella) ultrastructural arrangements of the wood cell wall components as described in other studies. We suggested that the dissimilar ultrastructural appearances may arise from the different pre-treatments and preparation methods. Hence, we propose the described polishing process as an alternative sample preparation strategy. In addition, we proved that the reported texture does not depend on drying and directional polishing. We also found that microtoming does cause preferential orientations of the structural components along the cutting direction. This leads to the conclusion that the observed texture reflects the underlying random nature of the cell wall nanostructure. Further studies are required to resolve the underlying interactions of the cellulose fibrils, lignin and hemicelluloses.

### Acknowledgments

We thank I. Burgert (Department of Biomaterials, Max-Planck-Institute of Colloids and Interfaces) for helpful dis-



cussions and our colleagues at the Empa Wood Laboratory for valuable suggestions and comments on the manuscript. Thanks are also due to S. Fink and his staff, University of Freiburg (D) for the microtoming of our sections. We are grateful to two anonymous reviewers whose valuable comments improved the quality of the paper.

## References

- Atalla, R.H., Isogai, A., 2005. Recent Developments in Spectroscopic and Chemical Characterization of Cellulose. Review in Polysaccharides: Structural Diversity and Functional Versatility. Marcel Dekker, New York. pp. 123–157.
- Babcock, K.L., Prater, C.B., 2004. Phase Imaging: Beyond Topography. Veeco Instruments Inc..
- Bailey, J.W., 1938. Cell wall structure of higher plants. *Ind. Eng. Chem.* 30, 40–47.
- Brändström, J., 2001. Micro- and ultrastructural aspects of norway spruce tracheids: a review. *IAWA J.* 22 (4), 333–353.
- Daniel, G., Nilsson, T., 1984. Studies on the S2 layer of *Pinus sylvestris*. Department of Forest Products, Uppsala. pp. 1–34.
- Donaldson, L.A., 2001. A three-dimensional computer model of the tracheid cell wall as a tool for interpretation of wood cell wall ultrastructure. *IAWA J.* 22 (3), 213–233.
- Donaldson, L., Frankland, A., 2004. Ultrastructure of iodine treated wood. *Holzforschung* 58 (3), 219–225.
- Fahlén, J., Salmén, L., 2002. On the lamellar structure of the tracheid cell wall. *Plant Biol.* 4 (3), 339–345.
- Fahlén, J., Salmén, L., 2003. Cross-sectional structure of the secondary wall of fibers as affected by processing. *J. Mater. Sci.* 38, 119–126.
- Fahlén, J., Salmén, L., 2005. Pore and matrix distribution in the fiber wall revealed by atomic force microscopy and image analysis. *Biomacromolecules* 6, 433–438.
- Fengel, D., 1970. Ultrastructural behavior of cell wall polysaccharides, In: Page, D.H. (Ed.), *The Physics and Chemistry of Wood Pulp Fibres*. Tappi.
- Frey-Wyssling, A., 1968. The ultrastructure of wood. *Wood Sci. Technol.* 2, 73–83.
- Harada, H., Côté, W.A., 1985. *Structure of Wood*. Academic Press, Orlando.
- Heyn, A.N.J., 1977. The ultrastructure of wood pulp with special reference to the elementary fibril of cellulose. *Tappi* 60 (11), 159–161.
- Jayme, G., Koburg, E., 1959. Ueber den elektronisch bestimmten Durchmesser der Mikrofibrillen von Laubholzzellelementen. *Holzforschung* 13, 37–43.
- Kataoka, Y., Saiki, H., Fujita, M., 1992. Arrangement and superimposition of cellulose microfibrils in the secondary walls of coniferous tracheids. *Mokuzai Gakkaishi* 38 (4), 327–335.
- Keckes, J., Burgert, I., Frühmann, K., Müller, M., Kölln, K., Hamilton, M., Burghammer, M., von Roth, S., Stanzl-Tschegg, S., Fratzl, P., 2003. Cell-wall recovery after irreversible deformation of wood. *Nat. Mater.* 2, 810–812.
- Kerr, A.J., Goring, D.A.I., 1975. Ultrastructural arrangement of the wood cell wall. *Cellulose Chem. Technol.* 9, 563–573.
- Larsen, M.J., Winandy, J.E., Green, F., 1995. A proposed model of the tracheid cell wall of southern yellow pine having an inherent radial structure in the S2 layer. *Material und Organismen* 29 (3), 197–210.
- Mark, R.E., 1967. *Cell Wall Mechanics of Tracheids*. Yale University Press, London.
- Matthäck, C., 1991. *Trees, the Mechanical Design*. Springer, Berlin, Heidelberg, New York.
- Meyer, E., Hug, H.J., Bennewitz, R., 2004. *Scanning Probe Microscopy, The Lab on a Tip*. Springer-Verlag, Berlin, Heidelberg, New York.
- Niklas, K.J., 1992. *Plant Biomechanics*. University Press, Chicago.
- Ruel, K.F., Goring, D.A.I., 1978. Lamellation in the S2 layer of softwood tracheids as demonstrated by scanning transmission electron microscopy. *Wood Sci. Technol.* 12, 287–291.
- Schwarze, F.W.M.R., Engels, J., 1998. Cavity formation and the exposure of peculiar structures in the secondary wall (S2) of tracheids and fibres by wood degrading basidiomycetes. *Holzforschung* 52 (2), 117–123.
- Sell, J., Zimmermann, T., 1993a. Das Gefüge der Zellwandschicht S2 - Untersuchungen mit dem Feldemissions-Rasterelektronenmikroskop an Querbruchflächen von Fichten- und Tannenholz. *Forschungs- und Arbeitsberichte Abteilung* 115 (28), 1–27.
- Sell, J., Zimmermann, T., 1993b. Radial fibril agglomerations of the S2 on transverse-fracture surfaces of tracheids of tension-loaded spruce and white fir. *Holz als Roh- und Werkst.* 51, 384.
- Sell, J., Zimmermann, T., 1998. The fine structure of the cell wall of hardwoods on transverse-fracture surfaces. *Holz als Roh- und Werkst.* 56 (5), 365–366.
- Timell, T.E., 1989. Chemical composition of wood. In: Schniewind, A.P. (Ed.), *Concise Encyclopedia of Wood and Wood-based Materials*. Pergamon Press, Oxford, New York, Beijing, Frankfurt, São Paulo, Sydney, Tokyo, Toronto. pp. 319–324.
- Wardrop, A.B., 1964. *The Structure and Formation of the Cell Wall in Xylem*. Academic Press, New York.
- Wenz, G., Liepold, P., Bordeanu, N., 2005. Synthesis and SAM formation of water soluble functional carboxymethylcelluloses: thiosulfates and thioethers. *Cellulose* (12), 85–96.



## Paper C



# **ARRANGEMENT OF CELL WALL CONSTITUENTS IN CHEMICALLY TREATED NORWAY SPRUCE TRACHEIDS**

*Tanja Zimmermann*

Research Scientist

*Klaus Richter*

Senior Scientist and Head of Wood Laboratory

*Nico Bordeanu*

Research Scientist

Swiss Federal Laboratories for Materials Testing and Research (Empa)

Ueberlandstrasse 129, 8600 Duebendorf, Switzerland

*Jürgen Sell*

Professor, former Head of Wood Laboratory (Empa)

Robaenkli 22, 8607 Aathal-Seegraeben, Switzerland

## ABSTRACT

The cell wall of tracheids in conifer wood has evolved to provide both water conduction and mechanical strength to the standing tree. However, its structure at the nanometer level is not yet accepted beyond doubt and little is known about the interactions between the cell wall components. In the present study, the fracture pattern of the S2 layer of Norway spruce tracheids was observed by field emission scanning electron microscopy (FE-SEM) after pre-treatment of the cell wall with various alkali solutions, acetic and nitric acid and ASAM delignification. The resulting cell wall arrangements were also studied in ultra thin sections of unfractured samples with transmission electron microscopy (TEM). In the case of untreated samples (reference), radial fracture patterns – perpendicular to the compound middle lamella – were regularly observed. A treatment with 10 % and 18 % NaOH or 24 % KOH at room temperature – associated with a slight decrease of glucomannan – resulted in the disappearance of these radial fracture formations. As the severity of the alkali treatment increased and acid and ASAM delignification was applied, concentric alignments in the cell wall became more and more discernable. The increasing loss of hemicelluloses and lignin led therefore to distinct changes in the fragmentation patterns of the cell walls. In addition, reduction in strength and stiffness were determined for all chemically treated cell walls. It is concluded that even slight changes in cell wall constitution influence the interactions of the cell wall components and thus fracture mechanics and ultrastructural appearance of wood cell walls.

Keywords: cell wall structure, interactions of cell wall components, S2 layer, chemical treatment, FE-SEM, TEM

## INTRODUCTION

The complex architecture of the wood cell wall determines the strength and stability of the standing tree, and therefore also the mechanical properties of solid wood. The structure of wood at all length scales makes it possible for tons of plant biomass to be supported by astonishingly slim stems to heights of sometimes more than 50 metres. The tree can withstand large static and dynamic forces of gravity and wind-loads. Moreover, the wood structure efficiently conducts water from the roots to the crown (Booker and Sell 1998). Natural selection has ensured that tree and wood structure at the cellular level are optimized to satisfy these engineering requirements (Mattheck 1991). However, the structure at the nano level and the specific molecular mechanistic phenomena are not yet fully understood (Fratzl et al. 2004). The organization as well as the interactions of the stiff cellulose fibrils and the softer matrix polymers lignin and hemicelluloses in the thickest secondary two wall layer, the S2 is still open to debate.

Microscopic studies on the ultrastructure of wood cell wall transverse sections revealed a lamellar (Daniel and Nilsson 1984; Fahlén and Salmén 2002; Kerr and Goring 1975; Ruel and Goring 1978), radial (Schwarze and Engels 1998; Sell and Zimmermann 1993) or random (Donaldson and Frankland 2004; Zimmermann et al. 2006) distribution of cell wall components in the S2. It has been suggested that different organization pattern do coexist (Sell and Zimmermann 1998; Singh and Daniel 2001). Another hypothesis is that the wood cell wall components re-arrange into various structural patterns under different stress conditions and preparation methods (Zimmermann et al. 2006). Indeed, a morphological re-arrangement process following plastic deformation of wood has been discovered by Keckes et al. (2003). They found evidence for a molecular stick-slip mechanism similar to the motion of dislocations in crystalline materials. In detail, a re-formation of the amorphous matrix between the cellulose fibrils within the cell wall was discussed. A similar mechanism may explain the formation of different ultrastructural patterns observed in the past.

Further studies are required to resolve the underlying interactions of the cell wall constituents. In this context, our study investigates the influence of chemical pre-treatment on fractured or ultra thin tracheid cross sections. For this purpose, spruce cell walls were modified by dissolving chemical components, mainly hemicelluloses and lignin using alkaline and acetic treatment. Possible changes in the supermolecular structure of cellulose due to alkali treatment were evaluated by using X-ray diffraction. The resulting morphological structures were then studied by field emission scanning electron microscopy (FE-SEM) and transmission electron microscopy (TEM).

## MATERIALS AND METHODS

### *Chemical Pre-Treatment*

3 mm thick panels were prepared from a spruce board (*Picea abies* Karst) by planing and cut with a circular saw into single sticks. Prior to preparation the wood was stored outside for months under cover and afterwards for several weeks in a climate chamber at 65 % RH and 23 °C. For each treatment, 50 small sticks of sound wood (cross-section 3 mm x 3 mm, each containing early- and latewood, 70 mm in length) were shaken in various solutions. The treatments were designed to dissolve distinct parts of the binding components of the cell wall (hemicelluloses and lignin) with increasing severity. 50 sticks were retained as reference material.

Alkaline treatment was used for hemicellulose degradation:

1. Sodium hydroxide, NaOH (10 % w/v at room temperature, 5 hrs)
2. Sodium hydroxide, NaOH (18 % w/v at room temperature, 5 hrs)
3. Potassium hydroxide, KOH (24 % w/v at room temperature, 5 hrs)
4. hot water extraction with addition of NaOH (10 % w/v, 100 °C, 5 hrs) in a rotary evaporator

Acetic treatment and ASAM pulping were designed for intensive degradation of both, hemicelluloses and lignin, leaving the cellulose generally unaltered. To represent the effect of ASAM-pulping industrial wood chips of spruce were used instead of small sticks:

5. Acetic acid, CH<sub>3</sub>COOH (80 % v/v) and nitric acid, HNO<sub>3</sub> (65 % v/v) = 10/1 (by volume) during 30 min at 120 °C
6. steaming with hot water vapour during 30 min at 1 bar pressure and 100-120 °C and ASAM pulping with sodium sulfite, Na<sub>2</sub>SO<sub>3</sub>/sodium hydroxide, NaOH= 80/20 (by volume), heating time 105 min, until T<sub>max</sub> =180 °C is reached

After treatment with the various chemicals all samples were washed in distilled water until the washing solutions became neutral. The wood was then conditioned to an equilibrium moisture content of about 10 %.

Samples of all treatments were submitted to total hydrolysis with sulphuric acid, the hydrolysed carbohydrates were separated by borate complex ion exchange chromatography, and detected photometrically with copper-2,2-bicinchonate reagent according to Uremovic et al. (1994).



### *X-Ray Diffraction Studies*

To assess the possible influence of the alkali treatments on the supermolecular structure of cellulose, XRD measurements were carried out. The tangential surfaces of the sample sticks treated with 10% (cold and hot water extraction) and 18% NaOH as well as 24 % KOH were prepared by microtoming the surface and a thoroughly washing with deionized water. The samples were then investigated with a diffractometer (X'Pert Pro, Panalytical, Netherlands) using Ni-filtered Cu K $\alpha$  radiation ( $\lambda = 0.15418$  nm). Lattice recognition was done by comparison with literature data.

### *Mechanical Tests*

3-point bending tests were applied to loosen the cell wall structure of the sticks on the fracture surface. For each combination of chemical treatment, at least 5 wood samples were loaded to failure (44 N load cell, loading speed 20  $\mu\text{m/s}$ ). Therefore, special equipment for the bending testing of small samples was used (Figure 1).

From the results, the bending strength and the Modulus of Elasticity (MOE) of the samples were calculated.

The wood chips (ASAM delignification) were manually broken without measuring strength and stiffness.

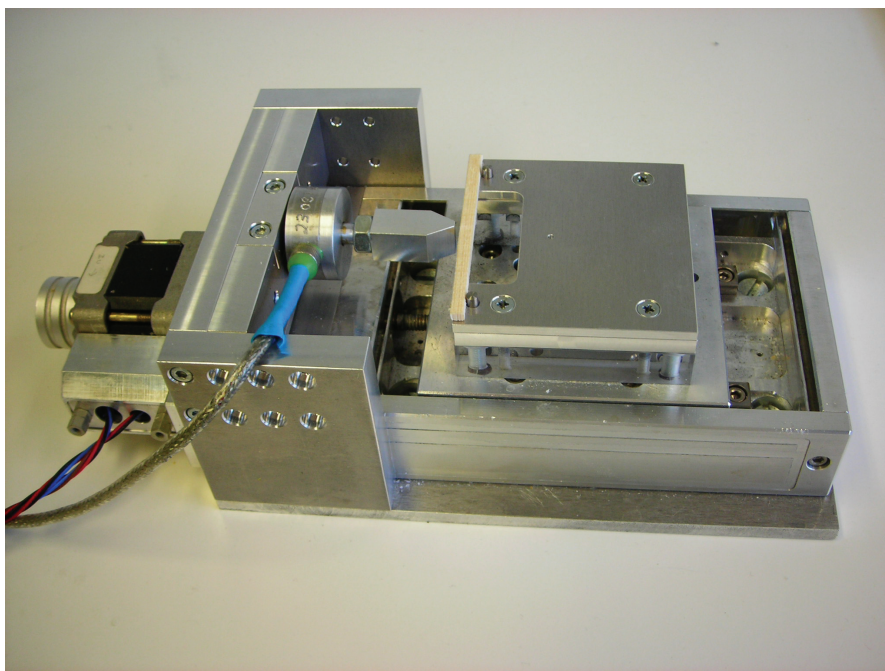


FIG. 1. The bending tests were carried out using special equipment for small samples

## *Structural analysis*

### *SEM studies*

Samples of the transverse fracture surfaces were extracted with razor blades in close proximity to the outermost tension zone. These were then prepared for SEM by drying in a vacuum oven at 40 °C and 10 mbar for 12 hours, glueing on a specimen holder using carbon-adhesive and sputtering with a platinum layer of approx. 10 nm. The samples were investigated in a Field Emission SEM (Jeol 6300F) at an acceleration voltage of 5 kV and working distance of 24 mm.

### *TEM studies*

From each combination of chemical treatment, three samples were embedded following the methodology proposed by Spurr (1969). Ultra thin sections (approx. 100 nm) of the samples were produced using a diamond knife (microtome type LKB Ultratome, 4801 A) and placed on Formvar coated copper grids. Half of the sections were stained for 4 minutes with a solution of  $\text{KMnO}_4$  (1 % w/v) in sodium citrate (0.1 % w/v). The remaining sections were stained with uranyl acetate (1 % w/v) and lead citrate (Reynolds 1963). After staining, the sections were washed in double-distilled water. Finally, the sections were examined with a Philips STEM CM30 transmission electron microscope.

## RESULTS AND DISCUSSION

### *Chemical Pre-Treatment*

The effects of the various chemical treatments applied are shown by the results of total hydrolysis, presented as relative percentages in Table 1.

It is well known that the hydrolysis residue represents a rough approximation of the Klason lignin content (Fengel and Wegener 1989). Thus, our own data is in good agreement with results cited in the literature and confirms that an increase in the severity of alkali treatment did not lead to lignin degradation, while the relative amounts of sugars, typical for the hemicelluloses did – as expected – decrease. A treatment with 10 % w/v and 18 % w/v NaOH or 24 % w/v KOH at room temperature led only to slight changes in the carbohydrate composition of the cell wall. Only small proportions of the hemicellulose glucomannan were solubilized, indicated by a decrease of mannose and simultaneously an increase of glucose. In contrast, the hot water extraction with NaOH (10 % w/v) caused a sharp decline in mannose. As intended, the treatment with acetic

acid and nitric acid or ASAM pulping (with Na<sub>2</sub>SO<sub>3</sub> and NaOH) led to a distinct degradation of both hemicelluloses and lignin.

TABLE 1. Determination of carbohydrates and unhydrolysed residues obtained from spruce wood submitted to various chemical treatments.

	Relative composition of the hydrolysates (by weight)						
	Glucose (%)	Xylose (%)	Galactose (%)	Arabinose (%)	Mannose (%)	4-O-Me- GluA <sup>1)</sup> (%)	unhydrolyzed residue <sup>2)</sup> (%)
Reference	71.37	6.97	1.03	1.35	18.32	0.95	27.48
10% NaOH	70.48	7.07	1.80	1.35	18.35	0.77	28.77
18% NaOH	73.38	6.21	1.70	1.32	16.50	0.89	28.13
24% KOH	74.17	5.73	1.34	1.60	16.23	0.94	28.20
10% NaOH 100°C	80.00	7.41	1.06	1.30	9.77	0.46	31.82
CH <sub>3</sub> COOH/ HNO <sub>3</sub>	86.19	4.08	-	-	9.05	0.69	10.27
ASAM Pulping	84.4	7.8	-	-	7.5	-	10.5

1) 4-O-Me-GluA: 4-O-methyl-glucuronic acid

2) Related to absolutely dry wood

### *X-Ray Diffraction Studies*

Different authors have reported that the lattice structure of cellulose changes due to mercerization by sodium hydroxide treatment (e.g. Borysiak and Doczekalska 2005; Mansikkamäki et al. 2005; Nishiyama et al. 2000; Okano and Sarko 1984). This might have an influence on the interactions of the cell wall constituents. The path from

cellulose I (parallel structure) to cellulose II (antiparallel structure) during mercerization goes by way of Na-cellulose I. If a cellulose sample is treated with an alkali solution, the cellulose swells to various extents depending on the type and the concentration of alkali, and also on the temperature (Fengel and Wegener 1989). At low concentrations, only the large pores in the cellulose structure are occupied. With increasing concentration, the smaller cation  $\text{Na}^+$  ( $\text{Na}^+ = 0.276 \text{ nm}$ ) can advance more easily into smaller pores.  $\text{Na}^+$  seems to have a favourable diameter which is able to widen the smallest pores down to the space between the lattice planes and advance into them. During intensive washing, the linked Na-ions are removed and another lattice is formed, the cellulose II lattice.

In our study, for all NaOH and KOH treatments in different concentrations no lattice conversion of cellulose (transformation of cellulose I to cellulose II) was observed (Figures 2a, 2b). This is also true for the samples treated with 10 % NaOH at 100 °C although these samples showed distinct losses in glucomannan. The diffraction peaks found are typical for cellulose I (Borysiak and Doczekalska 2003; Mansikkamäki et al. 2005). The results are in accordance to different studies reported in literature. Kim (2005) found for the sapwood of sound oak wood that the cellulose was converted more slowly to Na-cellulose I during mercerization than in delignified wood and that very little Na-cellulose was converted to cellulose II. During washing and drying Na-cellulose I of sound wood was reconverted to cellulose I.

Revol and Goring (1981) reported only a partial conversion of cellulose I to cellulose II although they impregnated  $0.5 \times 0.5 \text{ mm}^2$  samples under vacuum for 24 hrs. In our study larger  $3 \times 3 \text{ mm}^2$  samples were alkali treated for only 5 hrs but not with vacuum.

Lonikar et al. (1984) found no lattice conversion at all for white birch treated with 23 % aqueous NaOH. On the other hand, wood subjected to a pre-treatment that results in the loosening of its morphological texture showed varying degrees of lattice conversion during mercerization.

The authors explained the fact that alkali treatment caused only little or no transformation from cellulose I to cellulose II by the chemical composition of wood. Hemicelluloses and lignin are deposited in between the adjacent cellulose fibrils. Intramolecular as well as intermolecular interactions are present within and among these wood components so that none of the physical or physicochemical characters of an individual wood component is displayed independent of the other components. Even chemical bonds exist between wood components as detected in lignin-carbohydrate

complexes. Thus, wood displays a very tough and compact morphological texture which restricts either the penetration of the caustic solution or the subsequent swelling of cellulose and hence no lattice conversion is observed.

As no degradation of lignin could be observed in our study for all alkali treated samples, we conclude that lignin prevented the alkali swelling of the cellulose to some extent and therefore the transformation from cellulose I to cellulose II.

Recent results of Jungnickl (2006) support our conclusion. In her study, the influence of lignin on the formation of cellulose II was assessed. Semi-thin tangential slices of spruce earlywood were treated with 10 % and 20 % NaOH at 90 °C for 10 hours with and without prior delignification. A pronounced formation of cellulose II was observed from WAXS (Wide angle X-ray scattering) patterns of the delignified samples after treatment with 10 % and 20 % NaOH. A conversion to cellulose II in the samples treated with 10 % NaOH without prior delignification could not be observed.

Nevertheless, mercerization and a transformation from parallel cellulose I to antiparallel cellulose II occurs at another hierarchical level than the re-arrangements observed in the presented microscopic study. It is not likely that changes in the lattice structure affect the arrangement of wood cell wall components.

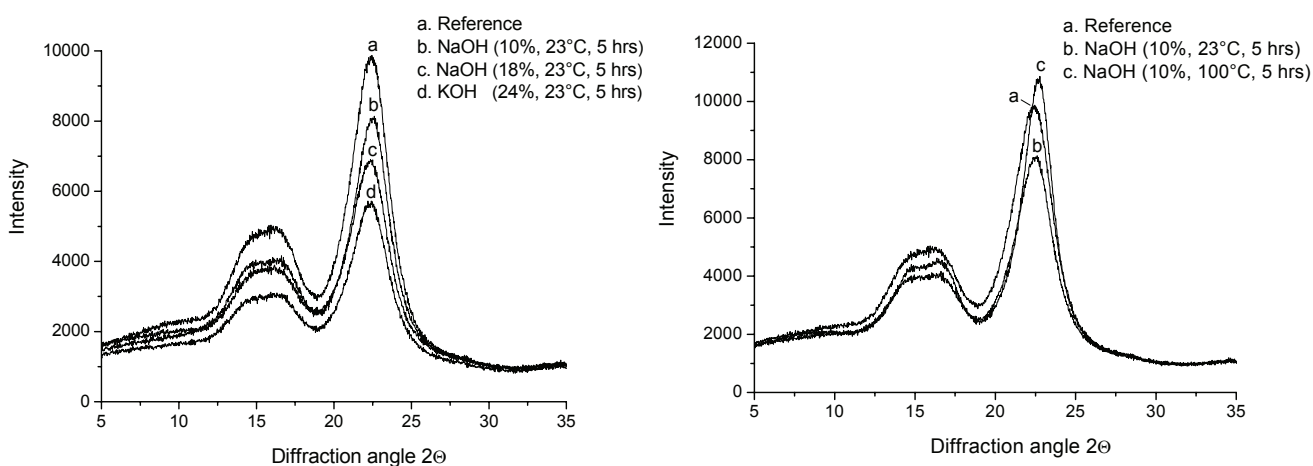


FIG. 2 a. b.: X-ray diffraction patterns of alkali treated spruce wood showing the typical peaks for cellulose I

### Mechanical Tests

Figs. 3a and 3b show the results of the 3-point bending tests.

The highest strength and stiffness was determined for the untreated samples (reference). The MOE values are in accordance with those known from the literature for sound wood (Sell 1989) while the calculated bending strength was even higher.

The lowest values were obtained for the samples treated with acetic acid ( $\text{CH}_3\text{COOH}$ ) and nitric acid ( $\text{HNO}_3$ ). These samples showed an intensive decrease in hemicelluloses and lignin residue (see Table 1) and were strongly deformed. Köhler and Spatz (2002) obtained similar results for the strengthening tissues of *Aristolochia macrophylla* Lam. with chemically altered cell wall assembly. They showed for wet sclerenchyma tissue, that a chemical extraction of hemicelluloses and lignin respectively, led to significant changes in the stress-strain behaviour of the samples. Removing the lignin or the hemicelluloses reduced the initial stiffness in the linear deformation stage. In addition, the samples where hemicelluloses were extracted lost their high toughness.

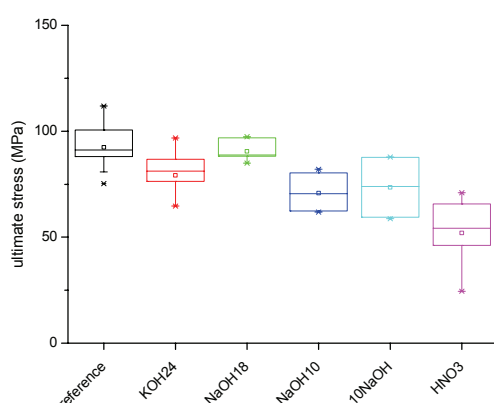


FIG. 3a. Bending strength of chemically treated Norway spruce samples.

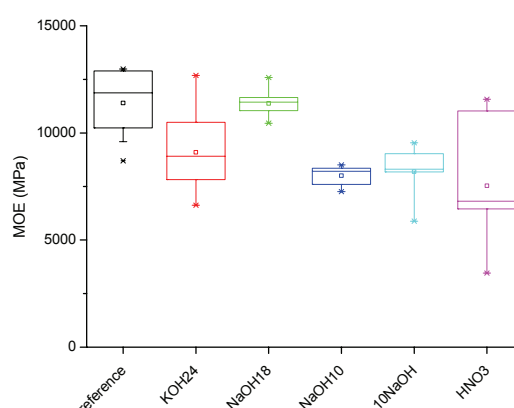


FIG. 3b. Modulus of Elasticity of chemically treated Norway spruce samples.

reference: untreated samples (n= 11)

KOH24: KOH 24 % w/v at room temperature, 5 hrs (n= 7)

NaOH18: NaOH 18 % w/v at room temperature, 5 hrs (n=7)

NaOH10: NaOH 10 % w/v at room temperature, 5 hrs (n= 6)

10NaOH: hot water extraction with NaOH, 10 % concentration, 6 hrs (n=5)

HNO3:  $\text{CH}_3\text{COOH}$ , 80 % v/v and  $\text{HNO}_3$ , 65 % v/v= 10/1 (by volume), 30 min, 120 °C (n=7)

Although alkaline treatment (with NaOH or KOH), extraction at room temperature) led only to a slight hemicellulose degradation (see Table 1), it had an influence on the measured MOE and bending strength. Generally, alkali treated samples showed lower values compared with the reference samples. One exception was the treatment with 18 % NaOH: The MOE and strength values are apparently not different from those determined for the reference samples. Fratzl et al. (2004) showed that the macroscopic mechanical properties depend to a large extent on the strength of the interface between cellulose fibrils and matrix polymers. A weakening of the interface might be caused by the permanent swelling of the cell wall during the alkali treatment and the starting solubilization of hemicelluloses. Consequently, molecular interaction between fibrils and the matrix polymers altered, bonds were solved and eventually new bonds were constituted. Recently, Keckes et al. (2003) observed cell-wall recovery mechanisms that lead to the re-formation of the amorphous matrix between the cellulose fibrils within the cell wall. It is conceivable that similar phenomena play a role when fracture mechanics change in chemically swollen wood.

Although only small proportions of glucomannan have been solubilized by alkaline treatment at room temperature, it is also possible that the degree of polymerization (DP) of the residual polymers changed, and as a consequence influenced strength and stiffness of the respective samples.

The samples extracted in hot water with 10 % NaOH had an intensive reduction in mannose (approximately 9 %) and showed a similar deformation as the specimens treated with  $\text{CH}_3\text{COOH}$  and  $\text{HNO}_3$ . Surprisingly, these samples showed slightly higher MOE and strength values than those treated with 10 % NaOH at room temperature without an apparent change in carbohydrate composition. A possible explanation might be derived from the respective X-ray diffraction patterns (Figure 2a and 2b). The X-ray diffraction experiments with samples treated with alkali at room temperature showed a decreasing peak intensity (Cellulose I peaks) with increasing alkali concentration (Fig. 2a). This indicates a decrease in crystallinity due to the alkali treatment. In contrast, the peak intensity of samples treated with 10 % NaOH at 100 °C was higher than for all the other alkali treated samples and even higher than for the reference samples. It is possible that due to a higher degradation of glucomannan the crystallinity of the remaining matrix increases and therefore no further losses in strength and stiffness occurred. However, as it was very difficult to determine the correct dimensions of the deformed small samples, required for the calculation of MOE and bending strength, slight measuring irregularities can also not be excluded.



In summary, it was evident that even a slight change in carbohydrate composition (e.g. 2 % reduction in mannose) resulted in strength and stiffness losses. A distinct degradation of all hemicelluloses and lignin (e.g. decrease of unhydrolyzed residue of about 18 %, compare Table 1) caused sample deformations as well as a sharp decline in MOE and bending strength.

### *Structural analysis*

#### *Reference samples*

In the case of untreated samples, radial fracture patterns (perpendicular to the compound middle lamella) were apparent on transverse surfaces of the cell wall layer S2 (Fig. 4). This result is in good agreement with earlier studies (Sell and Zimmermann 1993). As cellulose, hemicelluloses and lignin have similar electron optical densities, it is not possible to distinguish between both cell wall components. Consequently, the aligned features in the S2 of fractured samples will hereafter generally be described as fracture or fragmentation patterns.

In ultra thin TEM sections of reference samples, no consistent orientation of the cell wall components could be discerned. Lamellar as well as disordered and, in few cases, moderate striations perpendicular to the compound middle lamella were visible (Fig. 5).

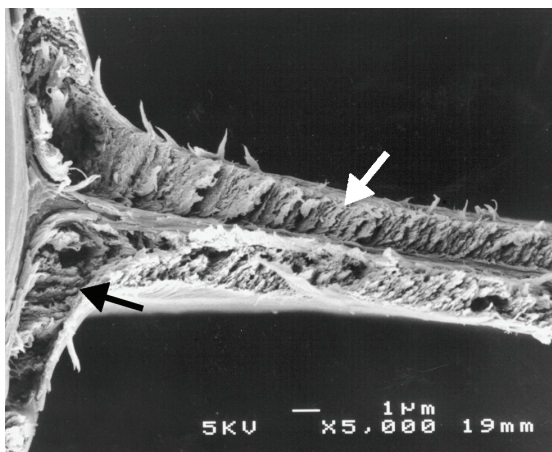


FIG. 4. FE-SEM micrograph: Transverse fracture surface (tension zone) of an untreated tracheid cell wall of spruce (earlywood). Distinct preferentially radial (perpendicular to the compound middle lamella) fragmentation of the S2 (arrows).

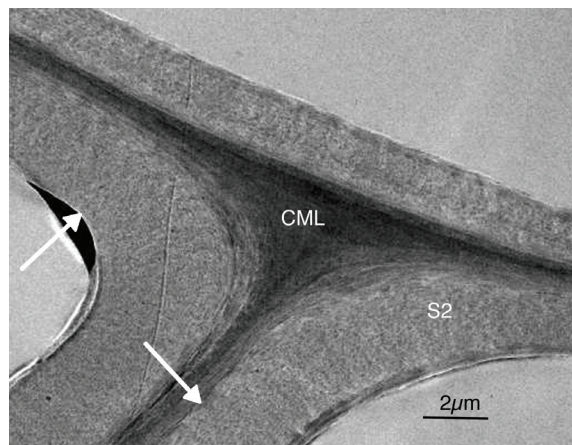


FIG. 5. TEM micrograph: Transverse ultra thin section of a cell wall of spruce (transition zone early-/latewood, reference sample). Stained with  $\text{KMNO}_4$ . No distinct preferential orientation of the cell wall components (arrows).



### *Chemically treated samples*

Figures 6 to 11 show FE-SEM micrographs of transverse fracture surfaces and a TEM micrograph of an ultra thin section of chemically treated wood cell walls.

Chemical treatment was associated with changes in the fragmentation of the thick S2 layer:

Swelling of the cell wall and a slight reduction in hemicelluloses after treatment with NaOH (10 % w/v and 18 % w/v) or KOH (24 % w/v) led to the disappearance of radial structures and resulted in a disordered fragmentation (Fig. 6).

On transverse fracture surfaces of samples treated with hot water and NaOH (10 % w/v), concentric layers within the S2 became apparent (Fig. 7).

Substantial degradation of hemicelluloses and lignin after treatment with CH<sub>3</sub>COOH and HNO<sub>3</sub> or Na<sub>2</sub>SO<sub>3</sub> and NaOH, respectively, was linked to increasing formation of distinct lamellar arrangements (concentric rings parallel to each other) within the S2. This could be observed both, on fractured samples by FE-SEM as well as in ultra thin sections of non-fractured samples (Figs. 7 - 11).

For the alkali treated samples it was remarkable that a swelling without an apparent change in the carbohydrate composition had an influence on the mechanical interactions of the cell wall components during the fracture process. This is also reflected in the reduction of strength and stiffness (see Fig. 3). The decomposition of small portions of the hemicellulose glucomannan, indicated by a decrease of mannose and simultaneously an increase of glucose (compare Table 1), results in the disappearance of formerly visible radial fracture patterns. It is well established that cellulose fibrils are surrounded with hemicelluloses forming larger units which are embedded in the hemicellulose/lignin matrix (Fengel and Wegener 1989). According to the observations of Salmén and Olsson (1998) on softwoods, the hemicellulose glucomannan is closely associated with cellulose, whereas xylan seems to appear in combination with lignin. Slight solubilization of glucomannan may influence the interactions between the cellulose fibril agglomerates (visible by SEM) and the matrix constituents of the cell wall and thus the cell wall assembly. Thus, fracture mechanics and as a consequence the fracture pattern will alter. According to Fratzl et al. (2004) a tight binding between matrix and cellulose fibrils is required for wood to be strong and tough. They postulated that hemicelluloses could play a role as special interface polymers, capable of binding to the cellulose fibrils and forming aqueous networks between them.

The samples with a significant loss in hemicellulose and/or lignin proportion are strongly deformed and show a significant decrease in strength and stiffness. The increasing losses of binding components result in a complete re-arrangement of initially radial to lamellar oriented cell wall components (Fig. 11). The severe chemical treatments applied loosen the tracheid cell wall structure. A distinct proportion of hemicelluloses and lignin is dissolved, whereas the cellulose remains probably unaltered. It is known that the cellulose fibrils are aligned at an angle of 5-30 degrees (microfibril angle) to the longitudinal axis in the secondary two wall layer, e.g. Liese (1970). As the cellulose fibrils are spirally arranged in this layer, its deformation due to the chemical treatment and the fracturing process may cause the structural re-arrangement in concentric slippage planes.

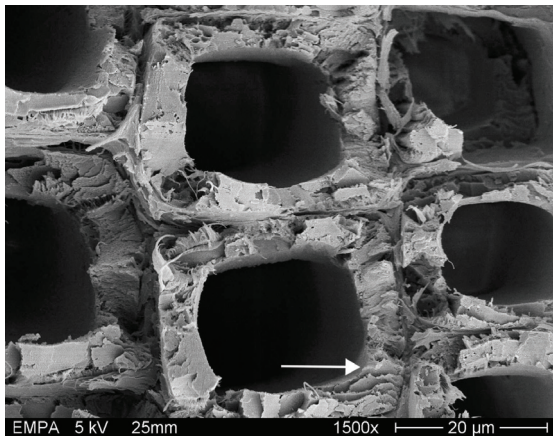


FIG. 6. FE-SEM micrograph: Transverse fracture surface (tension zone) of cell walls of spruce (transition zone early-/latewood); treated with KOH (24%, room temperature). Relatively brittle fracture surfaces, no preferential orientations in the S2 are visible. In exceptional cases radial fracture patterns were found (arrow).

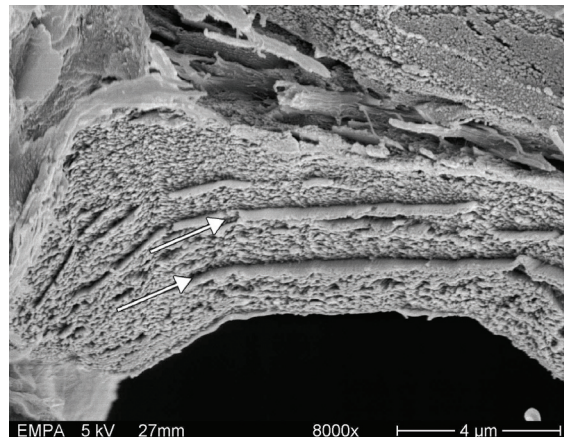


FIG. 7. FE-SEM micrograph: Transverse fracture surface (tension zone) of a cell wall of spruce (latewood); treated with NaOH (10 %, 100 °C). Within the S2 layer distinct concentric fracture patterns are discernible (arrows).

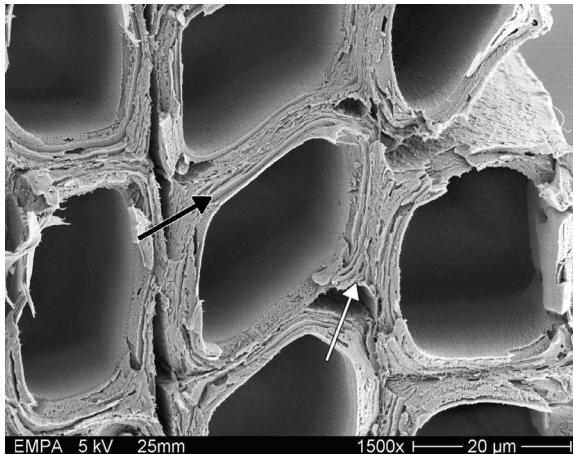


FIG. 8. FE-SEM micrograph: Transverse fracture surface (tension zone) of cell walls of spruce (transition zone early-/latewood); boiled for 30 minutes at 120 °C with CH<sub>3</sub>COOH (80 %) and HNO<sub>3</sub> (65 %) in a ratio of 10:1. Concentric lamellas within the S2 are clearly visible (arrows).

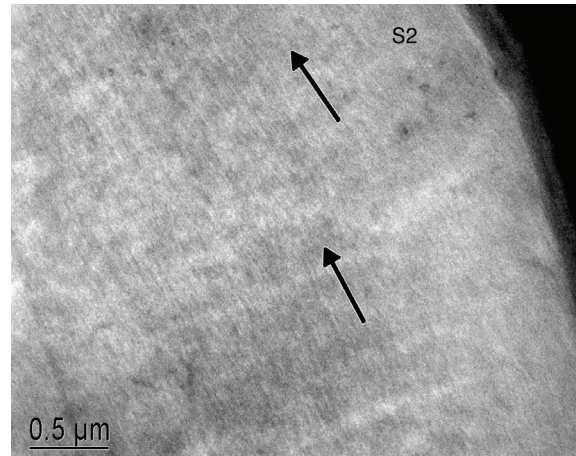


FIG. 9. TEM micrograph: Transverse ultra thin section of a latewood cell wall of spruce; boiled for 30 minutes at 120 °C with CH<sub>3</sub>COOH (80 %) and HNO<sub>3</sub> (65 %) in a ratio of 10:1. Stained with KMNO<sub>4</sub>. Concentric lamellar striations (light and dark areas parallel to the other layers) within the S2 are noticeable (arrows).

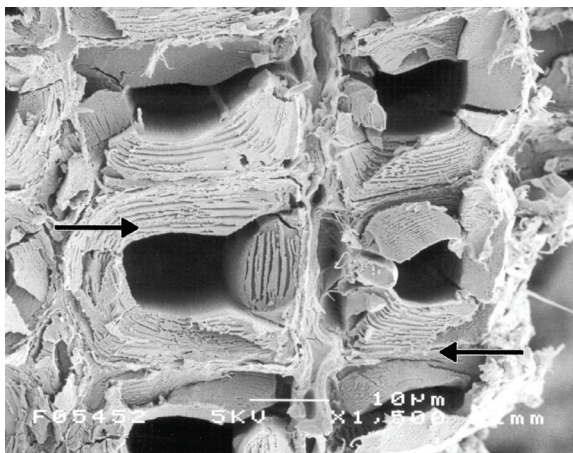


FIG. 10. FE-SEM micrograph: Transverse fracture surface (tension zone) of latewood cell walls of spruce; treatment with chemicals of ASAM pulping (Na<sub>2</sub>SO<sub>3</sub> and NaOH). Concentric lamellas within the S2 are recognizable in almost every cell wall (arrows). No radial or disordered fracture patterns could be found.

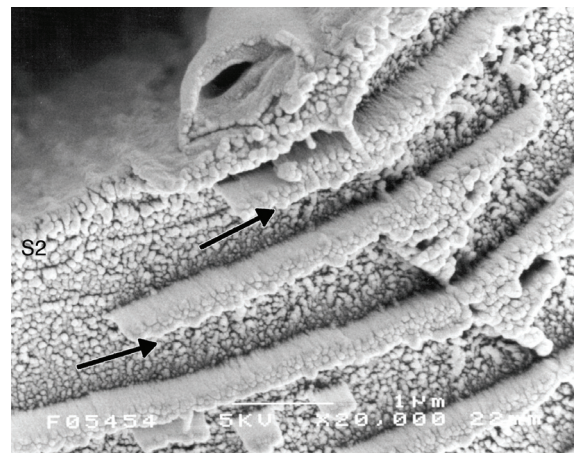


FIG. 11. FE-SEM micrograph: Transverse fracture surface (tension zone) of the S2 layer of a latewood cell wall of spruce; same sample as in Figure 8. With high magnifications, a graduation of agglomerated cellulose fibrils (slippage planes) in the circumferential direction (parallel to the compound middle lamella) is discernible (arrows).

## CONCLUSIONS

- Depending on the applied chemical treatment, transverse fracture surfaces and ultra thin sections of the S2 layer of Norway spruce tracheids showed radially, randomly or concentrically arranged cell wall constituents.



- A slight change in carbohydrate composition resulted in strength and stiffness losses. A distinct degradation of all hemicelluloses and lignin caused sample deformations as well as a sharp decline in MOE and bending strength.
- Hemicelluloses and lignin appear to be important components that are associated with fracture mechanics and the resulting fracture patterns. The fracture process and the resulting fragmentation pattern of the cell wall are very sensitive to alterations of the chemical composition of the wood cell wall.
- The hemicellulose glucomannan seems to play a special role for the interactions between the cell wall constituents. Even small losses of glucomannan influence their interactions and therefore the ultrastructural appearance of transverse sections.
- For all NaOH and KOH treatments in different concentrations no lattice conversion of cellulose (transformation of parallel cellulose I to antiparallel cellulose II) was observed. The X-ray diffraction patterns for all alkali treated samples were typical for cellulose I. Thus, mercerization and therefore changes in the lattice structure of cellulose are not the reason for the observed re-arrangements of cell wall constituents.
- The natural arrangement of the structural components in unaffected wood could not be derived from these studies.

For future studies it is of foremost importance to investigate underlying interactions of cell wall components and to understand the mechanisms of re-orientations of cell wall constituents.

#### ACKNOWLEDGEMENTS

The authors wish to thank U. Klotz (Empa, Laboratory for Joining and Interface Technology) and R. Wessicken (ETH Zürich) for support with the TEM operation. We are also grateful to D. Eckstein for critical reading as well as to O. Kordsachia and J. Puls for carrying out the total hydrolysis and analysis of the sugar composition of the hydrolysates (Federal Research Centre for Forestry and Forest Products, Hamburg, D). Thanks are due to I. Burgert and M. Eder (Max-Planck Institute of Colloids and Interfaces, Golm, D) for performing the bending tests on a special equipment for small samples. The support of E. Strub (Empa, Wood Laboratory) on the chemical treatment of the samples is gratefully acknowledged. The idea for the chemical treatments arised from a collaboration with Prof. J. Fromm, Institute for Wood Research, TU München, D.

## REFERENCES

- BOOKER, R. E., AND J. SELL. 1998. The nanostructure of the cell wall of softwoods and its functions in a living tree. *Holz Roh-Werkst.* 56:1-8.
- BORYSIK, S., AND B. DOCZEKALSKA. 2005. X-ray diffraction study of pine wood treated with NaOH. *Fibres & Textiles in Eastern Europe* 13(5):87-89.
- DANIEL, G., and T. NILSSON 1984. Studies on the S2 layer of *Pinus sylvestris*. Report 154, Department of Forest Products, Uppsala, 34 pp.
- DONALDSON, L., AND A. FRANKLAND. 2004. Ultrastructure of iodine treated wood. *Holzforschung* 58(3):219-225.
- FAHLÉN, J., AND L. SALMÉN. 2002. On the lamellar structure of the tracheid cell wall. *Plant Biology* 4(3):339-345.
- FENGEL, D., AND G. WEGENER 1989. *Wood-Chemistry, Ultrastructure, Reactions*. De Gruyter, Berlin. 613 pp.
- FRATZL, P., I. BURGERT, AND H. S. GUPTA. 2004. On the role of interface polymers for the mechanics of natural polymeric composites. *Physical Chemistry Chemical Physics* 6(24):5575-5579.
- FRATZL, P., I. BURGERT, AND J. KECKES. 2004. Mechanical model for the deformation of the wood cell wall. *Zeitschrift für Metallkunde* 95(7):579-584.
- JUNGNICKL, K. 2006. Personal Communication.
- KECKES, J., I. BURGERT, K. FRÜHMANN, M. MÜLLER, K. KÖLLN, M. HAMILTON, M. BURGHAMMER, S. VON ROTH, S. STANZL-TSCHEGG, AND P. FRATZL. 2003. Cell-wall recovery after irreversible deformation of wood. *Nature Materials* 2:810-812.
- KERR, A. J., AND D. A. I. GORING. 1975. Ultrastructural arrangement of the wood cell wall. *Cellulose Chem. and Technol.* 9:563-573.
- KIM, N.-H. 2005. An investigation of mercerization in decayed oak wood by white rot fungus (*Lentinula edodes*). *Journal of Wood Science* 51:290-294.
- KÖHLER, L., AND H.-C. SPATZ. 2002. Micromechanics of plant tissues beyond the linear-elastic range. *Planta* 215:33-40.
- LIESE, W. 1970. Elektronenmikroskopie des Holzes. In Freund, H. *Handbuch der Mikroskopie in der Technik*. Umschau-Verlag, Frankfurt. pp. 109-170.
- LONIKAR, S. V., N. SHIRAISHI, AND T. YOKOTA. 1984. Effect of the Loosening of the Wood Texture on the Mercerization of Cellulose in Wood. *Journal of Wood Chemistry and Technology* 4(4):483-496.
- MANSIKKAMÄKI, P., M. LAHTINEN, AND K. RISSANEN. 2005. Structural changes of cellulose crystallites induced by mercerisation in different solvent systems; determined by powder X-ray diffraction method. *Cellulose* 12:233-242.

- MATTHECK, C. 1991. Trees, the mechanical design. Springer, Berlin, Heidelberg, New York.
- NISHIYAMA, Y., S. KUGA, AND T. OKANO. 2000. Mechanism of mercerization revealed by X-ray diffraction. *Journal of Wood Science* 46:452-457.
- OKANO, T., AND A. SARKO. 1984. Mercerization of Cellulose. I. X-Ray Diffraction Evidence for Intermediate Structures. *Journal of Applied Polymer Science* 29:4175-4182.
- REVOL, J.-F., AND D. A. I. GORING. 1981. On the Mechanism of the Mercerization of Cellulose in Wood. *Journal of Applied Polymer Science* 26:1275-1282.
- REYNOLDS, E. S. 1963. The use of lead citrate at high pH as an electron-opaque stain in electron microscopy. *Journal of Cell Biology* 17:208.
- RUEL, K. F., AND D. A. I. GORING. 1978. Lamellation in the S2 layer of softwood tracheids as demonstrated by scanning transmission electron microscopy. *Wood Sci. Technol.* 12:287-291.
- SALMÉN, L., AND A. M. OLSSON. 1998. Interaction between hemicelluloses, lignin and cellulose: Structure-property relationships. *Journal of pulp and paper science* 24(3):99-103.
- SCHWARZE, F. W. M. R., AND J. ENGELS. 1998. Cavity formation and the exposure of peculiar structures in the secondary wall (S-2) of tracheids and fibres by wood degrading basidiomycetes. *Holzforschung* 52(2):117-123.
- SELL, J. 1989. Eigenschaften und Kenngrößen von Holzarten. Baufachverlag AG, Zürich. 80 pp.
- SELL, J., AND T. ZIMMERMANN. 1993. Radial fibril agglomerations of the S2 on transverse-fracture surfaces of tracheids of tension-loaded spruce and white fir. *Holz Roh-Werkst.* 51:384.
- \_\_\_\_\_. 1998. The fine structure of the cell wall of hardwoods on transverse- fracture surfaces. *Holz Roh-Werkst.* 56(5): 365-366.
- SINGH, A. P., AND G. DANIEL. 2001. The S2 layer in the tracheid walls of *Picea abies* wood: Inhomogeneity in lignin distribution and cell wall microstructure. *Holzforschung* 55(4): 373-378.
- SPURR, A. R. 1969. A Low-Viscosity Epoxy Resin Embedding Medium for Electron Microscopy. *Journal of Ultrastructure Research* 26(1-2): 31 ff.
- UREMOVIC, A., T. DOKK GLAWISCHNIG, J. SCHUSEIL, B. SAAKE, A. BORCHMANN, A. HERRMANN, AND J. PULS. 1994. Chromatographische Untersuchungen zur quantitativen Bestimmung der Holzzucker. *Holz Roh-Werkst.* 52:347-354.

ZIMMERMANN, T., V. THOMMEN, P. REIMANN, AND H. J. HUG. 2006. Ultrastructural appearance of embedded and polished wood cell walls as revealed by Atomic Force Microscopy. *Journal of Structural Biology* 156:363-369.





## Paper D



dioxide and nitric acid. The wafers were stored for several days under these conditions and the changes were observed by measuring the water contact angle in air using a Gonionometer from Dataphysics (OCA 15+).

Received: December 21, 2003

Final version: June 11, 2004

- [1] S. Schultz, G. Wagner, J. Ulrich, *Chem. Ing. Tech.* **2002**, 74, 901.
- [2] V. Schröder, H. Schubert, *Colloid Surface A* **1999**, 152, 103.
- [3] S. M. Joscelyne, G. Trägårdh, *J. Membr. Sci.* **2000**, 169, 107.
- [4] V. Schröder, O. Behrend, H. Schubert, *J. Colloid Interf. Sci.* **1998**, 202, 334.
- [5] S. M. Joscelyne, G. Trägårdh, *J. Food Eng.* **1999**, 39, 59.
- [6] K. Kandori, in *Food Processing: Recent Developments* (Ed.: A. G. Ganokar), Elsevier Science **1995**, Chapter 7.
- [7] N. C. Christov, D. N. Ganchev, N. D. Vassileva, N. D. Denkov, K. D. Danov, P. A. Kralchevsky, *Colloid Surface A* **2002**, 209, 83.
- [8] G. T. Vladislavjevic, H. Schubert, *Desalination* **2002**, 144, 167.
- [9] I. Kobayashi, M. Yasuno, S. Iwamoto, A. Shono, K. Satoh, M. Nakajima, *Colloid Surface A* **2002**, 207, 185.
- [10] G. T. Vladislavjevic, S. Tesch, H. Schubert, *Chem. Eng. Process.* **2002**, 41, 231.
- [11] A. J. Abrahamse, R. van Lierop, R. G. M. van der Sman, A. van der Padt, R. M. Boom, *J. Membrane Sci.* **2002**, 204, 125.
- [12] C. J. M. van Rijn, M. C. Elwenspoek, *IEEE proc. MEMS* **1995**, 83.
- [13] B. V. Zhmud, J. Sonnefeld, L. Bergström, *Colloid Surface A* **1999**, 158, 327.
- [14] R. Maboudian, W. R. Ashurst, C. Carraro, *Tribol. Lett.* **2002**, 12, 95.
- [15] M. H. Hu, S. Noda, T. Okubu, Y. Yamaghuchi, H. Komiyama, *Appl. Surf. Sci.* **2001**, 181, 307.
- [16] V. V. Tsukruk, I. Luzinov, D. Julthongpiput, *Langmuir* **1999**, 15, 3029.
- [17] B. C. Bunker, R. W. Carpick, R. A. Assink, M. L. Thomas, M. G. Hankins, J. A. Voigt, D. Sipola, M. P. de Boer, G. L. Gulley, *Langmuir* **2000**, 16, 7742.
- [18] U. Srinivasan, M. R. Houston, R. T. Howe, R. Maboudian, *J. Microelectromech. S.* **1998**, 7, 252.
- [19] G. J. Kluth, M. M. Sung, R. Maboudian, *Langmuir* **1997**, 13, 3775.
- [20] M. M. Sung, G. J. Kluth, R. Maboudian, *J. Vac. Sci. Technol. A* **1999**, 17, 540.
- [21] W. R. Ashurst, C. Carraro, R. Maboudian, W. Frey, *Sens. Act. A* **2003**, 104, 213.
- [22] B. H. Kim, T. D. Chung, C. H. Oh, K. Chun, *J. Microelectromech. S.* **2001**, 10, 33.
- [23] K. Iimura, T. Kato, *Colloid Surface A* **2000**, 171, 249.

- [24] M.-W. Tsao, J. F. Rabolt, H. Schönherr, D. G. Castner, *Langmuir* **2000**, 16, 1734.
- [25] S. R. Wasserman, Y.-T. Tao, G. M. Whitesides, *Langmuir* **1989**, 5, 1074.
- [26] M. D. Lechner, K. Gehrke, E. H. Nordmeier, *Makromolekulare Chemie*, Birkhäuser Verlag, **1993**.
- [27] C. J. M. van Rijn, *Nano and Micro Engineered Membrane Technology*, Elsevier Science, **2004**.
- [28] L. Baberi, G. Kulik, H.-J. Mathieu, P. Hoffmann, Presentation, *Euromat* **2003**, Lausanne.

## Cellulose Fibrils for Polymer Reinforcement\*\*

By Tanja Zimmermann,\* Evelyn Pöhler and Thomas Geiger

Lignocellulosic fibres obtained from renewable resources such as wood become of more and more interest as reinforcing components in composites,<sup>[1,2]</sup> because they are biodegradable and harmless for the ecological system. Furthermore, they have promising mechanical properties and are less expensive than conventional synthetic fibres.

Within the different cell wall layers of fibres the high tensile-strength cellulose exists as a system of fibrils embedded in the matrix substance lignin. Depending on the break down by disintegration processes the dimensions of the partly crystalline fibrils of wood vary as it is shown in Figure 1. Fibrils have diameters in the nanometer and lengths in the micrometer scale.

[\*] T. Zimmermann, E. Pöhler  
Swiss Federal Laboratories for Materials Testing and Research  
Wood Laboratory  
Ueberlandstrasse 129, CH-8600 Dübendorf, Switzerland  
E-mail: Tanja.Zimmermann@EMPA.CH

Dr. Th. Geiger  
Swiss Federal Laboratories for Materials Testing and Research  
Laboratory for Functional Polymers  
Ueberlandstrasse 129, CH-8600 Dübendorf, Switzerland

[\*\*] We thank J. Schleuniger for his support and advice on the disintegration of cellulose fibers and the tensile tests. Thanks are due to K. Weiss for his support on the evaluation of the data and to F. Ammann for the determination of the polymerisation degrees. We are also grateful to P. Gasser for his electron microscopical help and to D. Eckstein, R. Klingner, K. Richter, F.W.M.R. Schwarze and J. Sell for helpful suggestions and comments on the manuscript.  
This work was supported by the Commission for Technology and Innovation (KTI).

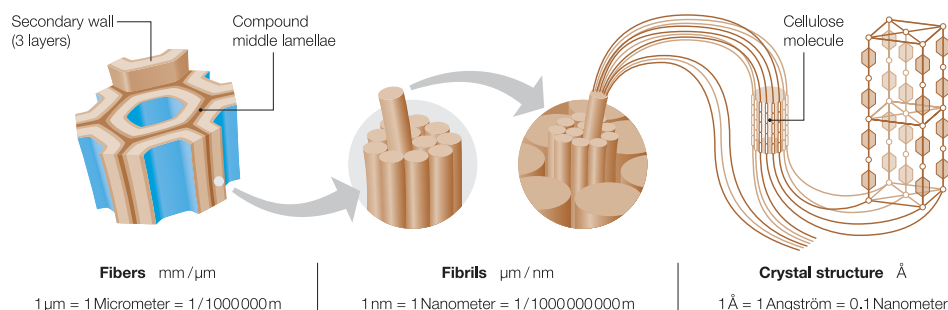


Fig. 1. Scheme of a wood cell wall showing the compound middle lamella (middle lamella and primary wall), and three layers of the secondary wall. Cellulose, the principal component of the cell wall, exists as a system of fibrils. Parts of the fibrils are arranged in an orderly fashion and provide crystalline properties to the wall (in the style of [3])

Each fibril can be considered as a chain of crystalline units, linked together by amorphous domains.<sup>[4]</sup> The modulus of elasticity of the perfect crystal of native cellulose was calculated by different authors<sup>[5–9]</sup> and estimated between 130 GPa up to 250 GPa. The tensile strength of the crystal structure was assessed to be approximately 0.8 GPa up to 10 GPa (Tab. 1).

To use the potential of fibrils, the fragmentation of cellulose fibres into smaller units has been attempted many times. The literature differentiates between two products. The Microfibrillated Cellulose (MFC) is a form of expanded high-volume cellulose, obtained through a mechanical homogenisation process of e.g. wood pulp.<sup>[10,11]</sup> The Microcrystalline Cellulose (MCC) is generated by chemical treatment of various plant fibres.<sup>[10–12]</sup> After dissolving or degrading of the accessible amorphous regions, the crystalline regions remain. MFC with aspect ratios (fiber length divided by diameter) between 50 and 100<sup>[13]</sup> and MCC with aspect ratios of about 3<sup>[13]</sup> are normally not used for reinforcement purposes. However, they form a stable gel which is used as paint or ink thickener, pharmaceutical tablet binder or rheology-control agent in food.

Table 1. Interrelation between structure, disintegration process, the obtained component, the modulus of elasticity and the tensile strength (modified after [6]).

Disintegration process	Component	Modulus of elasticity	Tensile strength
pulping	wood	10 GPa	100 MPa
mechanical/chemical dissolving	fibre	40 GPa	400 MPa
mechanical/chemical dissolving	fibre	70 GPa	700 MPa
	crystal structure	130 – 250 GPa	800–10000 MPa

Some studies report on cellulose whiskers or fibrils obtained from organic materials like sugar beet pulp,<sup>[14,15]</sup> potato tuber cells,<sup>[16]</sup> wheat straw,<sup>[17,18]</sup> tunicin<sup>[19–23]</sup> or crab shell chitin.<sup>[24]</sup> These whiskers or fibrils were used as reinforcement components in synthetic polymers and biopolymers for the production of films and lacquers. Depending on the portion of cellulose, the composites showed improved mechanical properties. A review of cellulose based nanocomposites is given by Berglund.<sup>[25]</sup>

The production of cellulose nanocomposites with fibrils of a high aspect ratio for load-bearing applications is fairly new. In particular, the possible fields of application of cellulose fibrils separated from wood pulp were hardly investigated. Wood as basis material for the extraction of cellulose fibrils offers next to the expected high strength advantages like low costs and a constant availability.

Although there are several studies on the separation of cellulose fibrils from plant fibres or special sea animals, certain problems are not sufficiently solved: The disintegration of cellulose without severe degradation and at reasonable cost is still difficult. Another problem is the dispersion of cellulose fibrils in polymer matrices, especially when they are hydrophobic.

The objective of our investigations was to separate cellulose fibrils from sulphite wood pulp with ordinary methods at the greatest possible lengths and diameters below 100 nm without severe degradation. Furthermore, the suitability of the obtained fibrils for the reinforcement of polymers was tested.

#### Materials and Methods:

The following steps were carried out in the project:

- Separation of cellulose fibrils or fibril bundles from sulphite pulp by a combination of chemical and/or mechanical processes.
- Electron microscopical and chemical characterisation of the obtained fibrils or fibril bundles.
- Reinforcement of polymers with the obtained fibrils and their mechanical and morphological investigation.

**Separation of cellulose fibrils:** As basis material sulphite pulp (mainly composed of softwood tracheids) from the Company Booregard was used.

Table 2. Mixing ratio polymer/fibrils

Polymer	Fibril content <sup>[a]</sup>			
	1%	5%	10%	20%
Polyvinyl alcohol (PVA)	x	x	x	—
Hydroxypropyl cellulose (HPC)	x	x	x	x

[a] weight percent based on the weight of the polymer

**Mechanical separation:** 5 g of wet sulphite pulp with a dry content of 30 % was dispersed in 300 ml of deionised water. The suspension was treated with an ultra-turrax (FA IKA; 24000 rpm, 8 h) to separate the fibril bundles from the wooden cell wall. A dispersing and homogenisation of the cellulose fibrils was achieved by application of a microfluidizer M-100 y (FA Microfluidics; 1000 bar, 60 min).

**Chemical/mechanical separation:** 5 g of oven dried pulp was weighted in a 200 ml solution of sulphuric acid (10 wt %) and stirred at 60 °C for 16 h. The obtained suspension was centrifugated (5000 rpm) and washed several times in deionised water. Afterwards the solution was neutralised with sodium hydroxide (0.1 N) and homogenised with a microfluidizer M-100 y (FA Microfluidics; 1000 bar, 60 min).

**Morphological characterisation:** For the morphological characterisation the following electron microscopes were used:

Field-Emission Scanning Electron Microscope (FE-SEM, Jeol 6300 F)

Transmission Electron Microscope (TEM, Philips CM30)

For the preparation of samples for FE-SEM, glimmer plates were fixed with a conducting carbon on a specimen holder. A drop of a diluted fibril/water suspension (1:20) was put on the glimmer plate. The samples were air-dried and the remaining fibrils were sputtered with a platinum layer of about 5 nm.

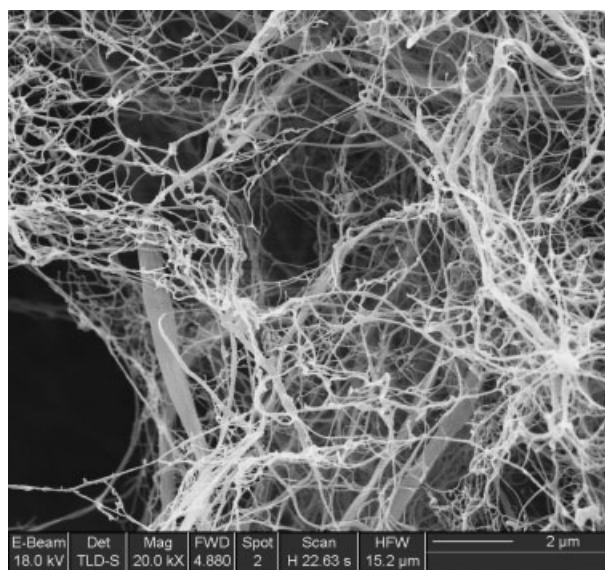
For TEM investigations uncoated 300 mesh copper grids were drawn through the fibril suspension (see above). The sticked fibrils were stained with 1 wt % uranyl acetate.

**Chemical characterisation:** The wood pulp as reference material and the fibrils were dried for 16 h at a temperature of 105 °C. A defined portion of cellulose (about 50 mg) was solved in acetone. From the pure solvents and also from the testing solutions the running time through a marked distance of a viscosimeter was determined. The viscosity number as well as the degree of polymerisation (DP) of the cellulose was then calculated by the obtained running times and the defined cellulose portion.<sup>[26]</sup>

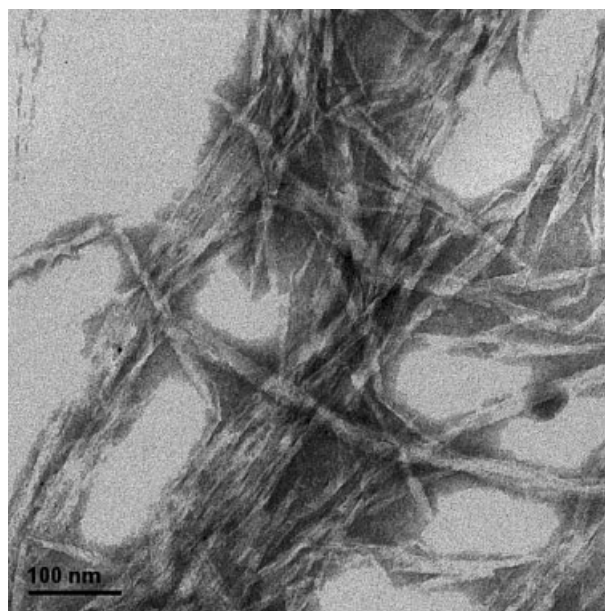
**Dispersion into polymers:** Two water soluble polymers were used: Polyvinyl alcohol (PVA, FA Aldrich) with an average molecular weight of 85000–146000 g/mol and low viscosity hydroxypropyl cellulose (HPC, FA Aqualon). Fibril solutions with different solid contents obtained by mechanical or chemical/mechanical separation were mixed with the two polymers at a temperature of 60 °C (Tab. 2). The achieved suspensions were casted in a silicone form and dried at room

temperature (23 °C) and a relative humidity of 50 % for seven days (solution casting method). Films out of pure cellulose fibril suspensions were also prepared. Samples for tensile tests were stamped out of the produced films after EN ISO 527-4.<sup>[27]</sup>

**Mechanical tests:** With the obtained films tensile tests were conducted after EN ISO 527-4.<sup>[27]</sup> The tests were carried out at 20 °C/65 % r.H. and a loading speed of 50 mm/min with



(a)



(b)

Fig. 2. (a) FE-SEM micrograph: Mechanically isolated cellulose fibrils and fibril bundles out of sulphite pulp. A fibril network with single filaments with thicknesses in the nanometer range and estimated lengths of several tens of micrometers becomes visible. (b) TEM micrograph: Chemically and mechanically isolated cellulose fibrils out of sulphite pulp. Fibril structures with diameters below 50 nanometers become visible. The lengths are still in the range of micrometers.



an universal testing machine Zwick Z010. For the measurement of the tensile strength a 200 N load cell was chosen. The strain was determined by the longitudinal motion of the testing machine. From the obtained results stress-strain diagrams and bar charts were drawn. The tensile fracture surfaces were characterised by FE-SEM.

#### Results and Discussion

**Morphological characterisation:** Mechanical dispersion of pulp fibres leads to fibril structures with diameters between 20 and 100 nm and estimated lengths of several tens of micrometers. Due to the expected high density of hydroxyl groups at the fibril surface, they strongly interact and tend to agglomerate. Thus, a network of single fibril filaments becomes visible on SEM micrographs after preparation on glimmer plates (Fig. 2a).

Chemical breakdown with sulphuric acid combined with mechanical dispersion results in even finer fibril structures with diameters below 50 nanometers (Fig. 2b). Accordingly, the fibrils become shorter but their length is still in the range of micrometers. We suggest that the finer and shorter fibrils interact to a lower extent, consequently the fibrils are not as strong networked than the ones treated solely mechanically. Furthermore, less fibril agglomerations could be observed.

In the presented study fibrils with diameters clearly below 100 nm and a high aspect ratio could be isolated from sulphite pulp purely mechanically. For the disintegration process an ultra-turrax and a microfluidizer were used. Taniguchi and Okamura<sup>[28]</sup> also used wood pulp and a super-grinding method to obtain fibrils with diameters in the range of 20 to 90 nm. The method consists of a simple mechanical treatment which is designed to expose shearing-stress to the longitudinal fibre axis of the fibre samples. The same principle acts in our study by using a microfluidizer that separates the fibrils under high pressure and therefore also applies shearing-stress to the fibre axis. The resulting fibril dimensions are similar in both methods. Turbak et al.<sup>[11]</sup> and Herrick et al.<sup>[10,29]</sup> — who introduced MFC — also obtained fibrillar structures with diameters in the range 25–100 nm from wood pulp after a homogenisation process.

A chemical disintegration of sulphite pulp led in our investigation to fibril diameters clearly below 50 nm. This is concordant with whisker or fibril diameters determined in other studies after the hydrolysis of various plant fibres or tunicin. Chanzy et al.,<sup>[20]</sup> e.g., isolated fibrils out of tunicin with diameters of approximately 2–30 nm and estimated aspect ratios greater than 60. Wu et al.<sup>[30]</sup> used cellulose crystals obtained by acid sulphuric hydrolysis of cellulose fibres with diameters of about 50 nm. A dependence on acid concentration, disintegration temperature and time seems obvious.

In our study, the mechanically isolated fibrils interacted and formed networks that were well observable by SEM. The shorter fibrils, obtained after disintegration with sulphuric acid seemed to interact to a lower extend. The importance of percolating network formation for a high reinforcement efficiency even with small amounts of cellulose is a main theme

Table 3. The degree of polymerisation of the reference material sulphite pulp and the fibrils disintegrated mechanically or chemically.

Disintegration	DP
Sulphite Pulp (Reference)	1381
Fibrils: 8 h ultra-turrax, 60 min microfluidizer	643
Fibrils: H <sub>2</sub> SO <sub>4</sub> (10 wt %), 16 h mixed, neutralised with NaOH; 60 min microfluidizer	304

in many studies carried out with fibrils obtained from different organic fibers (not wood pulp).<sup>[17,18,31]</sup> However, the studies did not illustrate the network formation until now. A strong cellulose network formation seems to be intimately associated with the solution casting method that is also used in our study. Probably, a special filling threshold for the formation of such networks is necessary. Well dispersed and homogenized cellulose fibrils form a stable gel.<sup>[11]</sup> This observation leads to the suggestion of a high complexity of cellulose microfibril organisation in aqueous suspensions with physical crosslinkage and support the evidence for fibril network formation. It would be interesting to find a method that could analyse whether the fibril networks are still intact after casting the films. Thus, we are planning TEM investigations on fibril and fibril/polymer films to visualise the fibril arrangement.

**Chemical characterisation:** Table 3 shows the degrees of polymerisation (DP) of the basis material (sulphite pulp) and of samples disintegrated either mechanically or chemically.

The degree of polymerisation (DP) of the basis material sulphite pulp is around 1400. After mechanical isolation of cellulose fibrils the DP decreases by about 50 %. A chemical disintegration with sulphuric acid leads to a stronger drop of the DP of about 80 %. This could be explained by the degradation of amorphous domains in cellulose. Anyhow, the fibril lengths are still in the range of micrometers (see above). After Battista,<sup>[32]</sup> the DP correlates strongly with the aspect ratio of the fibril. Thus, the longer fibrils obtained in our study by mechanical disintegration and even the fibrils isolated by a comparatively mild hydrolysis process have much higher DPs than MCC (DP 145<sup>[13]</sup>).

**Mechanical tests:** The fibril/polymer solutions could be casted to homogeneous and translucent films with thicknesses between 0.04 and 0.1 mm. Pure fibril films had thicknesses around 0.01 mm.

The results of the tensile tests are presented in Figures 3,4. The stiffness of the polyvinyl alcohol composites (PVA) was higher than the stiffness of the hydroxypropyl cellulose composites (HPC). This can be explained by a higher stiffness of pure PVA compared to pure HPC. Remarkably, PVA samples initially showed a very stiff and then abruptly a ductile behaviour. All together the variation was higher with the PVA-composites. HPC-composites showed a more homogeneous behaviour. Even though the fibrils are oriented at random in

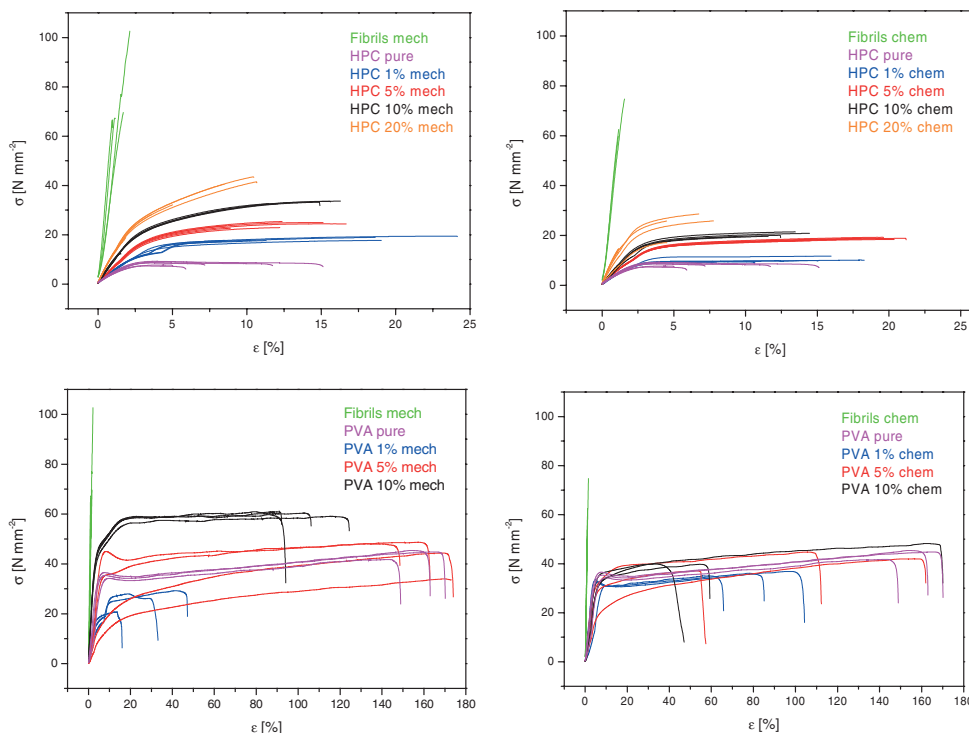


Fig. 3. Stress-strain diagrams of films out of HPC or PVA and different portions of cellulose fibrils.

the matrix material, the Modulus of Elasticity (MOE) arises for the composites with mechanically isolated fibrils up to a factor of 2.5 (fibril content 10 wt %) for the PVA-composites and up to a factor of 3 (fibril content 20 wt %) for the HPC-composites compared to the unfilled polymers. The tensile strength even showed an up to fivefold increase. Pure films of cellulose fibrils are reaching almost the strength properties of clear wood. Over all, the mechanically isolated fibrils with comparatively high DPs showed a better performance than the chemically isolated ones.

With a fibril portion of 1 or 5 % no reinforcing effect or increase in MOE at all could be obtained in the case of the PVA-composites. With the assumption that networked fibrils lead to a higher reinforcing effect than discrete fibrils, possibly no network formation took place. Probably, it needs a higher filling threshold to induce intense interactions between the fibrils and thus the formation of networks. Anyhow, the polymer HPC showed even with a filling threshold of 1 % an improved tensile strength and MOE. One must be aware that the elongation was determined by the longitudinal motion of the testing machine. For following studies it would be reasonable to use specific optical strain measurement methods.

In various studies cellulose microcrystals or whiskers with low aspect ratios were isolated from different natural fibres like wheat straw, tunicin or potato tuber cells for the production of nanocomposites using different synthetic or natural amorphous polymer matrices.<sup>[17,31,33]</sup> In most of the cases, the mechanical properties could be substantially improved depending on the amount and a homogeneous dispersion of the cellulose filler.

Nanocomposites containing fibrils isolated from wood pulp with higher aspect ratios were produced to a lesser extent. Taniguchi and Okamura<sup>[28]</sup> obtained by high pressure homogenisation of wood pulp Microfibrillated Cellulose (MFC). Out of this material they produced films without using an organic solvent. The films obtained had about 3–100  $\mu\text{m}$  thickness and were homogeneous and translucent. The tensile strength of films based on wood pulp MFC was 2.4 times that of commercial print grade paper and 2.7 times that of polyethylene. The determined values for the tensile strengths were not specified. In our studies pure films of randomly oriented cellulose fibrils obtained a tensile strength like clear wood between 80 and 100 MPa. However, both results indicate the high reinforcing potential of the fibrils.

A few studies are dealing with the production of cellulose nanocomposites with hydrophobic matrices.<sup>[13,30,34,35]</sup> Wu and Berglund<sup>[30]</sup> synthesized a polyurethane/cellulose nanocomposite containing 3, 5 and 10 wt % cellulose. The cellulose fibrils obtained by acid sulphuric hydrolysis were almost homogeneously dispersed into the polyurethane matrix. For the nanocomposite with 5 wt % cellulose loading they found a 1.6-fold increase in modulus, a 2-fold increase in tensile strength and a 1.5-fold increase in the elongation to rupture as compared to that of pure PU. Therefore, it was possible to improve the mechanical properties and elastomeric properties synergistically. Frequently, filler addition is accompanied by increasing strength and stiffness at the expense of reduced elongation to rupture.<sup>[36]</sup> Also in our study it is remarkable that the modulus of elasticity next to the tensile strength could be increased for composites using water soluble poly-

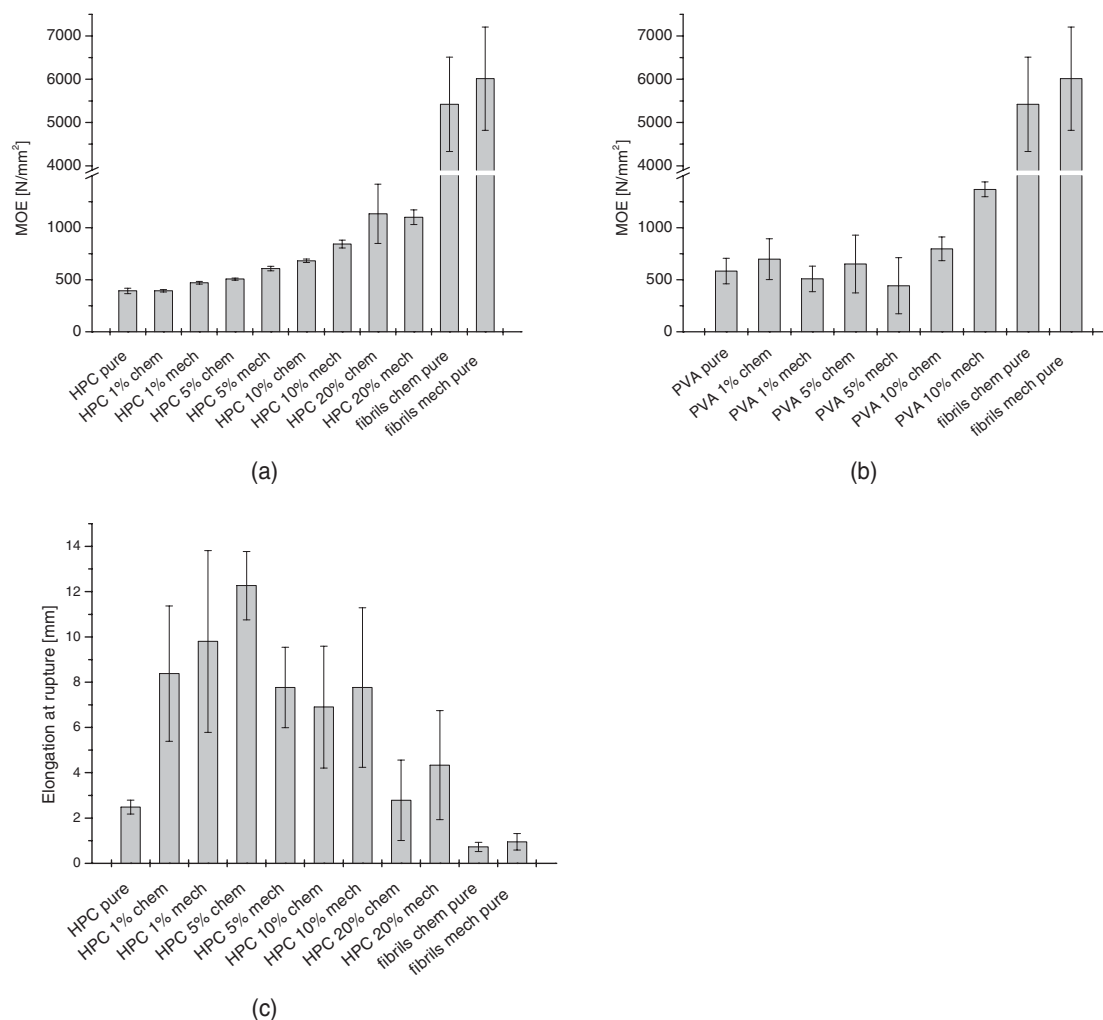


Fig. 4. (a,b). Modulus of Elasticity of the composites with different fibril portions based on the pure polymers HPC and PVA (6 samples per variant). The standard deviation is indicated by error bars. (c). Elongation to rupture for HPC composites (6 samples per variant). The standard deviation is indicated by error bars.

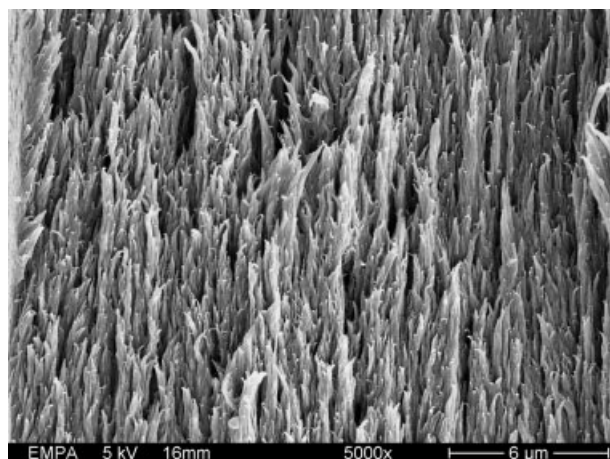
mers. In our case the MOE of HPC could be increased up to 3 times with 20 wt % of mechanically isolated cellulose fibrils. A 5-fold rise of the elongation to rupture was achieved with a loading of 5 wt % of chemically disintegrated fibrils (Fig. 4(c)). Thus, the values were much higher than found by Wu et al.<sup>[30]</sup> Even with a loading of 10 or 20 wt % of cellulose fibrils the elongation to rupture was up to 3 times higher compared to the pure polymer.

Different studies and also our own results show a high reinforcing effect of cellulose whiskers or fibrils for various matrices. Some studies are available where fibrils obtained from wood pulp were embedded in organic matrices but water soluble polymers like in our study were not used until now. Due to the high density of hydroxyl groups at the fibril surfaces we had little problems to disperse the fibrils in the polymer matrices.

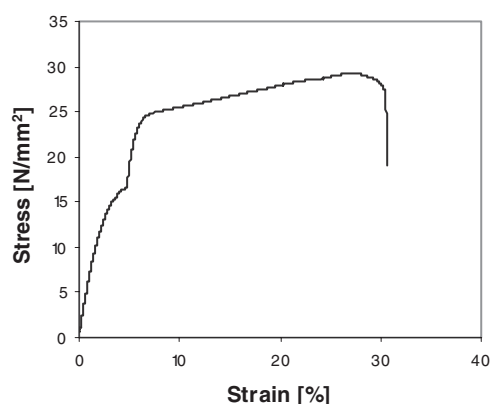
The DP of the cellulose and thus the aspect ratio appears to play an important role for the mechanical properties of the composites. For mechanically isolated fibrils it seems that the fibrillation works predominantly in longitudinal direction so

that only little transverse cutting of the fibrils takes place, keeping the inherent tensile strength of the fibrils intact and resulting in a larger surface area per mass unit. Due to the larger surface area of the fibrils, stronger hydrogen bonding can be expected and a probable network formation enhances the tensile strength when the film is dried. This could be the reason for a higher reinforcing effect found for purely mechanically isolated compared to additionally chemically isolated fibrils. The good mechanical performance and particularly the high elongation to rupture also could benefit from the interfacial coupling or a crosslinking between cellulose and polymer matrix. Tensile fracture surfaces of reinforced PVA show that the fibrils seem to be surrounded by the matrix material (Fig. 5a). Furthermore, after fracturing, the fibrils are aligned into the testing direction. Thus, an intended alignment of multidirectional embedded fibrils in PVA might be conceivable by a preloading. Interesting is also the stress-strain diagram of some of the tensile samples (Fig. 5b). After a slow drop of the curve an anew increase takes place, possibly indicating the alignment of the initially multidirectional





(a)



(b)

Fig. 5. (a) FE-SEM micrograph: Tensile fracture surface of polyvinyl alcohol with a cellulose fibril portion of 10 wt %. (b) Stress-strain diagram of polyvinyl alcohol with a cellulose fibril portion of 1 wt %.

embedded fibrils that leads to a restiffening of the composite. These features could not be observed with HPC composites.

**Conclusions:** According to the main aim of the study, cellulose fibrils were separated from wood fibres. Further, the usability of the obtained fibril structures as reinforcement material for two polymers was shown.

From the results it is concluded that cellulose fibrils with diameters below 100 nm can be isolated out of sulphite pulp by a combination of chemical and/or mechanical processes. According to the isolation process, the fineness of the fibrils varies.

Mechanical dispersion of the pulp leads to fibril structures without severe degradation and diameters between 20 and 100 nm and estimated lengths of several tens of micrometers.

Chemical breakdown with sulphuric acid combined with mechanical dispersion results in even finer fibril structures with diameters below 50 nm. Accordingly, the fibrils become shorter but their length is still in the range of micrometers.

The high Modulus of Elasticity (MOE) as well as the good aspect ratio of cellulose fibrils are ideal requirements for a reinforcing application in polymers. Thus, fibril reinforced

PVA and HPC show - compared with the basis material - a up to 3 times higher MOE and a 5 times higher tensile strength. Pure films of cellulose fibrils are reaching almost the strength properties of clear wood. Remarkably is the fivefold increase of the elongation to rupture for the HPC composites with a fibril loading of 5 %.

Application areas of fibrils are supposable in biopolymers where degradability and at the same time a high strength and visual transparency are required (e.g. medicine, gardening etc.). Further, the fibrils could be used in adhesives (e.g. instead of synthetic fibres) to improve systematically their application and exploitation as well as thermal creep. Due to their ability to form aqueous gels, cellulose fibrils could also be used as rheological modifier e.g. in water-borne coatings.

In the next steps, larger quantities of cellulose fibrils will be produced and the embedding process into different polymers will be optimized. The morphological, mechanical and chemical properties of the different obtained pilote products will be determined.

- [1] A. K. Bledzki, J. Gassan, *Progr. Polymer Sci.* **1999**, 24, 221.
- [2] S. J. Eichhorn, C. A. Baillie, N. Zafeiropoulos, L. Y. Mwaikambo, M. P. Ansell, A. Dufresne, K. M. Entwistle, P. J. Herrera-Franco, G. C. Escamilla, L. Groom, M. Hughes, C. Hill, T. G. Rials, P. M. Wild, *J. Mater. Sci.* **2001**, 36, 2107.
- [3] P. H. Raven, R. F. Evert, S. E. Eichhorn, *Biology of Plants*, Freeman and Company, New York, **2000**.
- [4] D. Fengel, G. Wegener, *Wood – Chemistry, Ultrastructure, Reactions*, Walter de Gruyter, Berlin, New York, **1989**.
- [5] M. G. Northolt, H. de Vries, **1985**, 133, 183.
- [6] A. J. Michell, in *Composites Asia Pacific 89*, Composites Institute of Australia, Adelaide, Australia, **1989**, pp. 66.
- [7] I. Sakurada, Y. Nukushina, I. Ito, *J. Polymer Sci.* **1962**, 651.
- [8] S. A. Wainwright, W. D. Biggs, J. D. Currey, J. M. Gosline, Princeton University Press, Princeton, **1982**.
- [9] K. Tashiro, M. Kobayashi, *Polymer* **1991**, 32, 1516.
- [10] F. W. Herrick, R. L. Casebier, J. K. Hamilton, K. R. Sandberg, *J. Appl. Polymer Sci. Appl. Polymer Symp.* **1983**, 37, 797.
- [11] A. F. Turbak, F. W. Snyder, K. R. Sandberg, *J. Appl. Polymer Sci. Appl. Polymer Symp.* **1983**, 37, 815.
- [12] A. F. Turbak, F. W. Snyder, K. R. Sandberg, in *United States Patent*, International Telephone and Telegraph Corporation, New York, US, **1983**.
- [13] A. Boldizar, C. Klason, J. Kubat, P. Naslund, P. Saha, *Int. J. Polymeric Mater.* **1987**, 11, 229.
- [14] E. Dinand, H. Chanzy, M. R. Vignon, *Food Hydrocolloids* **1999**, 13, 275.
- [15] L. Heux, E. Dinand, M. R. Vignon, *Carbohydrate Polymers* **1999**, 40, 115.

- [16] M. N. Angles, A. Dufresne, *Macromol.* **2001**, 34, 2921.
- [17] W. Helbert, J. Y. Cavaille, A. Dufresne, *Polymer Composites* **1996**, 17, 604.
- [18] A. Dufresne, J. Y. Cavaille, W. Helbert, *Polymer Composites* **1997**, 18, 198.
- [19] M. N. Angles, A. Dufresne, *Macromol.* **2000**, 33, 8344.
- [20] H. Chanzy, B. Ernst, J.-Y. Cavaille, V. Favier, Elf Atochem. S. A., France, United States Patent, **2000**.
- [21] A. Dufresne, *Composite Interfaces* **2000**, 7, 53.
- [22] V. Favier, G. R. Canova, J. Y. Cavaille, H. Chanzy, A. Dufresne, C. Gauthier, *Polymers Adv. Technol.* **1995**, 6, 351.
- [23] V. Favier, H. Chanzy, J. Y. Cavaille, *Macromol.* **1995**, 28, 6365.
- [24] K. G. Nair, A. Dufresne, *Biomacromol.* **2003**, 4, 657.
- [25] L. A. Berglund, (Ed.: M. A. D. Mohanty), CRC Press LLC, **2004**.
- [26] Anonymus, *ISO 5351/2*, **1981**.
- [27] Anonymus, *ISO 527-4*, **1997**.
- [28] T. Taniguchi, K. Okamura, *Polymer Int.* **1998**, 47, 291.
- [29] F. W. Herrick, United States Patent, **1984**.
- [30] Q. Wu, X. Liu, L. A. Berglund, in *Proc. 23rd Riso International Symposium on Material Science: Sustainable Natural and Polymeric Composites - Science and Technology* (Ed.: H. Lilholt, Madsen, B., Toftegaard, H. L., Cendre, E., Megnis, M., Mikkelsen, L. P., Sorensen, B. F.), Riso National Laboratory, Roskilde, Denmark, **2002**, pp. 107.
- [31] P. Hajji, J. Y. Cavaille, V. Favier, C. Gauthier, G. Vigier, *Polymer Composites* **1996**, 17, 612.
- [32] O. A. Battista, *Microcrystal Polymer Science*, Chapter 2, Mc Graw Hill, New York, **1975**.
- [33] A. Dufresne, D. Dupeyre, M. R. Vignon, *J. Appl. Polymer Sci.* **2000**, 76, 2080.
- [34] A. N. Nakagaito, H. Yano, *Appl. Phys. A* **2003**.
- [35] A. N. Nakagaito, H. Yano, *Appl. Phys. A* **2004**, 78, 547.
- [36] C. Zilg, R. Thomann, R. Mülhaupt, J. Finter, *Adv. Mater.* **1999**, 11, 49.

## Cutting of SiC Fibers for Ti-MMC Applications\*\*

By Manuel Herkt,\* Falko Heutling, and Ursula Koch

Modern materials research in the field of aeronautics seeks new methods to improve the performance of combustion engines and turbines by reducing weight using materials with high specific strength and stiffness.<sup>[1]</sup> Since the growth of international air traffic is about 5 % per year and the market demands economical turbines the need of lightweight materials becomes clear.<sup>[2]</sup> One way to achieve this objective is to use metal matrix composites (MMC). Most promising is the combination of SiC fibers together with TiAl6V4 (Ti-MMC). As Titanium 6-4 can be easily diffusion bonded, one fabrication route is the hot isostatic pressing (HIP) of Ti-coated SiC fibers.

A feasibility study has been carried out by MTU Aero Engines, which proofed a possible weight reduction by 25 % using Ti-MMC.

Most recently the successful application of this composite material as a landing gear component has been reported in literature.<sup>[3]</sup>

The aim of this combination is to take advantage of the high Young's modulus of the SiC fibers and the low weight of Titanium (high specific stiffness). The SiC fibers, which are

- [\*] M. Herkt,<sup>[+]</sup> Prof. Dr. U. Koch  
Department of Precision-, Microengineering &  
Engineering Physics  
Munich University of Applied Sciences  
Lothstraße 34, 80323 Munich, Germany  
E-mail: u.koch@fhm.edu
- Dr. F. Heutling  
MTU Aero Engines GmbH  
Materials Engineering, Rotor and New Materials  
Dachauer Straße 665, 80995 Munich, Germany  
E-mail: falko.heutling@muc.mtu.de
- [+] EADS Corporate Research Center Germany,  
Dept. LG-CT, 81663 Munich, Germany  
E-mail: manuel.herkt@eads.net

[\*\*] We would like to thank Stephen Hoffmann-Ivy for the many enriching remarks and comments. Special thanks go to Dr. Jürgen Wehr of EADS Corporate Research Center Germany for performing the bending tests. We also would like to thank Manfred Dietrich from the university's laboratory for laser techniques for performing the laser cutting. Furthermore we would like to express our gratitude Prof. Dr. Ortner from Darmstadt University of Technology for his willingness to discuss the found "onion-structure". Our very special thanks go to Dr. Gese from MATFEM for the FEM simulations of the breaking fibers.

## Paper E



# Mechanical and Morphological Properties of Cellulose Fibril Reinforced Nanocomposites\*\*

By Tanja Zimmermann,\* Evelyn Pöhler and Patrick Schwaller

Cellulose fibrils with diameters in the nanometer and lengths in the micrometer range offer great advantages for the use as a reinforcing phase in different polymer matrices. They combine good mechanical properties with low density, biodegradability and renewability. A review on such cellulose based nanocomposites is given by Berglund.<sup>[1]</sup>

In an earlier study, cellulose fibrils obtained from sulphite wood pulp were successfully used for the reinforcement of water soluble polymers like polyvinyl alcohol (PVA) and hydroxypropyl cellulose (HPC).<sup>[2]</sup> An investigation on the mechanical properties of the nanocomposites revealed that the addition of fibrils increased the modulus of elasticity (MOE) up to three-fold and the tensile strength up to five-fold compared to the raw polymer. However, the numeric MOE values calculated from these tests may be underestimated because the elongation of the samples was only determined from the longitudinal motion of the testing machine.

[\*] T. Zimmermann, E. Pöhler

Wood Laboratory  
Empa, Swiss Federal Laboratories for Materials Testing  
and Research  
Ueberlandstrasse 129  
CH-8600 Duebendorf, Switzerland  
E-mail: Tanja.Zimmermann@empa.ch

Dr. P. Schwaller  
Laboratory for Materials Technology  
Empa, Swiss Federal Laboratories for Materials Testing  
and Research  
Feuerwerkerstrasse 39  
CH-3602 Thun, Switzerland

[\*\*] We thank T. Geiger and J. Schleuniger (empa, Laboratory for Functional Polymers) for their support and advice on the disintegration of cellulose fibres and the tensile tests. Thanks are also due to M. Pinnow and Mrs. Schlawne (Dept. of Structural Characterisation, Fraunhofer Institute Golm, D) for helping us with the TEM investigations and to A. Fischer who supported us with the image analysis. We appreciated very much the hospitality of the University of Basel (P. Reimann and V. Thommen) that made our AFM investigations possible. We are also grateful to our colleagues at the Empa Wood Laboratory for helpful suggestions and comments on the manuscript.

A homogeneous fibril distribution as well as the formation of a rigid network resulting from hydrogen bonds between adjacent and overlapping fibrils was proposed to explain the improved mechanical behaviour of reinforced composites.<sup>[2,3]</sup> The importance of percolating network formation for a high reinforcement efficiency of different matrices is also discussed in studies carried out with cellulose whiskers obtained from different organic fibres (not wood pulp).<sup>[4-6]</sup> However, evidence for the existence of a network formation has not been provided so far.<sup>[1]</sup>

The objective of the present study was to determine the MOE as well as the hardness of fibril reinforced HPC films by nanoindentation. The modulus results were compared with those obtained by tensile tests carried out with an universal testing machine in an earlier study.<sup>[2]</sup> Further, the fibril alignment and the assumption of network formation in reinforced HPC films was analysed by Transmission Electron Microscopy (TEM) and Atomic Force Microscopy (AFM).

**Results and Discussion. Mechanical properties:** The nanoindentation experiments led to 2–3-fold (significance level  $p < 0.001$ ) higher MOE values for the HPC composites when compared with those obtained in tensile tests (Fig. 1). This indicates an apparent difference in the deformation behaviour between tensile and compressive loading and confirms results of other studies.

Xu et al.<sup>[10]</sup> determined indentation moduli on polymer-based nanocomposites with nanosilica. They obtained 2.6 to 3-fold higher MOE values than calculated in tensile tests and explained the differences in terms of the hydrostatic stress component which enhances the compressive modulus values in the isotropic polymer portion. The elastic properties of the polymer are mainly related to the uncoiling or sliding of chains over one another in response to the applied stress. The molecular mobility of the chains is strongly influenced by the available free volume. If the polymer is compressed, the free volume is reduced, the intermolecular forces between segments increase and thus the MOE is also expected to increase.<sup>[12]</sup>

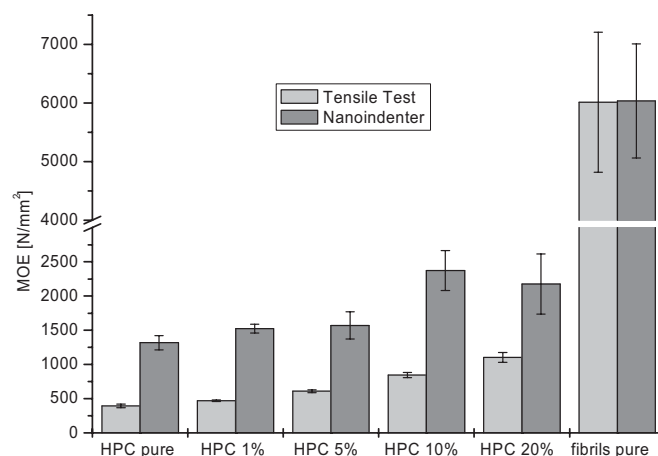


Fig. 1. Comparison of the Modulus of Elasticity of the hydroxypropyl cellulose composites with different fibril portions determined in tensile tests and from nanoindentation.

Stauss et al.<sup>[13]</sup> evaluated several galvanofomed Nickel samples and observed that the modulus obtained from nanoindentation was systematically about 15 % higher than the values calculated in tensile tests. The difference was explained by the fact that tensile and indentation tests do not probe the same material volumes and regions. In fact, tensile tests analyse a large volume of material, which includes defects such as pores, cracks and impurities whereas in nanoindentation the deformation zone is localised to a volume of a few hundred micrometer. Even in the case of our study where a large number ( $n = 50$ , resp. 100) of indentation tests was carried out for each composite film this explanation seems plausible.

Another important factor is the difference in strain rate between displacement-controlled tensile tests (deformation rate 50 mm/min, constant strain rate of  $0.008 \text{ sec}^{-1}$ ) and nanoindentation, where a constant load-rate of 0.4 mN/sec was used. The strain rate in our nanoindentation experiments thus decreased from  $2.25 \text{ sec}^{-1}$  at the beginning of the loading cycle to  $0.03 \text{ sec}^{-1}$  when attaining the maximum load. It is well known that the stiffness of certain materials depends on the strain rate. Wood e.g. shows an increased stiffness with high strain rates. Also in the case of the present study we assume that the strain rate differences contribute to the discrepancy of the MOE values as obtained from tensile tests and nanoindentation. Effects of different strain rates in nanoindentation experiments on our samples will be studied in future work.

Finally, an uncertainty of the tensile tests is related to the determination of the elongation by the longitudinal motion of the testing machine. As considerable higher moduli were obtained by nanoindentation it is reasonable that due to the shift of the tensile testing machine, the measured strain was too high for all composite films and therefore the calculated MOE values were too low. For an accurate optical strain measurement the application of a video-extensometer will be invaluable in future studies.

For the pure fibril films almost equal MOE values were measured with both methods (Fig. 1). The reason could be related to the extremely brittle nature of these films with almost no elongation at fracture and therefore only a small influence of the strain measurements.

As it was our objective in these studies to derive MOE values to relatively compare the stiffness of the fibril reinforced composite films among themselves, the accuracy of the single numerical values was therefore negligible.

For nanoindentation experiments the maximum stiffness was found for HPC with a fibril content of 10 wt%; these films had 2 times higher indentation moduli compared to the pure polymer. The highest increase in MOE (about 35 %) was found between a fibril loading of 5 wt% and 10 wt% ( $p < 0.001$ ). In comparison, films with a fibril portion of 20 wt% showed slightly lower MOE values ( $p < 0.05$ ). On the other hand, the highest MOE values measured by conventional tensile testing were obtained for the films with a fibril loading of 20 wt%, in this case even 3-fold higher values compared to pure HPC. Thus, the optimal filling rate of HPC is determined between 10 wt% and 20 wt%.

This is in good agreement with results of Borges et al.<sup>[14]</sup> who studied the tensile properties of cross-linked (with 1,4-butyl-diisocyanate) and uncross-linked composite films prepared from HPC with incorporation of microcrystalline cellulose fibres. The concentration of fibres in the composites ranged from 0 to 30 wt%. Maximum values of the MOE were observed at 10 wt% for the cross-linked and 20 wt% for the uncross-linked composites.

As indicated in Figure 2 the hardness of the hydroxypropyl cellulose composites increased with the fibril portion. The standard deviation of the hardness values is quite large. This phenomenon reflects a certain inhomogeneity of the material even on the micrometer scale. In accordance with the results obtained for the MOE, an abrupt increase in hardness could be observed ( $p < 0.001$ ) for the films with a fibril content of 10 wt% compared with HPC films with a fibril portion of 5 wt%. Thus, both nanoindentation tests provide evidence that a 10 % fibril ratio is optimal to enhance the mechanical properties of HPC films.

**Morphological Properties. TEM characterisation:** TEM micrographs of transverse surfaces of the HPC composite with a fibril content of 20 wt% show lighter and darker structures that can be explained by a contrast of crystalline fibril areas and the amorphous polymer matrix. The fibrils are homogeneously dispersed within the polymer matrix and form networks (Fig. 3(a,b)). According to the size of the fibrils, the transparency of the film also confirms the good fibril dispersion, i.e. no bigger aggregates are present. This indicates that during the drying step no fibril agglomeration occurs even when the stabilization by the fibril suspension is broken down.

Figure 3(c) shows the way in which the image processing software schematized a highlighted region in Figure 3(b). From the obtained image it is possible to calculate the interspace mesh areas of the cellulose fibril network. Figure 3(d) shows the distribution of mesh sizes expressed in cumulative percent. According to these results 90 % of the fibril interspace areas within the network are smaller than  $34000 \text{ nm}^2$ . The mean is

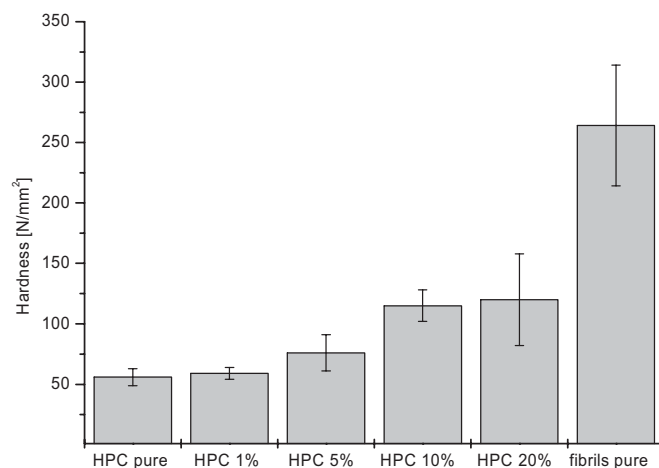


Fig. 2. Hardness of the hydroxypropyl cellulose composites with different fibril portions determined from nanoindentation.



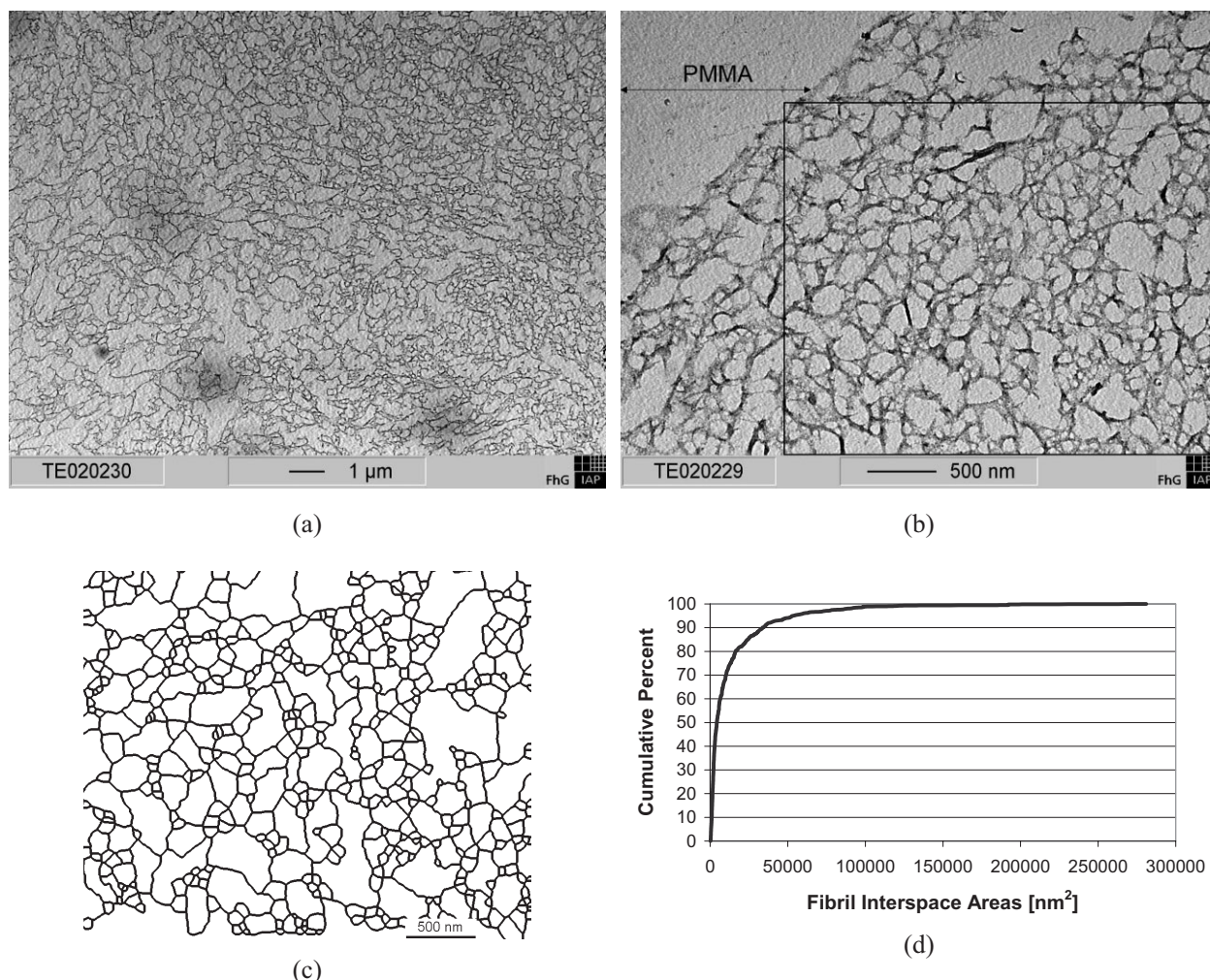


Fig. 3. a) TEM micrograph: Transverse section of a HPC film with a fibril content of 20 wt%. The fibrils are homogeneously dispersed within the polymer and form a conspicuous network structure. b) TEM micrograph: Like Figure 3(a), but higher magnification. The area that is selected for image analysis is indicated by the black border (PMMA= Polymethylmethacrylate). c) Model of the fibril network, highlighted in Figure 3(b), automatically schematised and segmented using the Image Processing Tool Kit 5.0 of Adobe Photoshop. d) Distribution of mesh sizes expressed in cumulative percent. 90% of the fibril interspace areas within the network are smaller than 34000 nm<sup>2</sup>.

13311 nm<sup>2</sup>, the smallest area 186 nm<sup>2</sup> and the largest area 281000 nm<sup>2</sup>. Thus, the statistical spread is very high (standard deviation 25712) with predominantly small mesh sizes. One must be aware that only a small and randomly selected area of the composite film was analysed. No other studies are known where mesh size areas of cellulose fibril network structures were measured. Thus, no comparisons are possible at present.

So far morphological characterisations have been carried out by TEM to measure the dimensions of cellulose whiskers or fibrils.<sup>[2,4,15–22]</sup> Scanning electron microscopy (SEM) was performed for investigation of the surface morphology of fractured nanocomposite films.<sup>[2,4,5,15,18,23–25]</sup> The objective of these studies was to analyse the filler/fibril distribution within the polymer matrices. From the results obtained it has been assumed that transversal sections of cellulose fibrils or whiskers appear as white dots, and the authors concluded that the filler must be homogeneously dispersed within the matrix. Thus, the dispersion of the fibrils could be shown but not the

apparent network formation within the polymer matrices as demonstrated in our study for the first time (Fig. 3(a,b)). Evidence for network formation was only indirectly derived from the mechanical and physical behaviour of the composites,<sup>[17,18]</sup> for example from the reduced swelling behaviour of filled polymers.<sup>[15]</sup>

Favier et al.<sup>[3]</sup> used TEM for the investigation of films consisting of cellulose whiskers obtained from tunicin and latex. They found that the whiskers were distributed throughout the structure, without segregation or association. Also Ruiz et al.<sup>[26]</sup> characterised the microstructure of nanocomposites consisting of tunicate and epoxy resin with TEM. In accordance to our results, their micrographs showed a good dispersion of the whiskers within the epoxy matrix and equal dimensions similar to the initial whisker suspension.

**AFM characterisation:** Only few studies report on characterisation of cellulose nanocomposites by AFM. Matsumara and Glasser<sup>[27]</sup> evaluated the phase dimensions of thermoplastic

cellulose composites by AFM. Some investigations used AFM for the characterisation of pulp fibres.<sup>[28,29]</sup>

Even though some limitations of AFM are mentioned in these studies, the authors demonstrated the usefulness of this method.

The AFM phase images obtained in our study give information about the fibril/polymer composition on the surfaces of the casted films, but in contrast to the TEM investigations no information about the distribution of the fibrils across the thickness of the films. Lower magnifications (e.g. 25  $\mu\text{m}$  scans) of hydroxypropyl cellulose films with fibril contents between 1 wt% and 20 wt% show that the fibrils are quite well dispersed within the matrix. However, structural irregularities and inhomogeneities with denser and more translucent areas were also detected (Fig. 4(a)). Higher magnifications of the composites with a fibril loading of 10 wt% and 20 wt% show network structures without indication for fibril agglomerations (Fig. 4(b)) and support the TEM findings. For the films with a fibril content of 1 wt% or 5 wt% no network formation could be detected. The fibril concentrations seem to be too small for intensive interactions between single filaments.

According to the results obtained, the direct use of the aqueous fibril suspensions for the compounding with HPC was an effective method of dispersing the fibrils within the polymer matrix. Chakraborty et al.<sup>[30]</sup> obtained similar results for microfibrils in water suspension used to make a biocomposite with polylactic acid (PLA). After a mixing procedure at 190 °C, they got a uniform dispersion of the microfibrils in the matrix.

The microscopic characterisations of the HPC films with different fibril contents provide valuable information for the interpretation of the results obtained from nanoindentation and, respectively in tensile testing. A significant increase in the mechanical properties was obtained for the films with fibril contents of 10 wt% compared to the films with lower fibril

portions. As a network formation could only be observed for composites with a fibril portion of at least 10 wt% it seems clear that the existence of fibril networks is of great importance for the mechanical properties of nanocomposites. The findings support earlier discussions about the importance of percolating cellulose fibril or whisker networks for a high reinforcement efficiency.<sup>[2,4-6]</sup>

According to the results of the present and earlier studies,<sup>[2]</sup> cellulose fibrils could be very useful for an application in waterborne coatings or adhesives to systematically improve their mechanical properties (hardness, tensile strength, MOE), their application and exploitation as well as thermal creep. In future, it is conceivable that characteristics of different matrices (e.g. fire resistance) could be directly influenced by functionalising the hydroxyl groups of cellulose fibrils.

**Conclusions:** Nanoindentation is a suitable method for mechanical characterisations of wood based nanocomposites. With small sized samples the handling is much easier than for conventional testing facilities and the results seem to be reliable. The apparent differences in the deformation behaviour between tensile (conventional testing) and compressive (nanoindentation) loading require further investigation.

TEM und AFM are very useful for the morphological characterisation of cellulose/HPC-composites. At higher magnifications, both methods indicated a homogeneous distribution of cellulose fibrils. Network formation within the polymer for fibril contents of at least 10 wt% could be shown for the first time. Nevertheless, on a larger scale some irregularities were apparent. These inhomogeneities may explain the reason for partly high standard deviations of the mechanical testing results.

The combination of the methods applied in this study allowed to explain the mechanical behaviour of the HPC nanocomposites and to determine the optimal filling rate for cellulose fibrils.

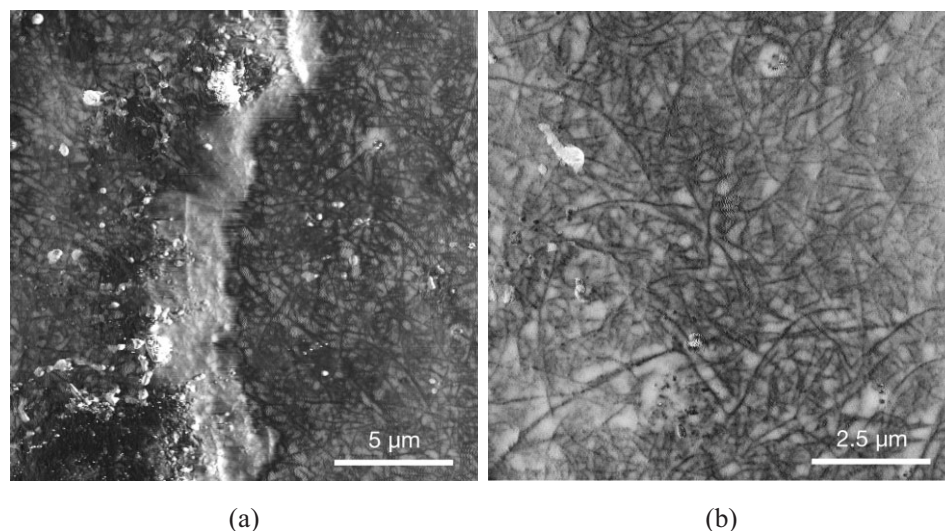


Fig. 4. a) AFM micrograph: Surface of a HPC film with a fibril content of 20 wt%. The fibrils are well dispersed within the polymer matrix and form network structures. Nevertheless, on a larger scale also some inhomogeneities are visible. b) AFM micrograph: Higher magnifications show that the fibrils are locally, homogeneously dispersed without any irregularities or agglomerations.



## Experimental

As basis material for the separation of cellulose fibrils sulphite pulp mainly composed of softwood tracheids from Borregaard ChemCell CH was used. The fibrils were mechanically separated as previously described.<sup>[2]</sup> Fibril solutions with different solid contents (1, 5, 10 and 20 wt%) were mixed with low viscosity hydroxypropyl cellulose (HPC) at a temperature of 60 °C. The obtained suspensions were casted in silicone forms and dried at standardised climate (23 °C/50 % r. H.) for seven days. Additionally, films consisting of pure cellulose fibril suspensions and pure HPC were also prepared.

**Tensile Tests:** Tensile tests – previously described in<sup>[2]</sup> – were performed on the casted films according to EN ISO 527-4<sup>[7]</sup> using a Zwick Z010 universal testing machine with a 200 N load cell. The tests were carried out at 20 °C/65 % r. H. and with a loading speed of 50 mm/min. The strain was determined by the longitudinal motion of the testing machine.

**Nanoindentation:** In a typical nanoindentation experiment a diamond indentation body is pressed into the specimen. The applied normal load  $P$  and the displacement into the surface  $h$  are continuously measured during loading and unloading.<sup>[8]</sup> A schematic example for such a load-displacement curve is shown in Figure 5. The Modulus of Elasticity (or indentation modulus)  $E_{\text{Indent}}$  can be calculated from the unloading part of the curve as the unloading is a purely elastic recovery process. The procedure however is not as straightforward as in tensile tests. We will therefore describe the method for the determination of  $E_{\text{Indent}}$  in more detail. The full procedure is described by Oliver and Pharr.<sup>[9]</sup>

The first step of the Oliver-Pharr data analysis procedure consists in fitting the unloading part of the load displacement data to the power-law relation derived from contact mechanics theory.

$$P = B(h - h_f)^m \quad (1)$$

$P$  is the applied load,  $h$  the displacement into the surface,  $h_f$  the residual depth of the indent after complete unloading (see Fig. 5).  $B$  and  $m$  are empirically determined fitting parameters. The unloading stiffness  $S = dP/dh$  can be calculated by differentiating Equation 1 and evaluating it for  $h = h_{\text{max}}$ .

$$S = Bm(h_{\text{max}} - h_f)^{m-1} \quad (2)$$

Using  $S$ , the so-called contact depth  $h_c$  can be calculated according to

$$h_c = h - \varepsilon P/S \quad (3)$$

where  $\varepsilon$  is a constant depending on the indenter geometry. We used  $\varepsilon = 0.75$  for the three-sided pyramidal indenters (so-called Berkovich-tips) used in the experiments for this work. Using  $h_c$ , the projected contact area as a function of the penetration,  $A(h_c)$  can be calculated. With  $S$  and  $A$ , the so-called reduced modulus  $E_r$  can be determined:

$$E_r = \frac{(\sqrt{\pi} \cdot S)}{2\beta \cdot A} \quad (4)$$

In Equation 4  $\beta$  depends on the indenter geometry and is equal to 1.034 for Berkovich pyramids. Finally,  $E_{\text{Indent}}$  of the sample can be extracted from the relation

$$\frac{1}{E_r} = \frac{(1-\nu^2)}{E_{\text{Indent}}} + \frac{(1-\nu_i^2)}{E_i} \quad (5)$$

where  $\nu$  is the Poisson's ratio of the test material and  $E_i$  (1141 GPa) and  $\nu_i$  (0.07) are the MOE and the Poisson's ratio, respectively, of the diamond indenter. Xu et al.<sup>[10]</sup> assumed  $\nu = 0.3$  for amorphous polymer samples and  $\nu = 0.35$  for

semicrystalline ones. Gindl et al.<sup>[11]</sup> used for their calculation of  $E_{\text{Indent}}$  a Poisson's ratio of 0.1 for cellulose. As we did not know the exact elastic constants for our HPC composites, we applied an intermediate value of 0.26 for the Poisson's ratio. It may seem counterintuitive that the Poisson's ratio of the investigated material has to be known. However, an uncertainty of  $\pm 0.1$  thus, a relatively big alteration of the Poisson's ratio, only induces a relative variation of  $E_{\text{Indent}}$  of  $\leq 5\%$ .

The hardness in nanoindentation experiments is understood as the mean contact pressure and can be calculated according to

$$H = \frac{P}{A(h_c)} \quad (6)$$

An important aspect is the function used to calculate the contact area from the displacement. Only for an ideal (i.e. infinitely sharp) Berkovich indenter the relation

$$A = 24.5 \cdot h_c^2 \quad (7)$$

is valid. In reality each tip will be blunted or may have other defects. This can be corrected to some extent by using an area function of the form

$$A(h_c) = a_0 \cdot h_c^2 + \sum_{i=1}^n a_{i+1} \cdot h_c^{1/2^i} \quad (8)$$

The parameters  $a_i$  are determined by performing nanoindentation experiments on materials with a known MOE (e.g. fused silica and sapphire).

The nanoindentation experiments were performed at ambient temperature using a MTS Nanoindenter XP (MTS, Oak Ridge TN, USA). Small pieces ( $10 \times 10 \text{ mm}^2$ ) of each composite (containing 1, 5, 10 and 20 wt% of cellulose fibrils) as well as pure HPC and pure fibril films were fixed with superglue (Turbo Klebstofftechnik GmbH, Bazenheid, CH) on aluminium specimen holders. The load-displacement curves have been measured with a peak load of 12 mN, the loading rate was 0.4 mN/sec, the unloading rate 0.8 mN/sec. The peak load was kept constant for a period of 15 sec to account for possible creep effects of the sample material. After unloading 90 % of the peak load, a second hold segment (i.e. keeping a constant load) of 50 sec was performed to measure the thermal drift. The latter was used to correct the load-displacement data. For each sample 50 (100 for the HPC samples with a fibril portion of 20 %) single load-displacements were measured and the average hardness and modulus values as well as the standard deviations were calculated. The large number of tests was necessary because the samples are laterally not homogeneous. Independent T-tests were carried out to demonstrate differences in means. A sample Poisson number of 0.26 was used for the calculation of the Modulus of Elasticity.

**TEM characterisation:** A small extract ( $2 \times 2 \text{ mm}^2$ ) of the HPC-composite containing 20 wt% fibrils was embedded in Polymethylmethacrylate (PMMA) resin. Ultra thin sections (approx. 60 nm thick) of the transverse film surfaces were sectioned using an ultramicrotome fitted with a diamond knife. The sections were mounted on Formvar coated grids and examined with a Philips CM200 transmission electron microscope at an accelerating voltage of 120 kV. Image processing software (Image Processing Tool Kit 5.0, Adobe Photoshop) was used for evaluation of the TEM images.

**AFM characterisation:** Small pieces ( $5 \times 5 \text{ mm}^2$ ) of the composite films of all fibril portions were glued (superglue, Turbo Klebstofftechnik GmbH, Bazenheid, CH) onto aluminium sample holders and examined with a NanoScope IVa Dimension™ 3100 AFM using Tapping Mode™. The samples were scanned using a silicon tip with a radius of approx. 10 nm. The length of the cantilever was 124  $\mu\text{m}$ , the spring constant was 37 N/m, and the resonant frequency was 300 kHz. The samples were investigated at ambient temperature and humidity. Images were taken in height mode, where the deflection of the cantilever is directly used to measure the  $z$  position, and in phase mode, where the phase shift of the cantilever is used to determine differences in material constitution.

Received: July 07, 2005

Final version: August 09, 2005

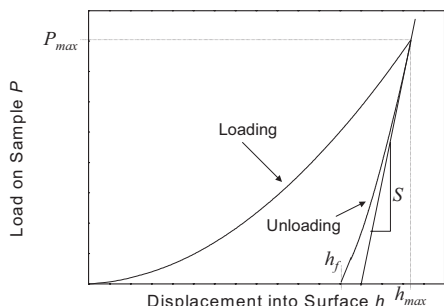


Fig. 5. Typical example of a load-displacement curve.

- [1] L. Berglund, in *Natural fibers, biopolymers, and their biocomposites* (Eds.: A. K. Mohanty, M. Misra, L. T. Drzol), CRC Press LLC, 2004, 560.
- [2] T. Zimmermann, E. Pöhler, T. Geiger, *Adv. Eng. Mater.* 2004, 6, 754.
- [3] V. Favier, H. Chanzy, J. Y. Cavaille, *Macromol.* 1995, 28, 6365.
- [4] W. Helbert, J. Y. Cavaille, A. Dufresne, *Polym. Compos.* 1996, 17, 604.

- [5] A. Dufresne, J. Y. Cavaille, W. Helbert, *Polym. Compos.* **1997**, 18, 198.
- [6] P. Hajji, J. Y. Cavaille, V. Favier, C. Gauthier, G. Vigier, *Polym. Compos.* **1996**, 17, 612.
- [7] Anonymus, EN ISO 527-4, **1997**.
- [8] A. Fischer-Cripps, in *Nanoindentation*, Springer, New York, **2002**.
- [9] W. C. Oliver, G. M. Pharr, *J. Mater. Res.* **2004**, 19, 3.
- [10] G. C. Xu, A. Y. Li, L. De Zhang, X. Y. Yu, T. Xie, G. S. Wu, *J. of Reinf. Plast. and Compos.* **2004**, 23, 1365.
- [11] W. Gindl, T. Schöberl, *Compos. Part A: Appl. Sci. and Manufacturing* **2004**, 35, 1345.
- [12] S. Roche, S. Bec, J. L. Loubet, *Mech. Properties Derived from Nanostructuring Mater. Symp. (Mater. Res. Soc. Symposium Proceedings Vol. 778)* **2003**, 117.
- [13] S. Stauss, P. Schwaller, J.-L. Bucaille, R. Rabe, L. Rohr, J. Michler, E. Blank, *Microelectron. Eng.* **2003**, 67 (8), 818.
- [14] J. P. Borges, M. H. Godinho, A. F. Martins, D. F. Stamatialis, M. N. De Pinho, M. N. Belgacem, *Polym. Compos.* **2004**, 25, 102.
- [15] M. N. Angles, A. Dufresne, *Macromol.* **2000**, 33, 8344.
- [16] E. Dinand, H. Chanzy, M. R. Vignon, *Food Hydrocolloids* **1999**, 13, 275.
- [17] A. Dufresne, M. R. Vignon, *Macromol.* **1998**, 31, 2693.
- [18] A. Dufresne, D. Dupeyre, M. R. Vignon, *J. of Appl. Polym. Sci.* **2000**, 76, 2080.
- [19] M. Samir, F. Alloin, M. Paillet, A. Dufresne, *Macromol.* **2004**, 37, 4313.
- [20] A. Morin, A. Dufresne, *Macromol.* **2002**, 35, 2190.
- [21] A. Dufresne, *Compos. Int.* **2003**, 10, 369.
- [22] V. Favier, R. Dendievel, G. Canova, J. Y. Cavaille, P. Gilormini, *Acta Mater.* **1997**, 45, 1557.
- [23] M. Samir, F. Alloin, J. Y. Sanchez, A. Dufresne, *Polym.* **2004**, 45, 4149.
- [24] A. P. Mathew, A. Dufresne, *Biomacromol.* **2002**, 3, 609.
- [25] A. F. Turbak, F. W. Snyder, K. R. Sandberg, *J. of Appl. Polym. Sci.: Appl. Polym. Symp.* **1983**, 37, 815.
- [26] M. M. Ruiz, J. Y. Cavaille, A. Dufresne, J. F. Gerard, C. Graillat, *Compos. Int.* **2000**, 7, 117.
- [27] H. Matsumura, W. G. Glasser, *J. of Appl. Polym. Sci.* **2000**, 78, 2254.
- [28] S. J. Hanley, D. G. Gray, *Holzforschung* **1994**, 18, 29.
- [29] R. Snell, L. H. Groom, T. G. Rials, *Holzforschung* **2001**, 55, 511.
- [30] A. Chakraborty, M. Sain, M. Kortschot, *Holzforschung* **2005**, 59, 102.



## Lebenslauf

Tanja Zimmermann Schütz

Geboren am		17. Dezember 1967 in Hamburg (D)
Familienstand		verheiratet, 3 Kinder
Schulausbildung	1974-1978	Grundschule Klosterbergen, Reinbek (D)
	1978-1987	Sachsenwaldgymnasium Reinbek (D) Abschluss: Abitur (1987)
Studium	1987-1993	Studium der Holzwirtschaft an der Universität Hamburg (D) Abschluss: Diplom-Holzwirtin (1993)
	1997-2001	Nachdiplomstudium Didaktischer Ausweis für das höhere Lehramt an der ETH Zürich (CH) (berufsbegleitend)
Berufliche Tätigkeit	seit 1994	Wissenschaftliche Mitarbeiterin der Abteilung Holz der Eidgenössischen Materialprüfungs- und Forschungsanstalt (EMPA) in Dübendorf (CH)
	seit 2001	Leiterin der Gruppe Holzwissenschaften/Biomimetik in der Abteilung Holz
	2002-2006	Doktorarbeit an der Empa, in Zusammenarbeit mit dem Institut für Holzbiologie und Holzschutz der Bundesforschungsanstalt für Forst- und Holzwirtschaft Hamburg (D) (berufsbegleitend)